National Library of Canada
Acquisitions and Bibliographic Services Branch
395 Wellington Street
Ottawa, Ontario
K1A 0N4

Bibliothèque nationale du Canada
Direction des acquisitions et des services bibliographiques
395, rue Wellington
Ottawa (Ontario)
K1A 0N4

Your file Votre référence

Our file Notre référence

NOTICE

The quality of this microform is heavily dependent upon the quality of the original thesis submitted for microfilming. Every effort has been made to ensure the highest quality of reproduction possible.

If pages are missing, contact the university which granted the degree.

Some pages may have indistinct print especially if the original pages were typed with a poor typewriter ribbon or if the university sent us an inferior photocopy.

Reproduction in full or in part of this microform is governed by the Canadian Copyright Act, R.S.C. 1970, c. C-30, and subsequent amendments.

AVIS

La qualité de cette microforme dépend grandement de la qualité de la thèse soumise au microfilmage. Nous avons tout fait pour assurer une qualité supérieure de reproduction.

S'il manque des pages, veuillez communiquer avec l'université qui a conféré le grade.

La qualité d'impression de certaines pages peut laisser à désirer, surtout si les pages originales ont été dactylographiées à l'aide d'un ruban usé ou si l'université nous a fait parvenir une photocopie de qualité inférieure.

La reproduction, même partielle, de cette microforme est soumise à la Loi canadienne sur le droit d'auteur, SRC 1970, c. C-30, et ses amendements subséquents.

Canada

University of Alberta

Analytical Investigation of Tension Fields in Lightweight Membrane Structures

by

Eliza M. Haseganu

©

A thesis submitted to the Faculty of Graduate Studies and Research in partial fulfillment of the requirements for the degree of **Doctor of Philosophy**.

Department of Mechanical Engineering

Edmonton, Alberta

Fall 1994

National Library
of Canada

Acquisitions and
Bibliographic Services Branch

395 Wellington Street
Ottawa, Ontario
K1A 0N4

Bibliothèque nationale
du Canada

Direction des acquisitions et
des services bibliographiques

395, rue Wellington
Ottawa (Ontario)
K1A 0N4

Your file Votre référence

Our file Notre référence

The author has granted an irrevocable non-exclusive licence allowing the National Library of Canada to reproduce, loan, distribute or sell copies of his/her thesis by any means and in any form or format, making this thesis available to interested persons.

L'auteur a accordé une licence irrévocable et non exclusive permettant à la Bibliothèque nationale du Canada de reproduire, prêter, distribuer ou vendre des copies de sa thèse de quelque manière et sous quelque forme que ce soit pour mettre des exemplaires de cette thèse à la disposition des personnes intéressées.

The author retains ownership of the copyright in his/her thesis. Neither the thesis nor substantial extracts from it may be printed or otherwise reproduced without his/her permission.

L'auteur conserve la propriété du droit d'auteur qui protège sa thèse. Ni la thèse ni des extraits substantiels de celle-ci ne doivent être imprimés ou autrement reproduits sans son autorisation.

ISBN 0-315-95200-8

Canada

University of Alberta

RELEASE FORM

Name of Author:	**Eliza M. Haseganu**
Title of Thesis:	**Analytical Investigation of Tension Fields in Lightweight Membrane Structures**
Degree:	**Doctor of Philosophy**
Year this degree granted:	**1994**

Permission is hereby granted to the University of Alberta Library to reproduce single copies of this thesis and to lend or sell such copies for private, scholarly or scientific research purposes only.

The author reserves all other publication and other rights in association with the copyright in the thesis, and except as hereinbefore provided neither the thesis nor any substantial portion thereof may be printed or otherwise reproduced in any material form whatever without the author's prior written permission.

Eliza Haseganu

Eliza M. Haseganu
Apt. 104A, 3815-107 Street
Edmonton, Alberta
Canada
T6J 2N7

Date: July 26, 1994

University of Alberta

Faculty of Graduate Studies and Research

The undersigned certify that they have read, and recommend to the Faculty of Graduate Studies and Research for acceptance, a thesis entitled **Analytical Investigation of Tension Fields in Lightweight Membrane Structures** submitted by **Eliza M. Haseganu**, in partial fulfillment of the requirements for the degree of **Doctor of Philosophy**.

David Steigmann

Dr. D. J. Steigmann (Supervisor)

Gary Faulkner

Dr. M. G. Faulkner

A. Mioduchowski

Dr. A. Mioduchowski

S. Łukasiewicz

Dr. S. A. Łukasiewicz

R. J. Tait

Dr. R. J. Tait

Date: May 4 1994

In memoria părinților mei

Abstract

The tension field generated by wrinkling in lightweight membrane structures has long been a problem of concern to structural designers and analysts.

A numerical method for the static analysis of elastic membranes is presented. The method is applicable to the study of tension fields associated with wrinkling in isotropic elastic membranes undergoing finite deformations.

A *relaxed strain energy density* is constructed and employed in the wrinkled regions in order to accommodate the wrinkling effect while retaining the analytical simplicity of membrane theory. As a consequence, tension field theory is automatically incorporated into ordinary membrane theory, extending the range of applicability of the membrane as a physical model.

The numerical procedure is based on the *Dynamic Relaxation Method.* This is an explicit, iterative technique in which the static solution forms the steady state part of the transient response of the structure. The numerical scheme is obtained from the spatial and temporal discretizations of the PDEs describing the damped motion of the membrane. The internal forces are obtained from the Euler-Lagrange equations. A finite difference technique derived from Green's theorem is used for the spatial discretization. The resulting system of ODEs is further integrated in time by a central difference time integrator. Fictitious mass and damping characteristics are chosen at each time step such that the static solution is achieved with the smallest number of steps. Arbitrary, conservative loading and arbitrary, planar geometries of the stress-free reference configuration are considered. Solutions of a number of boundary value problems are obtained and analyzed. The effects of various boundary and loading conditions on the response of the membrane are examined. A good agreement with existing exact solutions is observed. As well, the qualitative response obtained with experimental models confirms the predictions of the numerical method.

Acknowledgements

I would like to express my gratitude to my supervisor, Dr. D.J. Steigmann, for his advice, guidance and assistance in the preparation of this thesis. As well, I would like to thank Dr. M.G. Faulkner and Dr. A. Mioduchowski for their helpful suggestions and encouragement. Appreciation is extended to the University of Alberta, Department of Mechanical Engineering, Province of Alberta, Killam Trust and NSERC for the financial support received during the course of this research.

Table of Contents

Chapter 1

Introduction 1

Chapter 2

Membrane Theory 7

2.1 General Considerations 7

2.2 Kinematics of Deformation 8

2.3 Stress and Equilibrium 10

2.4 Relaxed Strain Energy Density 16

Chapter 3

Numerical Method 22

3.1 General Considerations 22

3.2 Dynamic Relaxation 23

3.2.1 Introduction. 23

3.2.2 History 24

3.2.3 Second-Order Richardson Method. 27

3.2.4 Transient Response and DR 28

3.2.5 DR Algorithm and Properties 31
3.2.6 Choice of Iteration Parameters 35
3.2.7 DR Algorithms for Nonlinear Problems 39
3.3 Spatial Discretization 42
3.3.1 Introduction 42
3.3.2 Green's Theorem Differencing Method 43
3.3.3 Internal and External Forces 48
3.3.4 Boundary Conditions 51
3.4 Adaptive DR Method for Analysis of Membranes 53

Chapter 4

DR Solutions to Membrane Problems 59
4.1 General Considerations 59
4.2 Neo-Hookean Membranes Subjected to
Displacement Boundary Conditions 67
4.2.1 Simple Shear of Square Membrane 67
4.2.2 Plane Twisting of Annular Membranes 72
4.2.3 Combined Twist and Lateral Deflection
of Annular Membranes 78
4.3 Neo-Hookean Membranes Subjected to
Mixed Displacement/Null Traction Boundary Conditions 86
4.3.1 Combined Stretching and Shearing of Rectangular
Membrane with Traction-Free Lateral Boundaries 86
4.3.2 Shearing of Square Sheet
with Traction-Free Circular Hole 94

4.3.3 Stretching of Rectangular Sheet with Traction-Free Slot . . . 100

4.4 Neo-Hookean and Ogden Membranes Subjected to Uniform Pressure and Displacement Boundary Conditions 105

4.4.1 Square Neo-Hookean Membrane Subjected to Simple Shear and Uniform Lateral Pressure 105

4.4.2 Circular Ogden and Neo-Hookean Membranes Subjected to Uniform Pressure Combined with Reduction in Boundary Circumference 109

4.5 Ogden Membranes Subjected to Point Loads, Uniform Pressure and Displacement Boundary Conditions 119

4.5.1 Circular Membrane Subjected to a Central Point Load 119

4.5.2 Circular Membrane Subjected to Uniform Pressure and a Central Point Load 122

Chapter 5

Experimental Models 134

Chapter 6

Summary and Conclusions 150

Bibliography 153

List of Figures

3.1 Mesh for spatial discretization, with integration paths used in Green's theorem method for differencing gradient components 45

3.2 Phantom mesh at boundary. 52

4.1a Original neo-Hookean strain energy function 61

4.1b Relaxed neo-Hookean strain energy function 62

4.2a Original Ogden strain energy function 64

4.2b Relaxed Ogden strain energy function 65

4.3a Square membrane; meshed reference configuration 68

4.3b Square membrane in simple shear; deformed configuration 69

4.4 Mesh dependent wrinkling for membrane with original, non-relaxed strain energy and boundary subjected to a simple shear deformation 71

4.5a Circular annular membrane; meshed reference configuration 73

4.5b Plane twisting of circular annular membrane; deformed configuration . . . 74

4.5c Plane twisting of circular annular membrane; deformed configuration, mesh removed 75

4.6a Square annular membrane; meshed reference configuration 76

4.6b Plane twisting of square annular membrane; deformed configuration 77

4.7a Circular annular membrane; radial displacement and reduction in circumference of inner boundary; intermediate deformed configuration . . . 79

4.7b Circular annular membrane; radial displacement and reduction in circumference of inner boundary; intermediate deformed configuration, mesh removed 80

4.7c Combined radial displacement and lateral deflection of circular annular membrane; intermediate deformed configuration 81

4.7d Combined radial displacement, lateral deflection and twist of circular annular membrane; final deformed configuration 82

4.8 Variation of stretch λ along a tension trajectory with initial radius r 84

4.9 Combined twist and lateral deflection of square annular membrane; deformed configuration 85

4.10a Rectangular membrane with traction free lateral boundaries; reference configuration 87

4.10b Combined stretching (20% of height) and shearing (30^{o}) of rectangular membrane with traction-free lateral boundaries; intermediate deformed configuration. 88

4.10c Combined stretching (30% of height) and shearing (30^{o}) of rectangular membrane with traction-free lateral boundaries; intermediate deformed configuration. 90

4.10d Combined stretching (30% of height) and shearing (45^{o}) of rectangular membrane with traction-free lateral boundaries; final deformed configuration. 91

4.10e Shearing (30^{o}) with no prestretch of rectangular membrane with traction-free lateral boundaries; deformed configuration 92

4.10f Shearing (30^o) with no prestretch of rectangular membrane with traction-free lateral boundaries; details of deformation in the proximity of the left free boundary 93
4.11a Square sheet with circular hole; reference configuration 95
4.11b Shearing of square sheet with traction-free circular hole; deformed configuration 96
4.11c Distribution of tense, wrinkled and slack regions mapped onto meshed reference configuration of square sheet with traction-free circular hole subjected to shearing. 97
4.11d Shearing of square sheet with traction-free central circular hole; details of deformation around the hole. 98
4.11e Contour plot representing lines of equal principal stretch λ on deformed configuration of square sheet with traction-free circular hole subjected to shearing. 99
4.12a Rectangular sheet with traction-free slot; meshed reference configuration . . 101
4.12b Stretching of rectangular sheet with traction-free slot; deformed mesh . . . 102
4.12c Stretching of rectangular sheet with traction-free slot; distribution of tense, wrinkled and slack regions, mesh removed 103
4.12d Stretching of rectangular sheet with traction-free slot; details of deformation near slot 104
4.13a Combined shear and pressurization of square membrane; deformed configuration for shear angle of 30^o. 106
4.13b Combined shear and pressurization of square membrane; deformed configuration for shear angle of 30^o, top view 107

4.13c Combined shear and pressurization of square membrane; deformed configuration for shear angle of 45^{o}, top view 108
4.14a Circular membrane; meshed reference configuration 110
4.14b Circular Ogden membrane subjected to a non dimensional pressure of 1.0 combined with a 20% reduction in the length of boundary circumference . . 111
4.14c Circular Ogden membrane subjected to a non dimensional pressure of 2.0 combined with a 20% reduction in the length of boundary circumference . . 112
4.14d Circular Ogden membrane subjected to a non dimensional pressure of 2.0 combined with a 50% reduction in the length of boundary circumference . . 113
4.15 Cross sections through meridian of deformed configurations of circular Ogden membrane for different numerical values of pressure 115
4.16a Cross sections through meridian of deformed configurations of circular neo-Hookean membrane for different numerical values of pressure 116
4.16b Comparison of cross sections through meridian of deformed configurations of circular neo-Hookean and Ogden membranes, for the same numerical values of pressure 117
4.17a Circular Ogden membrane subjected to a central vertical point load; deformed configuration 120
4.17b Circular Ogden membrane subjected to a central vertical point load, combined with a 20% reduction in the length of circumference of boundary; deformed configuration. 121
4.18a Pressurized circular membrane subjected to a central vertical point load directed downwards 123
4.18b Cross section through pressurized circular membrane subjected to a central vertical point load directed downwards 124

4.18c Cross section through pressurized circular membrane subjected to a central vertical point load directed downwards, combined with a 20% reduction in the length of boundary circumference 125

4.19a Pressurized circular membrane subjected to a central vertical point load directed downwards, combined with a 50% reduction in the length of boundary circumference. 127

4.19b Pressurized circular membrane subjected to a central vertical point load directed downwards, combined with a 50% reduction in the length of boundary circumference; top view 128

4.19c Pressurized circular membrane subjected to a central vertical point load directed downwards, combined with a 50% reduction in the length of boundary circumference; frontal view. 129

4.19d Cross section through pressurized circular membrane subjected to a central vertical point load directed downwards, combined with a 50% reduction in the length of boundary circumference; oblique view. 130

4.19e Cross section through pressurized circular membrane subjected to a central vertical point load directed downwards, combined with a 50% reduction in the length of boundary circumference; frontal view 131

4.19f Meridian of pressurized circular membrane subjected to a central vertical point load directed downwards, combined with a 50% reduction in the length of boundary circumference; frontal view 132

5.1a Experimental model of square membrane; initial configuration 135

5.1b Experimental model of square membrane subjected to shearing 137

5.2a Experimental model of rectangular membrane with traction-free lateral boundaries; initial configuration 138

5.2b Experimental model of rectangular membrane with traction-free boundaries subjected to shearing 139

5.3a Experimental model of square membrane with traction-free circular hole; initial configuration 140

5.3b Experimental model of square membrane with traction-free circular hole subjected to shearing. 142

5.4a Experimental model of circular annular membrane; initial configuration . . . 143

5.4b Experimental model of circular annular membrane subjected to plane twisting (5°) 144

5.4c Experimental model of circular annular membrane subjected to plane twisting (20°). 145

5.4d Experimental model of circular annular membrane subjected to combined lateral deflection and twisting (90°) 146

5.4e Experimental model of circular annular membrane subjected to combined lateral deflection and twisting (90°); details of deformation near hub. . . . 147

5.4f Experimental model of circular annular membrane subjected to combined lateral deflection and twisting (180°) 148

List of Symbols

$A^{k,l}$	—	nodal area
$A^{k+1/2,l+1/2}$	—	zonal area
c	—	damping matrix coefficient
$\boldsymbol{C}$	—	Cauchy-Green strain tensor
$\mathcal{D}$	—	damping matrix
$\boldsymbol{e}$	—	error vector
$\{\boldsymbol{e}_\alpha\}$	—	fixed orthonormal basis ($\alpha = 1,\ 2$)
$\{\boldsymbol{e}_i\}$	—	fixed orthonormal basis ($i = 1,\ 2,\ 3$)
$e_{\alpha\beta}$	—	2D alternator symbol
e_{ijk}	—	3D alternator symbol
E	—	total potential energy
$\boldsymbol{F}$	—	deformation gradient
$\mathcal{F}$	—	vector of external forces
G	—	shear modulus
h	—	time increment
$\boldsymbol{I}$	—	3D unit tensor
J	—	Jacobian
$\mathcal{K}$	—	stiffness matrix
${}^{l}\mathcal{K}$	—	local diagonal stiffness matrix
${}^{t}\mathcal{K}$	—	tangential stiffness matrix
$\boldsymbol{L}, \boldsymbol{M}$	—	principal vectors of strain in reference configuration

$\boldsymbol{l}, \boldsymbol{m}$	—	principal vectors of strain in deformed configuration
m_{ii}	—	element of diagonal mass matrix
$\mathcal{M}$	—	mass matrix
$\boldsymbol{n}$	—	unit normal to deformed surface at $\boldsymbol{r}$
N	—	total number of DOF of structure
p	—	pressure loading
P	—	load potential
$\mathcal{P}$	—	vector of internal forces
$\boldsymbol{r}$	—	position vector of material particle in deformed configuration
r_1, r_2, r_3	—	components of $\boldsymbol{r}$ with respect to $\{\boldsymbol{e}_i\}$
$\mathcal{R}$	—	residual vector
S	—	membrane analogue of 2nd Piola-Kirchhoff stress tensor
t	—	time
$\boldsymbol{T}$	—	Piola stress tensor
$\boldsymbol{u}$	—	displacement vector
U	—	strain energy per unit initial volume
v	—	natural width in simple tension
W, w	—	strain energy per unit area of reference configuration
w_λ, w_μ	—	principal stresses
$\boldsymbol{x}$	—	position vector of material particle in reference configuration
x_1, x_2	—	components of $\boldsymbol{x}$ with respect to $\{\boldsymbol{e}_\alpha\}$

Greek Symbols

Δ	—	2D unit tensor
λ, μ	—	principal stretches
$\xi_\alpha^{k,l}$	—	mesh distortion parameter
ω_0, ω_{max}	—	fundamental and maximum naural frequencies of structure
Ω	—	bounded region of (x_1, x_2)-plane
$\partial\Omega$	—	boundary of region Ω

Subscripts

i	—	component with respect to $\boldsymbol{e}_i$ $(i = 1,\ 2,\ 3)$
i	—	DOF $(i = 1, ..., N)$
α	—	component with respect to $\boldsymbol{e}_\alpha$ $(\alpha = 1,\ 2)$
$,\alpha$	—	partial derivative with respect to x_α $(\alpha = 1,\ 2)$
λ, μ	—	partial derivatives with respect to principal stretches

Left Superscripts

ℓ	—	local matrix
t	—	tangential matrix

Right Superscripts

(k, ℓ)	—	label of node
$(k+1/2, \ell+1/2)$	—	label of zone and zone center
n	—	label of time step
0	—	label of time step at $t = 0$
-1	—	inverse of matrix, tensor
T	—	transpose of tensor

Abbreviations

DOF	—	degree of freedom
DR	—	Dynamic Relaxation
ODE	—	ordinary differential equation
PDE	—	partial differential equation
2D	—	two dimensions
3D	—	three dimensions

Chapter 1

Introduction

Very thin, flexible tensile structures find an increased use in space, marine and terrestrial technology. The deformations occurring in such structures are mostly of the large rotation and/or strain type and as a consequence are inherently nonlinear. Partial or total wrinkling of membranes may be observed in some equilibrium configurations. The tension field generated by wrinkling has long been a problem of concern in the design and analysis of membrane structures.

Analysis of wrinkling is important for the prediction of structural response. Wrinkling is initiated by the loss of prestress and appearance of compressive stresses, under the action of a specific loading and/or certain boundary conditions. It represents a localized buckling phenomenon. The configuration of the wrinkled region depends on the small bending stiffness of the material. Membrane theory in its usual form neglects this bending stiffness, so it cannot give the details of deformation in a wrinkled region. Moreover, the presence of compressive stresses in equilibrium solutions makes such states unstable (Steigmann, 1986), and therefore physically meaningless. Stable solutions may be obtained by employing shell theory or alternatively, tension field theory, the latter being much simpler from the point of view of the analysis. Based on

these theories, various models of the wrinkled region have been reported in the literature.

One of the first investigations into wrinkling as a load transmission mechanism in membranes is due to Wagner (1929). He introduced the concept of the *tension field*, to simplify the post-buckling analysis of flexible shear panels used in aircraft construction. Applying shear loads to the edges of a thin panel and forcing it into the post-buckling range, the load is transmitted mainly along one of the principal axes of stress. Bending effects are minor. A wavy surface of the deformed panel is obtained, the trajectories of tensile stress being approximately coincident with the crests of the waves. Wagner neglected the bending stiffness and assumed the stress to be uniaxial. This uniaxial state of stress defines a tension field. Based on these assumptions, and considering the wrinkles as being spaced infinitesimally close together, Wagner formulated tension field theory.

Later, Reissner (1938) developed the first mathematical theory of tension fields for the case of plane stress and infinitesimal deformations. He generalized Wagner's results by introducing an artificial orthotropy into the membrane model, whereby a different elastic modulus is associated with each principal direction. In the presence of wrinkling, the corresponding modulus is set equal to zero. He assumed that the wrinkles are continuously distributed over a smooth surface and coincide with the trajectories of the active principal stress. A finite-deformation version of this theory was formulated by Wu and Canfield (1981), in the context of plane stress.

Further investigations into the wrinkling of membranes and the associated tension field are due to Kondo (1943) and Kondo et al. (1955), Stein and Hedgepeth (1961), Cherepanov (1963), Mansfield (1970), Zak (1982), Szyszkowski and Glockner (1984, 1987a,b) and others.

For isotropic elastic membranes with no bending stiffness, Pipkin (1986a) showed that all of the basic hypotheses of tension-field theory follow as consequences of the principle of minimum potential energy. In particular, states of strain associated with

unstable compressive stresses in conventional membrane theory may instead be constructed as limits of energy-minimizing sequences of deformations involving closely spaced wrinkles. Because of the absence of bending stiffness, there is no energetic penalty associated with spacing the wrinkles more and more closely together. The wrinkles are continuously distributed in the limit and the resulting configuration is, in general, perfectly smooth and free of compressive stresses. Pipkin (1986a) used these constructions to derive a *relaxed strain energy* that automatically accounts for states with continuously distributed wrinkles.

Subsequently, Steigmann (1990) used the relaxed energy to develop a general tension-field theory for application to the analysis of wrinkling in isotropic elastic membranes undergoing finite deformations, for curved geometries of the stress-free reference configuration. He derived a partial differential equation describing a geometrical property of tension trajectories. As well, he showed that the state of stress in the tension field is described by a statically determined system of two equations which is strongly elliptic at any stable solution. This system does not involve the deformation in the tension field, which is given by a system of parabolic type.

Pipkin (1986a) showed that tension field theory can be incorporated into ordinary membrane theory by replacing the strain energy function by the relaxed energy density. The relaxed strain energy represents the average energy per unit initial area over a region containing numerous wrinkles. The stresses delivered by the stress-strain relation derived from a relaxed strain energy are never compressive. In the presence of wrinkling one principal stress component vanishes, and this theory reproduces all of the main assumptions of tension field theory. However, a solution within this theory gives only the average deformation in a wrinkled region. To predict the details of the distribution, spacing and amplitude of the wrinkles, a theory that accounts for the strain energy due to bending must be employed (Hilgers and Pipkin, 1992). Nevertheless, if detailed information of this type is not of interest, then a pure membrane theory based on a relaxed energy density constitutes a much simpler alternative. A number of exact

solutions have been obtained in this way (Li and Steigmann, 1993, 1994, Haseganu and Steigmann, 1994a).

In this work a numerical method is developed for application to the analysis of partially wrinkled membranes undergoing finite deformations, for arbitrary conservative loading and planar geometries of the stress-free reference configuration. To accommodate the wrinkling effect while retaining the analytical simplicity of membrane theory, a relaxed strain energy is constructed and employed. The numerical procedure is based on the *Dynamic Relaxation Method* (Frankel, 1950, Otter, 1965, Day, 1965, Underwood, 1983). This is an explicit, iterative technique in which the static solution is obtained as the steady state part of the damped dynamic response of the structure. Dynamic Relaxation is particularly well suited for the class of problems considered here, since it does not require the construction or inversion of the stiffness matrix, which in the presence of wrinkling is ill-conditioned. Standard stiffness-based iterative methods such as Newton-Raphson and modified Newton-Raphson cannot be employed in this case, since such methods lead to ill-conditioned systems of equations and the iterations may not converge. Dynamic Relaxation has also the advantage of delivering asymptotically dynamically stable solutions. The numerical scheme is obtained from the spatial and temporal discretizations of the PDEs describing the damped motion of the membrane. The internal forces are obtained from the Euler-Lagrange equations. For the spatial discretization, a finite difference technique derived from Green's theorem is used (Wilkins, 1964, 1969, Silling, 1985). Besides its simplicity, this technique avoids the inconvenience of mapping methods, being applicable to uniform as well as irregular types of meshes, which can be fitted to any shape of the boundary. Also, this technique allows for the solution of problems involving concentrated loads. The analytical formulations of such problems contain singularities. However, the present model can be used to obtain the associated deformation, since the concentrated loads are applied at nodal points of the mesh, whereas the stretches are evaluated at zone-centered points, where they remain finite.

The system of ODEs obtained after the spatial discretization is then integrated in time by a central difference time integrator. Fictitious mass and damping characteristics are chosen at each time step, such that the static solution is achieved with the smallest number of steps. This general method can be employed to obtain solutions of a large variety of boundary value problems involving partially wrinkled membranes. As well, the method permits the analysis of the effects of various boundary and loading conditions on the response of the membrane.

The remainder of this section gives brief descriptions of each of the following chapters of the thesis.

Chapter 2 is concerned with the presentation of the direct theory of elastic membranes, and with the necessary modifications of the theory such as to account for the presence of wrinkling. Necessary conditions for stable equilibria are discussed and the concept of the relaxed strain energy is introduced. It is shown that by replacing the original strain energy with the relaxed strain energy, the effects of wrinkling are incorporated into conventional membrane theory. Further, the stress-strain relation obtained from the relaxed energy delivers stresses that are never compressive, and therefore deformations that satisfy this necessary condition for stability.

In Chapter 3, the method of Dynamic Relaxation is presented. Stability and convergence requirements for the numerical solution are discussed. A finite difference technique derived from Green's theorem for the use in the spatial discretization of the PDEs governing the damped motion of the membrane is described. An adaptive Dynamic Relaxation Method, especially developed for the analysis of partially wrinkled membranes is presented.

The application of this method to the solution of boundary value problems involving partially wrinkled membranes is discussed in Chapter 4. Two strain energy functions are used for illustrative purposes: the neo-Hookean strain energy and Ogden strain energy. Planar as well as 3D deformations are considered, starting in all cases from a planar reference configuration. Displacement boundary conditions as well as

mixed displacement/null-traction boundary conditions are used. A variety of geometrical shapes of the membrane are analyzed. Cases of zero distributed loading, uniform pressure loading and concentrated forces are studied. A good agreement with existing exact solutions is observed.

Chapter 5 contains a description of the experimental models constructed for the analysis of the real behaviour of the membranes. It is shown that the qualitative response obtained with these models confirms the predictions of the numerical method.

Chapter 2

Membrane Theory

2.1 General Considerations

An approach based on the direct theory of elastic membranes is considered (Green et al., 1965; Naghdi, 1972; Steigmann, 1990). According to the direct theory, a membrane is regarded as a two-dimensional elastic continuum, endowed with a strain energy $W(\boldsymbol{F})$ measured per unit area of a reference surface. Here $\boldsymbol{F}$ is the deformation gradient. The membrane is assumed to be perfectly flexible, its bending stiffness being considered as negligible. Further it is assumed to be isotropic, homogeneous and incompressible.

The equivalence of the direct theory and the conventional approach, based on the descent from three-dimensional elasticity (e.g. Green and Adkins, 1970), has been established by Naghdi and Tang (1977), for isotropic elastic materials that are either compressible or incompressible in bulk.

The case of finite deformations is considered.

2.2 Kinematics of Deformation

Attention is confined to planar geometries of the stress-free reference configuration. Consider a membrane that initially occupies a bounded region Ω of the (x_1, x_2)-plane with a piecewise smooth boundary $\partial\Omega$. The position of a point $\boldsymbol{x} \in \Omega$ is then given by $\boldsymbol{x} = x_\alpha \boldsymbol{e}_\alpha$, where Greek indices range over $\{1, 2\}$ and $\{\boldsymbol{e}_1, \boldsymbol{e}_2\}$ is a fixed orthonormal basis. A deformation carries the material point with coordinates (x_1, x_2) to the position $\boldsymbol{r}(\boldsymbol{x}) = r_i(\boldsymbol{x})\boldsymbol{e}_i$ in three-dimensional space, where Latin indices take values in $\{1, 2, 3\}$ and $\boldsymbol{e}_3 = \boldsymbol{e}_1 \times \boldsymbol{e}_2$ is the unit normal to the plane containing Ω. Here $r_i(\boldsymbol{x})$ are the Cartesian coordinates of the material point on the deformed surface. The basic kinematical variable in the direct theory is the deformation gradient $\boldsymbol{F}$, which maps the material element $d\boldsymbol{x}$ in the reference plane onto $d\boldsymbol{r}(\boldsymbol{x}) = \boldsymbol{F}\,d\boldsymbol{x}$, tangential to the deformed surface. This has the representation

$$\boldsymbol{F} = F_{i\alpha}(\boldsymbol{x})\boldsymbol{e}_i \otimes \boldsymbol{e}_\alpha; \quad F_{i\alpha} = r_{i,\alpha}. \tag{2.1}$$

The associated Cauchy-Green strain tensor $\boldsymbol{C}(\boldsymbol{x})$ is defined as

$$\boldsymbol{C} = \boldsymbol{F}^{\mathrm{T}}\boldsymbol{F} = C_{\alpha\beta}\,\boldsymbol{e}_\alpha \otimes \boldsymbol{e}_\beta; \quad C_{\alpha\beta} = F_{i\alpha}F_{i\beta}. \tag{2.2}$$

This is positive semi-definite, since $\boldsymbol{v} \cdot \boldsymbol{C}\boldsymbol{v} = |\boldsymbol{F}\boldsymbol{v}|^2$ for any vector $\boldsymbol{v} \in \mathbb{R}^3$. $\boldsymbol{C}(\boldsymbol{x})$ is also symmetric for every $\boldsymbol{x} \in \Omega$. Therefore it possesses an orthonormal pair $\{\boldsymbol{L}(\boldsymbol{x}), \boldsymbol{M}(\boldsymbol{x})\}$ of eigenvectors, with representations $\boldsymbol{L} = L_\alpha(\boldsymbol{x})\boldsymbol{e}_\alpha$ and $\boldsymbol{M} = M_\alpha(\boldsymbol{x})\boldsymbol{e}_\alpha$. These can be used to define non-negative scalars

$$\lambda(\boldsymbol{x}) = |\boldsymbol{F}\boldsymbol{L}| = (\boldsymbol{L} \cdot \boldsymbol{C}\boldsymbol{L})^{1/2}, \quad \mu(\boldsymbol{x}) = |\boldsymbol{F}\boldsymbol{M}| = (\boldsymbol{M} \cdot \boldsymbol{C}\boldsymbol{M})^{1/2} \tag{2.3}$$

and unit vectors

$$\boldsymbol{l}(\boldsymbol{x}) = \lambda^{-1}\boldsymbol{F}\boldsymbol{L}, \quad \boldsymbol{m}(\boldsymbol{x}) = \mu^{-1}\boldsymbol{F}\boldsymbol{M}. \tag{2.4}$$

The unit tensor $\boldsymbol{I}$ may be represented in the form $\boldsymbol{I} = \Delta + \boldsymbol{e}_3 \otimes \boldsymbol{e}_3$, where $\Delta = \boldsymbol{e}_\alpha \otimes \boldsymbol{e}_\alpha$. Using the orthonormality of $\{\boldsymbol{L}, \boldsymbol{M}\}$, Δ can be written as $\Delta = \boldsymbol{L} \otimes \boldsymbol{L} + \boldsymbol{M} \otimes \boldsymbol{M}$ for any $x \in \Omega$, and $\boldsymbol{F}$ becomes

$$\boldsymbol{F} = \boldsymbol{F}\Delta = \boldsymbol{F}\boldsymbol{L} \otimes \boldsymbol{L} + \boldsymbol{F}\boldsymbol{M} \otimes \boldsymbol{M}. \tag{2.5}$$

From equations (2.1) and (2.3) $\boldsymbol{F}$ is obtained as

$$\boldsymbol{F} = \lambda \boldsymbol{l} \otimes \boldsymbol{L} + \mu \boldsymbol{m} \otimes \boldsymbol{M}. \tag{2.6}$$

Then, the Cauchy-Green strain is

$$\boldsymbol{C} = \lambda^2 \boldsymbol{L} \otimes \boldsymbol{L} + \mu^2 \boldsymbol{M} \otimes \boldsymbol{M} + \lambda\mu \boldsymbol{l} \cdot \boldsymbol{m}(\boldsymbol{L} \otimes \boldsymbol{M} + \boldsymbol{M} \otimes \boldsymbol{L}). \tag{2.7}$$

As a consequence of the definition of $\boldsymbol{L}$ and $\boldsymbol{M}$, $\boldsymbol{l} \cdot \boldsymbol{m} = 0$, unless $\lambda = 0$ or $\mu = 0$. Thus, $\{\boldsymbol{l}(\boldsymbol{x}), \boldsymbol{m}(\boldsymbol{x})\}$ is an orthonormal basis for the tangent plane of the deformed surface at the material particle $\boldsymbol{x}$, representing the principal vectors of strain. $\{\boldsymbol{L}(\boldsymbol{x}), \boldsymbol{M}(\boldsymbol{x})\}$ are the principal vectors of strain in the reference plane. Then, λ and μ are the *principal stretches* representing the non-negative square roots of the eigenvalues of $\boldsymbol{C}$. The spectral form of $\boldsymbol{C}$ is

$$\boldsymbol{C} = \lambda^2 \boldsymbol{L} \otimes \boldsymbol{L} + \mu^2 \boldsymbol{M} \otimes \boldsymbol{M}. \tag{2.8}$$

The ratio J of the elemental area of the deformed surface to the elemental area of the (x_1, x_2)-plane can be obtained from (2.8) as:

$$J = (det\boldsymbol{C})^{1/2} = \lambda\mu. \tag{2.9}$$

2.3 Stress and Equilibrium

The basic constitutive hypothesis of elastic membrane theory assumes the existence of a strain energy $W(\boldsymbol{F})$ per unit area of reference configuration Ω (e.g. Cohen and Wang, 1984). The membrane is considered here to be uniform, in the sense that W does not explicitly depend on $\boldsymbol{x}$. Then, the total potential energy attributed to a deformation $\boldsymbol{x} \rightarrow \boldsymbol{r}(\boldsymbol{x})$ is

$$E[\boldsymbol{r}] = \iint_{\Omega} W(\boldsymbol{F})dA - P[\boldsymbol{r}], \tag{2.10}$$

where $dA = dx_1 dx_2$, and $P[\boldsymbol{r}]$ is a load potential associated with the particular type of conservative loading under consideration (e.g. certain kinds of pressure loading or dead loading). In the absence of any loading, the total potential energy of the deformation reduces to the strain energy

$$E[\boldsymbol{r}] = \iint_{\Omega} W(\boldsymbol{F})dA. \tag{2.11}$$

If the values of the function $W(\cdot)$ are required to be unaffected by superposed rotations, then there must be a function $\hat{W}(\cdot)$ of the Cauchy-Green strain such that $W(\boldsymbol{F}) = \hat{W}(\boldsymbol{C})$. The local response of the membrane thus depends only on the intrinsic or metric geometry of the surface, and not on the extrinsic or imbedding geometry. This is in accordance with the conventional notion of an ideal membrane. It is assumed that $\hat{W}(\cdot)$ is a C^2 function and that

$$\hat{W}(\boldsymbol{C}) \geq 0, \quad \hat{W}(\Delta) = 0. \tag{2.12}$$

A complete theory of material symmetry for membranes has been developed by Cohen and Wang (1984). Briefly, the symmetry group $\mathcal{G}$ of the membrane consists of

those tensors $\boldsymbol{P} = P_{\alpha\beta}\, \boldsymbol{e}_\alpha \otimes \boldsymbol{e}_\beta$ that satisfy $\hat{W}(\boldsymbol{C}) = \hat{W}(\boldsymbol{P}^{\mathrm{T}}\boldsymbol{C}\boldsymbol{P})$, for all $\boldsymbol{C}$ in the domain of $\hat{W}(\cdot)$. Attention is restricted here to isotropic solids, defined by

$$\mathcal{G} = \{\boldsymbol{P}: \quad \boldsymbol{P}^{\mathrm{T}}\boldsymbol{P} = \Delta\}. \tag{2.13}$$

For these, the strain energy depends on $\boldsymbol{C}$ only through its symmetric invariants

$$tr\boldsymbol{C} = \lambda^2 + \mu^2, \quad det\boldsymbol{C} = \lambda^2\mu^2, \tag{2.14}$$

and these in turn yield λ^2 and μ^2 as the roots of the quadratic equation

$$x^2 - (tr\boldsymbol{C})x + det\boldsymbol{C} = 0. \tag{2.15}$$

Thus, the relation between the invariants and the principal stretches is globally invertible. The strain energy may therefore be expressed as a symmetric function of λ and μ,

$$W(\boldsymbol{C}) = w(\lambda,\mu) = w(\mu,\lambda), \tag{2.16}$$

subject to the restrictions imposed by (2.12), namely $w(\lambda,\mu) \geq 0$ and $w(1,1) = 0$. For example, for neo-Hookean membranes the strain energy has the form

$$w(\lambda,\mu) = \frac{1}{2}G(\lambda^2 + \mu^2 + \lambda^{-2}\mu^{-2} - 3), \tag{2.17}$$

where G is a positive constant with dimensions of force/length (see § 4.1).

Stress-like variables $S_{\alpha\beta}$ may be defined as

$$S_{\alpha\beta} = \partial\hat{W} / \partial C_{\alpha\beta} + \partial\hat{W} / \partial C_{\beta\alpha}, \tag{2.18}$$

without restriction to strain energies of the form (2.16). These induce a tensor $\boldsymbol{S} = S_{\alpha\beta}\boldsymbol{e}_\alpha \otimes \boldsymbol{e}_\beta$ that is work-conjugate to $\boldsymbol{C}$ in the sense that

$$d\hat{W} = \tfrac{1}{2}\boldsymbol{S}:d\boldsymbol{C}, \tag{2.19}$$

where $d\hat{W}$ is the first-order change of strain energy due to an increment $d\boldsymbol{C}$ of strain. Here the notation $\boldsymbol{A}:\boldsymbol{B}$ is used to denote the scalar product $tr(\boldsymbol{A}^{\mathrm{T}}\boldsymbol{B})$. Thus $\boldsymbol{S}$ is the membrane-analogue of the second Piola-Kirchhoff stress of conventional elasticity.

For isotropic membranes, (2.16) yields $d\hat{W} = w_\lambda d\lambda + w_\mu d\mu$, where $d\lambda$ and $d\mu$ are the incremental stretches. The orthonormality of the eigenvectors $\{\boldsymbol{L}, \boldsymbol{M}\}$ of $\boldsymbol{C}$ may be used to show that

$$\lambda d\lambda = \tfrac{1}{2}(\boldsymbol{L}\otimes\boldsymbol{L}):d\boldsymbol{C} \quad \text{and} \quad \mu d\mu = \tfrac{1}{2}(\boldsymbol{M}\otimes\boldsymbol{M}):d\boldsymbol{C}. \tag{2.20}$$

Then for the two expressions for $d\hat{W}$ to agree for all $d\boldsymbol{C}$, it is necessary and sufficient that

$$\boldsymbol{S} = \lambda^{-1}w_\lambda \boldsymbol{L}\otimes\boldsymbol{L} + \mu^{-1}w_\mu \boldsymbol{M}\otimes\boldsymbol{M}. \tag{2.21}$$

This is the stress-strain relation for isotropic membranes.

As in conventional elasticity, a Piola stress $\boldsymbol{T}$ measuring forces in the membrane per unit length of arc in the reference surface, is defined by

$$\boldsymbol{T} = \boldsymbol{F}\boldsymbol{S}. \tag{2.22}$$

This may be represented in the form $\boldsymbol{T} = T_{i\alpha}\boldsymbol{e}_i\otimes\boldsymbol{e}_\alpha$, where $T_{i\alpha} = F_{i\beta}S_{\beta\alpha}$. From (2.2) and (2.18) it is then easily shown that

$$T_{i\alpha} = \partial W/\partial F_{i\alpha}. \tag{2.23}$$

For isotropic materials, (2.6), (2.21) and (2.22) combine to yield

$$\boldsymbol{T} = w_\lambda \boldsymbol{l}\otimes\boldsymbol{L} + w_\mu \boldsymbol{m}\otimes\boldsymbol{M}, \tag{2.24}$$

with component form

$$T_{i\alpha} = w_\lambda l_i L_\alpha + w_\mu m_i M_\alpha. \tag{2.25}$$

Consider the equilibrium of the membrane occupying the region Ω of the (x_1, x_2)-plane. The membrane is loaded by a pressure $p\boldsymbol{n}$ per unit of deformed area, body forces being neglected. The exterior unit normal $\boldsymbol{n}$ to the deformed surface at $\boldsymbol{r}$, may be expressed in terms of the unit tangent vectors $\boldsymbol{l}$ and $\boldsymbol{m}$ as

$$\boldsymbol{n} = \boldsymbol{l} \times \boldsymbol{m}. \tag{2.26}$$

Let $\boldsymbol{x}(s)$ be an arc length parametrization of a closed curve in Ω, enclosing an arbitrary region D. Let $\nu(s)$ be the unit normal to the arc, defined by $\nu = \boldsymbol{x}'(s) \times \boldsymbol{e}_3$. Then, the force transmitted across an element ds of the arc is $\boldsymbol{t}ds$, where $\boldsymbol{t} = \boldsymbol{T}\nu$ is the traction vector.

In the presence of pressure loading, the equilibrium of the arbitrary part $D \subset \Omega$ of the surface requires that

$$\oint_{\partial D} \boldsymbol{T}\nu ds + \iint_D p\boldsymbol{J}\boldsymbol{n} dA = \boldsymbol{0}. \tag{2.27}$$

The contour integral in (2.27) is transformed to an area integral by using Green's theorem. The theorem states that

$$\iint_D \phi_{,\alpha} dA = e_{\alpha\beta} \oint_{\partial D} \phi dx_\beta, \tag{2.28}$$

where $\phi(\boldsymbol{x})$ is any piecewise differentiable field in the plane, $e_{\alpha\beta}$ is the unit alternator ($e_{12} = -e_{21} = 1$, $e_{11} = e_{22} = 0$), and ∂D is the piecewise smooth boundary of D. Since $\boldsymbol{x}(s)$ is the parametric equation of ∂D, it follows that $e_{\alpha\beta} dx_\beta = \nu_\alpha ds$, where ν_α are the components of the unit normal ν. Substituting (2.28) with $\phi = T_{i\alpha}$ in (2.27) and then summing on α from 1 to 2, yields the global form of the equilibrium equation of region D, for any type of pressure loading:

$$\iint_D Div\boldsymbol{T}dA + \iint_D pJ\boldsymbol{n}dA = \boldsymbol{0}, \quad \forall D \subset \Omega. \tag{2.29}$$

Then, by the localization theorem, the local (pointwise) equilibrium equation is

$$Div\boldsymbol{T} + pJ\boldsymbol{n} = \boldsymbol{0}, \tag{2.30}$$

or in component form

$$T_{i\alpha,\alpha} + pJn_i = 0. \tag{2.31}$$

Using (2.24), equation (2.30) can be written in the form

$$[\nabla \cdot (w_\lambda \boldsymbol{L})]\boldsymbol{l} + w_\lambda (\boldsymbol{L} \cdot \nabla)\boldsymbol{l} + [\nabla \cdot (w_\mu \boldsymbol{M})]\boldsymbol{m} + w_\mu (\boldsymbol{M} \cdot \nabla)\boldsymbol{m} + pJ\boldsymbol{n} = \boldsymbol{0}, \tag{2.32}$$

where $\nabla = \boldsymbol{e}_\alpha (\cdot)_{,\alpha}$ is the two-dimensional gradient operator with respect to position $\boldsymbol{x} \in \Omega$.

Equations (2.30) - (2.32) represent the Euler-Lagrange equations for the total potential energy given by equation (2.10). The load potential $P[\boldsymbol{r}]$ in (2.10) is a potential associated with the particular type of conservative pressure loading under consideration. For example, if the pressure intensity p is spatially uniform and independent of deformation, and if the boundary $\partial\Omega$ is fixed, then the load potential has the form (Steigmann, 1992):

$$P[\boldsymbol{r}] = \frac{p}{6} \iint_\Omega e_{\alpha\beta} \boldsymbol{r} \cdot \boldsymbol{r}_{,\alpha} \times \boldsymbol{r}_{,\beta} \, dA. \tag{2.33}$$

This is the type of pressure loading considered in the present work.

If a concentrated force $\tilde{\mathcal{F}}$ is applied as a dead load at the point $\tilde{\boldsymbol{x}} \in \Omega$, then the load potential $P[\boldsymbol{r}]$ in (2.10) is

$$P[\boldsymbol{r}] = \tilde{\mathcal{F}} \cdot \tilde{\boldsymbol{r}}. \tag{2.34}$$

Here $\tilde{\boldsymbol{r}}$ is the corresponding $\boldsymbol{r}$ at the point $\tilde{\boldsymbol{x}} \in \Omega$ where the force is applied. For a vertical force $\tilde{\mathcal{F}} = \tilde{\mathcal{F}}\boldsymbol{e}_3$ for example, the load potential becomes $P[\boldsymbol{r}] = \tilde{\mathcal{F}}\,\tilde{r}_3$. The equilibrium equation of an arbitrary part D of Ω containing the application point $\tilde{\boldsymbol{x}}$ of the force is

$$\oint_{\partial D} \boldsymbol{T}\boldsymbol{\nu} ds + \tilde{\mathcal{F}} = 0, \qquad \tilde{\boldsymbol{x}} \in D. \tag{2.35}$$

For the case of zero pressure and in the absence of point loads, the local (pointwise) equilibrium equations are

$$Div\boldsymbol{T} = \boldsymbol{0}; \quad T_{i\alpha,\alpha} = 0 \text{ in } \Omega, \tag{2.36}$$

and can be identified with the Euler-Lagrange equations for the strain energy given by (2.11). Equations (2.36) have to be supplemented by the corresponding boundary conditions. For example, for the mixed displacement/zero-traction problem with $\boldsymbol{r}(\boldsymbol{x})$ assigned on part $\partial\Omega_{\boldsymbol{r}}$ of the boundary, the natural boundary condition is

$$\boldsymbol{T}\boldsymbol{\nu} = \boldsymbol{0} \text{ on } \partial\Omega \backslash \partial\Omega_{\boldsymbol{r}}. \tag{2.37}$$

If the dynamics of the membrane is of interest, the global equation of motion of an arbitrary part D of Ω, in the presence of pressure loading and having a concentrated force $\tilde{\mathcal{F}}$ acting at the point $\tilde{\boldsymbol{x}} \in D$, can be obtained as:

$$\oint_{\partial D} \boldsymbol{T}\boldsymbol{\nu} ds + \iint_{D} p J \boldsymbol{n} dA + \tilde{\mathcal{F}} = \iint_{D} \rho_0 \ddot{\boldsymbol{r}} dA, \quad \tilde{\boldsymbol{x}} \in D, \tag{2.38}$$

where ρ_0 is the mass density per unit initial area, and $\ddot{\boldsymbol{r}}$ is the acceleration.

2.4 Relaxed Strain Energy Density

In order for the Euler-Lagrange equations (2.30) or (2.36) to deliver stable equilibria, there are certain necessary conditions to be satisfied by the strain energy density $w(\lambda, \mu)$.

According to the energy criterion of elastic stability (Knops and Wilkes, 1973), a stable deformation $\boldsymbol{r}$ minimizes the functional $E[\,\cdot\,]$ (representing the potential energy of deformation given by equation (2.11)), in some specified class of functions. In particular, it is assumed that $\boldsymbol{r}$ is a strong relative minimizer (Morrey, 1966), i.e.

$$E[\boldsymbol{r}] \leq E[\boldsymbol{r} + \Delta\boldsymbol{r}], \tag{2.39}$$

for all continuous $\Delta\boldsymbol{r}(x_\alpha)$ vanishing on $\partial\Omega_r$, such that $|\Delta\boldsymbol{r}(x_\alpha)| < \delta$ for some $\delta>0$, and for every $(x_\alpha) \in \Omega$.

Further, Graves theorem (Graves, 1939) states that a deformation $\boldsymbol{r}(x_\alpha)$ is a strong relative minimizer of the energy $E[\,\cdot\,]$, only if its gradient $\boldsymbol{F}(x_\alpha)$ is a point of rank-one convexity of $W(\,\cdot\,)$ at every point $(x_\alpha) \in \Omega$, i.e.

$$W(\boldsymbol{F} + \boldsymbol{a} \otimes \boldsymbol{b}) - W(\boldsymbol{F}) - \boldsymbol{a} \cdot \boldsymbol{T}(\boldsymbol{F})\boldsymbol{b} \geq 0, \tag{2.40}$$

for all $\boldsymbol{a} = a_\alpha \boldsymbol{e}_\alpha + a_3 \boldsymbol{e}_3$, $\boldsymbol{b} = b_\alpha \boldsymbol{e}_\alpha$. Graves proved (2.40) for functionals of the form (2.11), but the result is easily shown to be valid for problems of dead loading, uniform pressure of fixed intensity as well as other types of conservative pressure loading (Steigmann, 1991).

In the case of isotropic membranes, the inequality (2.40) is equivalent to

$$w(\lambda^*, \mu^*) - w(\lambda, \mu) - w_\lambda (\boldsymbol{a} \cdot \boldsymbol{l})(\boldsymbol{b} \cdot \boldsymbol{L}) - w_\mu (\boldsymbol{a} \cdot \boldsymbol{m})(\boldsymbol{b} \cdot \boldsymbol{M}) \geq 0, \tag{2.41}$$

where λ and μ are the principal stretches furnished by $\boldsymbol{F}$, w_λ and w_μ are the associated values of the principal stresses, and λ^* and μ^* are the principal stretches delivered by the perturbed deformation gradient $\boldsymbol{F}^* = \boldsymbol{F} + \boldsymbol{a} \otimes \boldsymbol{b}$.

Inequality (2.41) implies that w_λ and w_μ are non-negative. This can be shown by setting $\boldsymbol{a} = a\boldsymbol{n}$ and $\boldsymbol{b} = \boldsymbol{L}$. Then, $\boldsymbol{F}^* = (\lambda \boldsymbol{l} + a\boldsymbol{n}) \otimes \boldsymbol{L} + \mu \boldsymbol{m} \otimes \boldsymbol{M}$, and it follows that $\lambda^* = (\lambda^2 + a^2)^{1/2}$, $\mu^* = \mu$. Consequently, (2.40) reduces to

$$w[(\lambda^2 + a^2)^{1/2}, \mu] - w(\lambda, \mu) \geq 0, \tag{2.42}$$

for all a. The choice $\boldsymbol{b} = \boldsymbol{M}$ leads similarly to

$$w[\lambda, (\mu^2 + a^2)^{1/2}] - w(\lambda, \mu) \geq 0, \tag{2.43}$$

for all a. Inequalities (2.42) and (2.43) imply that

$$\begin{aligned} w_\lambda &\geq 0, \\ w_\mu &\geq 0. \end{aligned} \tag{2.44}$$

Thus, the deformation $\boldsymbol{r}(x_\alpha)$ minimizes $E[\cdot]$ only if the associated principal stresses w_λ and w_μ are non-negative at every $(x_\alpha) \in \Omega$.

The following constitutive hypotheses on the behaviour of the function $w(\lambda, \mu)$ are adopted: It is assumed that $\mu = v(\lambda)$ is the unique solution of $w_\mu(\lambda, \cdot) = 0$, and that $w_\mu(\lambda, \cdot)$ is greater (respectively less) than zero when μ is greater (respectively less) than $v(\lambda)$. Further, it is assumed that $w_\lambda(\lambda, v(\lambda))$ is greater (respectively less) than zero when λ is greater (respectively less) than unity. In the terminology of Pipkin (1986a), $v(\lambda)$ is the *natural width in simple tension*. For isotropic, incompressible materials the natural width is $v(\lambda) = \lambda^{-1/2}$.

These assumptions imply that the function $w(\lambda, \cdot)$ attains its global minimum at the natural width:

$$\hat{w}(\lambda) = w(\lambda, v(\lambda)). \tag{2.45}$$

The partial derivative of $w(\lambda, \mu)$ with respect to λ, at the natural width is

$$w_\lambda = \hat{w}'(\lambda) - v'(\lambda) w_\mu, \tag{2.46}$$

and since $w_\mu = 0$, it follows that

$$w_\lambda = \hat{w}'(\lambda). \tag{2.47}$$

This is the uniaxial force-stretch relation.

Restrictions (2.44) and the adopted constitutive hypotheses require that

$$\begin{aligned} &\mu \geq v(\lambda) = \lambda^{-1/2}; \\ &\lambda \geq v(\mu) = \mu^{-1/2}, \end{aligned} \tag{2.48}$$

at every energy minimizing deformation. However, a solution of an equilibrium problem consisting of the Euler-Lagrange equations and assigned boundary conditions, will generally deliver principal stretches that violate at least one of the inequalities (2.48), on some parts of the domain Ω. Such deformations are necessarily unstable. Thus, the foregoing restrictions on λ and μ generally imply non-existence of energy minimizers. The explanation for this is that the equilibrium equations and the Gauss and Mainardi-Codazzi compatibility conditions together constitute six restrictions on six functions, namely the three components of the strain $\boldsymbol{C}$ and the three components of the second fundamental form on the deformed surface (e.g. the two principal curvatures and the angle defining the principal axes). Further restrictions such as (2.48) lead to an over-determined system, unless such restrictions happen to be satisfied automatically. This generally limits the class of problems that can be solved.

An alternative approach is considered here, consisting in the modification of membrane theory such as to account for the occurrence of a continuous distribution of

wrinkles. Such a theory was originally proposed by Wagner (1929) and subsequently developed by a number of investigators (e.g. Reissner, 1938, Kondo et al., 1955, Mansfield, 1970, Wu, 1978, Pipkin, 1986a, Steigmann, 1990). Pipkin (1986a) showed that such a theory emerges naturally from minimum-energy considerations.

The present model of the membrane is retained, but the original strain energy is replaced by a ***relaxed*** strain energy, $W_R(\boldsymbol{F})$, introduced by Pipkin (1986a). (The usage of this term in the present context will differ slightly from the original one.) In this way, the effects of wrinkling are incorporated into the conventional membrane theory.

The relaxed energy can be obtained from the original strain energy by constructing a sequence of finely wrinkled configurations, with closely spaced discontinuities in the deformation gradient. The limit of the sequence is a smooth deformation that is achieved without compressive stress and at no expense in strain energy (Pipkin, 1986a).

To illustrate this idea, consider a unit square of isotropic membrane deformed into a rectangle of dimensions $\lambda > 1$ and $\mu = v(\lambda) \equiv \lambda^{-1/2}$. According to the constitutive hypotheses introduced earlier, the associated stresses are $w_\lambda > 0$ and $w_\mu = 0$. Thus, the membrane is in a state of uniaxial tension. To make μ smaller than $v(\lambda)$, a compressive stress $w_\mu < 0$ would be required, violating the stability conditions (2.44). However, the following construction shows a way of reducing μ without compressive stress, and without expenditure of energy. Let the unit square be partitioned into n strips parallel to the tensile axis, each of width $1/n$. By folding the stretched membrane along the boundaries of the strips, a corrugated surface is obtained. A fold angle of $\theta \in [0, \pi/2)$ is used in alternating strips and $-\theta$ in the remaining strips. Then, taking the x_1-axis along the tensile axis, the deformation gradient is obtained as

$$\begin{aligned} &\boldsymbol{F}_n(\boldsymbol{x}) = \lambda \boldsymbol{e}_1 \otimes \boldsymbol{e}_1 + v(\lambda)\boldsymbol{m}_n \otimes \boldsymbol{e}_2; \\ &\boldsymbol{m}_n = \cos\theta \boldsymbol{e}_2 + S(x_2)\sin\theta \boldsymbol{e}_3, \end{aligned} \tag{2.49}$$

where $S(\cdot)$ is a square wave function, equal to ± 1 for x_2 belonging to a strip folded at angle $\pm\theta$. This construction induces no change in the stretches. Since the strain

energy in membrane theory is presumed to depend only on the stretches, it follows that

$$W(\boldsymbol{F}_n) = w(\lambda, v(\lambda)) \equiv \hat{w}(\lambda); \qquad n = 1,2,..... \tag{2.50}$$

To find the deformation $\boldsymbol{r}_n(\boldsymbol{x})$, (2.47) is integrated leading to

$$\boldsymbol{r}_n(\boldsymbol{x}) = \lambda x_1 \boldsymbol{e}_1 + v(\lambda) x_2 \cos\theta \boldsymbol{e}_2 + \left\{ \int_0^{x_2} S(x)dx \right\} v(\lambda) \sin\theta \boldsymbol{e}_3. \tag{2.51}$$

The integral in the last term is $O(1/n)$ for all x_2, so the sequence $\{\boldsymbol{r}_n\}$ converges uniformly to $\boldsymbol{r}(\boldsymbol{x}) = \boldsymbol{F}\boldsymbol{x}$, where

$$\boldsymbol{F} = \lambda \boldsymbol{e}_1 \otimes \boldsymbol{e}_1 + \mu \boldsymbol{e}_2 \otimes \boldsymbol{e}_2; \qquad \mu = v(\lambda)\cos\theta. \tag{2.52}$$

Thus, the limit of the sequence of wrinkled states is a smooth continuously wrinkled deformation whose gradient yields a transverse stretch $\mu \le v(\lambda)$. Moreover, μ can take any value in the interval $\mu \in (0, v(\lambda)]$ by an appropriate selection of $\theta \in [0, \pi/2)$. In view of (2.50), the strain energy associated with the limiting deformation is $\hat{w}(\lambda)$, independent of μ, and represents the global minimum of the function $w(\lambda, \cdot)$.

Similarly, smooth deformations with stretches $\mu > 1$ and $\lambda \in (0, v(\mu)]$ may be obtained by allowing fine scale wrinkling with folds parallel to the x_2-axis. The associated strain energy is $\hat{w}(\mu)$. Deformations with $\lambda \le 1$ and $\mu \le 1$ can be achieved by double wrinkling (Pipkin, 1986b), with no stress at all. These correspond to slack states of the membrane. The associated stain energy is $w(1, 1)$, which is taken to be zero.

Thus, the issue of non-existence of energy minimizers is addressed by allowing for the presence of continuously distributed wrinkles. The associated deformations deliver principal stretches that violate (2.48) but nevertheless satisfy the requirement (2.44).

The minimum energy principle may be reformulated so as to account for fine scale

wrinkling directly. This is achieved by replacing the original strain energy $w(\lambda,\mu)$ by the relaxed strain energy $w_R(\lambda,\mu)$, defined by

$$W_R(\boldsymbol{F}) = w_R(\lambda,\mu) \equiv \begin{cases} w(\lambda,\mu); & \lambda > v(\mu), \quad \mu > v(\lambda), \\ \hat{w}(\lambda); & \lambda > 1, \quad \mu \le v(\lambda), \\ \hat{w}(\mu); & \mu > 1, \quad \lambda \le v(\mu), \\ 0; & \lambda \le 1, \quad \mu \le 1. \end{cases} \tag{2.53}$$

The constitutive hypotheses imply that the principal stresses furnished by the relaxed strain energy automatically satisfy the necessary conditions (2.44) for all $(\lambda,\mu) \ge 0$. The inequality constraints in (2.48) are no longer required.

For deformations with $\lambda > 1$ and $\mu \le v(\lambda)$, $w_\mu = 0$ and $w_\lambda = \hat{w}'(\lambda)$ is a function of λ alone. The associated state of stress is given by

$$\boldsymbol{T} = w_\lambda \boldsymbol{l} \otimes \boldsymbol{L}, \tag{2.54}$$

and is called a *tension field.* The unit vectors $\boldsymbol{L}$ and $\boldsymbol{l}$ are tangential to the tension trajectories.

By employing the relaxed strain energy in the Euler-Lagrange equations, tension field theory is automatically incorporated into ordinary membrane theory, extending the range of applicability of the membrane as a physical model.

Chapter 3

Numerical Method

3.1 General Considerations

A wide variety of numerical solution methods are available for nonlinear static analysis of tensile structures (Barnes, 1980, Jenkins and Leonard, 1991). A review by Barnes (1980) gives the following classification: iterative matrix methods, incremental methods and direct vector methods, also termed minimization and relaxation methods.

Standard stiffness-based iterative methods such as Newton-Raphson and modified Newton-Raphson have been widely applied to static analysis and form-finding of tension structures (Mollman and Mortensen, 1966, Poskitt, 1967, Haug and Powell, 1971, Haug, 1972, Argyris, Angelopoulos and Bichat, 1974, Felippa, 1974, Stricklin and Haisler, 1977 and many other researchers). However, when wrinkling is indicated, the equilibrium equations (2.32) are not strongly elliptic (Steigmann, 1990), and the element stiffness becomes ill-conditioned. For this class of problems, such methods lead to ill-conditioned systems of equations and the iterations may not converge. Modifications of such methods, designed to account for the abrupt stiffness changes that occur at the transition from tense states to wrinkled or slack states, have been developed by Miller and Hedgepeth (1982), Miller et al. (1985), Magara, Okamura and

Kawaguchi (1984), Nishimura, Tosaka and Honma (1986), Roddeman et al. (1987), Contri and Schrefler (1988), Roddeman (1991) and Jeong and Kwak (1992). These modifications typically involve iterative algorithms that eliminate compressive stress in each stage of an incremental loading procedure.

From the incremental methods, the self-correcting Euler method (Barnes, 1980) has been more often employed for the analysis of membrane structures (Greenberg, 1970, Jensen, 1971, Bergan and Soreide, 1973, Jonatowski, 1974). This is a combination of the Euler and Newton-Raphson methods, and suffers from the same difficulties as the previous method, when applied to partially wrinkled membranes.

An explicit vector method widely and very successfully applied to nonlinear static analysis and form-finding of tensile structures, as well as to the solution of nonlinear equilibrium problems of structural mechanics in general, is the Dynamic Relaxation Method. This technique does not require the construction and inversion of the stiffness matrix, thus avoiding the convergence problems that Newton-Raphson or similar iterative methods experience when modeling loss of ellipticity. Therefore, the method is particularly well suited to the class of problems considered here. Other vector methods, such as the conjugate gradient method or the fixed point method, require the inversion of the stiffness matrix and consequently are less appropriate for the analysis of partially wrinkled membrane structures.

3.2 Dynamic Relaxation

3.2.1 Introduction

Dynamic Relaxation (DR) is an explicit iterative method developed for the static analysis of structural mechanics problems. This numerical technique is based on the

fact that the static solution represents the steady state part of the transient response of the structure.

As a solution strategy for static problems, DR involves converting first the equilibrium equation into an equation of a damped motion, by artificially adding an acceleration term as well as a viscous damping term, and then integrating explicitly in time from the initial conditions until the transient dynamic response has damped out to the static solution, with equilibrium satisfied.

Due to its explicit nature, the method is highly suitable for computations, since all quantities may be treated as vectors, eliminating the need for matrix manipulations of any kind. Therefore, the method is easily programmable and has low storage requirements. Its explicit form makes it also ideal for the case of large deformations and finite strains, the method being especially attractive for problems with highly nonlinear geometric and material behavior, which include limit points or regions of very soft stiffness characteristics (Underwood, 1993).

Since DR solutions are large-time limits of time-dependent motions, equilibrium solutions obtained by DR may be regarded as asymptotically dynamically stable, as they do not spontaneously decay to other configurations (Silling, 1988a).

Moreover, the simplicity, versatility, tenacity and reliability of the method make it an attractive alternative for the solution of nonlinear structural mechanics problems.

3.2.2 History

The DR method originates from the *second-order Richardson method* developed by Frankel (1950). Richardson (1911, 1925) used central difference approximations for partial derivatives to obtain numerical solutions to PDEs describing a variety of boundary value problems by an iterative process, the technique being termed "the Richardson method" (Shortley, Weller and Fried, 1942). Frankel (1950) states that the

formal equivalence of the Richardson algorithm to first order time dependent equations suggests the extension to a solution algorithm equivalent to a second order time dependent equation. Thus Frankel first made the connection with dynamics. The second-order Richardson algorithm is also known as "Frankel's method", as it was referred to by Rutishauser (Engeli et al., 1959, Cassel, 1970). Hansen (1956) developed independently a similar algorithm for tidal computations. After analyzing this algorithm (Otter and Day, 1960), Day suggested in 1961 to Otter the idea of applying it to obtain static solutions of elastic continuum problems by introducing a viscous damping term (Otter, 1965). Day named the method ***Dynamic Relaxation*** and later described it in a paper (Day, 1965) containing applications to the static analysis of a portal frame, a flat plate and a thick cylinder. However, Otter was the first to develop and apply the method (with near critical damping) in the context of stress and displacement analysis in prestressed concrete reactor pressure vessels (Otter, 1965). A description of the technique identifying the second order Richardson method developed by Frankel as the basis for DR, is given by Otter, Cassel and Hobbs (1966), together with a comparison with other iterative methods and some applications to the analysis of elastic structures. Another early paper that compares DR with other iterative methods is due to Wood (1967). The use of fictitious mass densities was suggested by Welsh (1967), leading to a substantial improvement of DR. This idea was first employed by Cassel, Kinsey and Sefton (1968) for the analysis of a cylindrical shell. Later Cassel (1970) analyzed the relation between fictitious densities and the numerical stability of DR. The use of finite elements for the spatial discretization in DR was first approached by Lynch, Kelsey and Saxe (1968), in the context of plane stress analysis. They also employed fictitious mass densities and mass proportional damping to optimize the iteration process. Rushton (1968a) made the first application of DR to a nonlinear problem.

Since 1970 the DR literature has expanded considerably. More complex problems concerned with a large variety of structural configurations have been analyzed using

DR. Geometrical and material nonlinearities have been successfully incorporated in the procedure. The technique has been successfully used for form-finding as well as nonlinear static analysis of lightweight tensile structures, such as cable networks and membranes (Barnes, 1974, 1975, 1976, 1984, 1986, Lewis et al., 1984, Wakefield, 1986, Barnes and Wakefield, 1988, Moncrieff and Topping, 1990, Lewis and Gosling, 1993). Cundall (1976) suggested an effective damping procedure, termed "kinetic damping", which has been frequently applied in the context of form-finding and static analysis of cable nets and membranes (Wakefield, 1986, Barnes and Wakefield, 1988, Lewis, 1989, Lewis and Shan, 1990, and others). Solutions of plate and shell problems - especially the large deflection case - have also been successfully obtained with DR (Alwar and Ramachandra Rao, 1974, Frieze, Hobbs and Dowling, 1978, Pica and Hinton, 1980, Lim and Turvey, 1985, Al-Shawi and Mardirosian, 1987, Zhang and Yu, 1989, Turvey and Salehi, 1990, Salehi and Turvey, 1991, Turvey and Osman, 1993, Kant and Kommineni, 1993, Ramesh and Krishnamoorthy, 1993). As well, a variety of other problems have been solved using DR, such as large deformation inelastic response of solids (Key, Stone and Krieg, 1981), tensegrity systems analysis (Motro, 1984, Motro, Najari and Jouanna, 1986), incompressibility in large deformations (Silling, 1987), phase changes and localization in elasticity (Silling, 1988a,b, 1989), elasto-plastic response (Caridis and Frieze, 1988, 1989, Zhang and Yu, 1989, Zhang, Yu and Wang, 1989, Turvey and Der Avanessian, 1989), and nonlinear viscoelastic response (French and Jensen, 1991). Contributions to a better understanding and improvement of the DR method were made by many authors: Wood (1971), Brew and Brotton (1971), Bunce (1972), Cassel and Hobbs (1976), Cundall (1976), Papadrakakis (1981, 1986), Underwood (1983), Tarakanow (1984), Zienkiewicz and Löhner (1985), Silling (1985), Zhang and Yu (1989), Lewis (1989), and Sauve and Metzger (1992). Of special importance is the work by Underwood (1983), which presents a detailed review on the subject of DR, as well as an adaptive DR algorithm for nonlinear problems. Also, the papers by Papadrakakis (1981) and Silling (1985) should be

mentioned. The former presents a method for the automatic evaluation of the DR iteration parameters, whereas the latter introduces – in the context of DR analysis in finite elastostatics – a versatile spatial discretization method based on Green's theorem that avoids the inconvenience of mapping techniques.

3.2.3 Second- Order Richardson Method

DR is based on the *second-order Richardson algorithm* (Frankel, 1950). This is an explicit iterative technique for the solution $\tilde{\phi}(x,y)$ of boundary-value problems described by PDEs approximated as difference equations in the form

$$\mathcal{L}\tilde{\phi} = 0, \tag{3.1}$$

where $\mathcal{L}$ is a finite difference operator.

Frankel (1950) introduced artificial second order time dependency of ϕ, transforming equation (3.1) into

$$\frac{\partial^2 \phi}{\partial t^2} + \mathcal{B}\frac{\partial \phi}{\partial t} - \mathcal{L}\phi = 0. \tag{3.2}$$

By using central difference approximations for the temporal derivatives, an iteration process is carried out in time until the long-term solution ϕ of equation (3.2) is obtained. This solution eventually satisfies equation (3.1) too, i.e. $\phi \equiv \tilde{\phi}$.

This method proved to be very successful in solving structural mechanics problems (Otter, 1965, Day, 1965) and it is in this context that it evolved to the method known as DR.

3.2.4 Transient Response and DR

The discretized equilibrium equation of a structure may be represented in the general form:

$$\mathcal{F} + \mathcal{P}(\tilde{u}) = \mathbf{0}, \tag{3.3}$$

where $\mathcal{F}$ is the vector of external forces (body forces, point loads, forces due to distributed loads such as pressure acting on a membrane, and forces prescribed on the boundary), $\tilde{u}$ is the displacement vector ($\tilde{r} = x + \tilde{u}$) and $\mathcal{P}(\tilde{u})$ is the vector of internal forces.

Equation (3.3) may be obtained by a finite difference or a finite element discretization technique, applied to the equilibrium equations governing the structural behaviour.

For a membrane structure, a spatial discretization of the global equilibrium equation (2.29) or (2.35) would lead to an equation of the form (3.3). In this case, the problem is highly nonlinear, due to the geometric and material behavior and a tangent stiffness matrix ${}^{t}K(\tilde{u})$ may be obtained from

$${}^{t}K(\tilde{u}) = -\frac{\partial \mathcal{P}(\tilde{u})}{\partial \tilde{u}}. \tag{3.4}$$

As mentioned at § 3.1, when wrinkling is present the equilibrium equations of the membrane are not strongly elliptic (Steigmann, 1990), and the element stiffness derived from (3.4) becomes ill-conditioned. For this class of problems, standard stiffness-based iterative methods such as Newton-Raphson and modified Newton-Raphson lead to ill-conditioned systems of equations and the iterations may not converge. Therefore, one cannot employ this type of methods to obtain a solution $\tilde{u}$ to equation (3.3).

If a displacement vector u which is not an equilibrium solution (i.e. $u \neq \tilde{u}$) is introduced in equation (3.3), then $\mathcal{F} + \mathcal{P}(u) \neq \mathbf{0}$, and an oscillatory motion of the

structure will occur. However, if damping is present, the oscillations will decrease in time and the structure will eventually reach the equilibrium configuration $\tilde{\boldsymbol{r}} = \boldsymbol{x} + \tilde{\boldsymbol{u}}$ given by (3.3). Thus, by transforming the static problem to a damped dynamic problem, the static solution of (3.3) may be obtained as the steady-state part of the transient response of the structure, with no need to construct or invert stiffness matrices.

For a membrane, the transient response is described by the global equation of motion (2.38). A spatial discretization of this equation may be represented as a form of Newton's second law:

$$\mathcal{M}\,\ddot{\boldsymbol{u}}^n + \mathcal{D}\,\dot{\boldsymbol{u}}^n = \mathcal{F}^n + \mathcal{P}(\boldsymbol{u}^n), \tag{3.5}$$

where $\mathcal{M}$ is the mass matrix, $\mathcal{D}$ is the damping matrix, superscript n represents the label of the time increment (with $n = 0$ corresponding to $t = 0$, t being the time), and a superimposed dot indicates a temporal derivative (thus $\dot{\boldsymbol{u}} = \dot{\boldsymbol{r}}$ is the velocity vector and $\ddot{\boldsymbol{u}} = \ddot{\boldsymbol{r}}$ is the acceleration vector).

The DR algorithm (second order Richardson) developed by Frankel (1950) is obtained by employing central difference approximations for the temporal derivatives in equation (3.5) (Underwood, 1983):

$$\dot{\boldsymbol{u}}^{n-1/2} = (\boldsymbol{u}^n - \boldsymbol{u}^{n-1})/h, \tag{3.6}$$

$$\ddot{\boldsymbol{u}}^n = (\dot{\boldsymbol{u}}^{n+1/2} - \dot{\boldsymbol{u}}^{n-1/2})/h, \tag{3.7}$$

where h is the time increment. The expression for $\dot{\boldsymbol{u}}^n$ is given by the average value:

$$\dot{\boldsymbol{u}}^n = \tfrac{1}{2}(\dot{\boldsymbol{u}}^{n-1/2} + \dot{\boldsymbol{u}}^{n+1/2}). \tag{3.8}$$

Since only the steady-state part of the dynamic response is of interest, the mass matrix and damping matrix need not characterize the physical structure. However, $\mathcal{F}$ and

$\mathcal{P}\,\boldsymbol{u}$) must represent the physical problem. A diagonal mass matrix as well as mass proportional damping (Lynch, Kelsey and Saxe, 1968, Underwood, 1983) is an advantageous choice, resulting in decoupled scalar equations for each degree of freedom of the structure. Thus

$$\mathcal{D} = c\mathcal{M}, \tag{3.9}$$

where c is the damping coefficient. Substituting (3.6) - (3.9) into (3.5) gives the pair of equations needed to advance to the next velocity and displacement:

$$\begin{aligned} \dot{\boldsymbol{u}}^{n+1/2} &= \frac{(2-ch)}{(2+ch)}\dot{\boldsymbol{u}}^{n-1/2} + \frac{2h}{(2+ch)}\mathcal{M}^{-1}(\mathcal{F}^{n} + \mathcal{P}(\boldsymbol{u}^{n})), \\ \boldsymbol{u}^{n+1} &= \boldsymbol{u}^{n} + h\dot{\boldsymbol{u}}^{n+1/2}. \end{aligned} \tag{3.10}$$

The differencing method is explicit, since $\boldsymbol{u}^{n+1}$ depends only on quantities which are known from time step n. Denoting the sum of the forces as the residual $\mathcal{R}^{n}$

$$\mathcal{R}^{n} = \mathcal{F}^{n} + \mathcal{P}(\boldsymbol{u}^{n}), \tag{3.11}$$

the scalar equations corresponding to (3.10) are :

$$\begin{aligned} \dot{u}_i^{n+1/2} &= \frac{(2-ch)}{(2+ch)}\dot{u}_i^{n-1/2} + \frac{2h}{(2+ch)}(m_{ii})^{-1}\mathcal{R}_i^{n}, \\ u_i^{n+1} &= u_i^{n} + h\dot{u}_i^{n+1/2}, \qquad\qquad n = 1,\ldots\ldots,N, \end{aligned} \tag{3.12}$$

where N is the total number of degrees of freedom of the structure, and m_{ii} the i^{th} diagonal element of $\mathcal{M}$ (no sum on i). As already mentioned, equations (3.12a) are decoupled, since $\mathcal{M}$ is diagonal.

To start the DR algorithm, the initial conditions are usually of the form

$$\boldsymbol{u}^{0} \neq \boldsymbol{0}; \quad \dot{\boldsymbol{u}}^{0} = \boldsymbol{0}. \tag{3.13}$$

Equations (3.8) and (3.13b) give

$$\dot{\boldsymbol{u}}^{-1/2} = \dot{\boldsymbol{u}}^{1/2}, \tag{3.14}$$

and the velocity at time step 1/2 can be determined from (3.10a), where (3.11) is also substituted:

$$\dot{\boldsymbol{u}}^{1/2} = \frac{h}{2}\mathcal{M}^{-1}\,\mathcal{R}^{0}. \tag{3.15}$$

It can be observed that the damping coefficient c is not needed to start the algorithm. Hence, the central difference time integrator for mass proportional damping and diagonal mass matrix has the form (Underwood, 1983):

$$\begin{aligned}
&\dot{\boldsymbol{u}}^{1/2} = \frac{h}{2}\mathcal{M}^{-1}\,\mathcal{R}^{0}, && \text{for } n = 0,\\
&\dot{\boldsymbol{u}}^{n+1/2} = \frac{(2-ch)}{(2+ch)}\dot{\boldsymbol{u}}^{n-1/2} + \frac{2h}{(2+ch)}\mathcal{M}^{-1}\,\mathcal{R}^{n}, && \text{for } n \neq 0, \qquad (3.16)\\
&\boldsymbol{u}^{n+1} = \boldsymbol{u}^{n} + h\dot{\boldsymbol{u}}^{n+1/2}, && \text{for all } n.
\end{aligned}$$

The mass matrix $\mathcal{M}$, damping coefficient c and the time increment h needed in (3.16) are chosen such that the static solution $\mathcal{R} = \mathbf{0}$ is obtained in a minimum number of steps. However, the choice of h must ensure stability of the iterations.

3.2.5 DR Algorithm and Properties

Based on the central difference time integrator (3.16), the DR algorithm may be written in the form (Cassel, 1970, Bunce, 1972, Underwood, 1983):

(I) choose c, h, and $\mathcal{M}$; $\boldsymbol{u}^0$ given; $\dot{\boldsymbol{u}}^0 = \mathbf{0}$; $n = 0$,

(II) $\mathcal{R}^n = \mathcal{F}^n + \mathcal{P}(u^n)$,

(III) if $\mathcal{R}^n \cong \mathbf{0}$ stop, else continue,

(IV) for $n = 0$, $\dot{u}^{1/2} = \frac{h}{2}\mathcal{M}^{-1}\mathcal{R}^0$, (3.17)

for $n \neq 0$, $\dot{u}^{n+1/2} = \frac{(2-ch)}{(2+ch)}\dot{u}^{n-1/2} + \frac{2h}{(2+ch)}\mathcal{M}^{-1}\mathcal{R}^n$,

(V) $u^{n+1} = u^n + h\dot{u}^{n+1/2}$,

(VI) $n = n+1$; return to (II).

The transient response obtained with this algorithm does not represent the real behavior of the structure, due to the fictitious mass and damping characteristics. However, since $\mathcal{F}$ and $\mathcal{P}(u)$ correspond to the physical problem, the steady state part of the response, which satisfies the equilibrium equation (3.3), represents the static solution. A rapid convergence of the solution u obtained from (3.17f) to the static solution $\tilde{u}$ of the equilibrium equation (3.3) is desirable, and the stability of the solution u has also to be ensured. Therefore the choice of c, $\mathcal{M}$ and h must satisfy certain conditions.

The optimum convergence rate of the solution u to $\tilde{u}$ is of interest. For this purpose, the characterization of the mode-by-mode convergence rate in terms of the spectral radius of the iterative error equation may be used. Frankel (1950), Lynch, Kelsey and Saxe (1968), Cassel (1970), Key, Stone and Krieg (1981), Papadrakakis (1981) and Underwood (1983) present discussions on this topic.

For linear structural mechanics problems (Underwood, 1983), $\mathcal{P} = -\mathcal{K}u$, where $\mathcal{K}$ is the stiffness matrix, and the residual becomes

$$\mathcal{R} = \mathcal{F} - \mathcal{K}u. \tag{3.18}$$

Equations (3.17e, f), (3.6), (3.18) and the notation

$$\alpha = \frac{2h^2}{2+ch}, \qquad \beta = \frac{2-ch}{2+ch}, \tag{3.19}$$

give the displacement needed to advance to the next iteration

$$u^{n+1} = u^n + \beta(u^n - u^{n-1}) + \alpha(\mathcal{M}^{-1}\mathcal{F}^n - \mathcal{A}u^n), \tag{3.20}$$

where $\mathcal{A} = \mathcal{M}^{-1}\mathcal{K}$. The error e of the iteration at the n^{th} time step is defined as:

$$e^n = u^n - \tilde{u}. \tag{3.21}$$

Substituting (3.20) in (3.21) gives the error equation, showing the relationship between successive error vectors:

$$e^{n+1} = (1+\beta-\alpha\mathcal{A})e^n - \beta e^{n-1}. \tag{3.22}$$

A solution of (3.22) may be obtained by assuming the error vector to decay with each iterative step

$$e^{n+1} = \kappa e^n, \tag{3.23}$$

where $|\kappa| = \rho$ is the spectral radius (Strang, 1980). Obviously, convergence requires $|\kappa| < 1$. Denoting by $\mathcal{A}$ any eigenvalue of $\mathcal{A}$, and using (3.22) and (3.23) leads to a quadratic equation for κ:

$$\kappa^2 - (1+\beta-\alpha\mathcal{A})\kappa + \beta = 0. \tag{3.24}$$

Optimum convergence is obtained for $\hat{\kappa}$, which is the minimum κ that produces uniform convergence over the entire range of eigenvalues $\mathcal{A}_0 \le \mathcal{A} \le \mathcal{A}_{max}$. This condition is achieved for

$$(1+\beta-\alpha\mathcal{A}) = \pm 2\beta^{1/2}, \tag{3.25}$$

which gives

$$|\hat{\kappa}| = \hat{\rho} = \beta^{1/2}. \tag{3.26}$$

Since (3.25) holds for all possible eigenvalues of $\mathcal{A}$, the two equations that satisfy the condition for $\hat{\rho}$ are

$$1+\beta-\alpha\lambda_0 = 2\beta^{1/2}, \qquad 1+\beta-\alpha\lambda_{max} = -2\beta^{1/2}, \tag{3.27}$$

leading to

$$\hat{\rho} = \beta^{1/2} \approx \left|1-2\sqrt{\frac{\lambda_0}{\lambda_{max}}}\right|, \tag{3.28}$$

where $\lambda_0 << \lambda_{max}$ has been assumed. Deoting the fundamental and the highest circular frequencies of the undamped equation (3.5) by ω_0 and ω_{max} respectively, equation (3.28) becomes:

$$\hat{\rho} \approx \left|1-2\frac{\omega_0}{\omega_{max}}\right|. \tag{3.29}$$

Minimizing $\hat{\rho}$ produces more rapid convergence. This can be achieved by maximizing the ratio ω_0/ω_{max} through a judicious choice for $\mathcal{M}$, which is tantamount to scaling $\mathcal{A}$ to maximize the ratio λ_0/λ_{max}.

For optimum convergence, the values of the time increment h and damping coefficient c to be used in the DR algorithm (3.17) have to satisfy the condition (3.25). Equations (3.9), (3.27), (3.19) and the earlier assumption $\lambda_0 << \lambda_{max}$ lead to:

$$h \le \frac{2}{\sqrt{\lambda_{max}}} = \frac{2}{\omega_{max}}, \tag{3.30}$$

$$c \approx 2\sqrt{\lambda_0} = 2\omega_0. \tag{3.31}$$

Equation (3.30) derived from the optimum convergence condition represents the expression for the stability limit for the central difference time integrator (O'Brien, Hyman and Kaplan, 1951, Leech, 1965). This is the Courant–Friedrichs–Lewy condition (Courant, Friedrichs and Lewy, 1928), which states that h can be no larger then the time it takes for the information to travel between two adjacent nodes in the mesh. This condition has been exploited to develop the idea of *fictitious mass* (Welsh, 1967, Lynch, Kelsey and Saxe, 1968, Cassel, 1970, Key, Stone and Krieg, 1981 and many others), which minimizes $\hat{\rho}$, while retaining stability. Equation (3.31), derived from the optimum convergence condition as well, is the expression for the critical damping of the fundamental natural frequency (Thompson, 1988). The critical damping property of ensuring optimum convergence has been extensively used in the choice of c.

3.2.6 Choice of Iteration Parameters

There are different approaches described in the literature for the choice of the iteration parameters $\mathcal{M}$, h and c, from the simple trial and error technique based on visualizing the evolution of the solution in time (Day, 1965, Frieze, Hobbs and Dowling, 1978, Turvey and Salehi, 1990), to automatic and adaptive methods based on optimum convergence conditions (Papadrakakis, 1981, Underwood, 1983, Zhang and Yu, 1989).

Choice of $\mathcal{M}$ and h

Several methods are used to determine the elements m_{ii} of the fictitious mass matrix $\mathcal{M}$ and the time step h.

The simplest approach, proposed by Day (1965), consists in using the real mass and adjusting the time increment h by trial and error, until a suitable value which satisfies the stability condition is found. This is achieved by visualizing the behavior of the solution in time, at representative nodes. However, this is not an efficient method, unless the damping coefficient c satisfies the optimum convergence condition, i.e. damping is near critical. Otter (1965) also used real mass, but calculated the stable time increment from the Courant-Friedrichs-Lewy condition, mentioned at § 3.2.5.

A frequently used method based as well on the Courant-Friedrichs-Lewy condition, introduces a fictitious diagonal mass matrix, whose elements m_{ii} have to be chosen such that the transit time for information transfer for degree of freedom i to adjacent and like degrees of freedom is a constant. This approach, proposed by Welch (1967), has been used for linear as well as nonlinear problems (Cassel and Hobbs, 1976, Key, Stone and Krieg, 1981, Silling, 1988a). However, it is considered cumbersome for discrete structural models containing different element types (Underwood, 1983).

Another common method to determine the elements m_{ii} of the fictitious mass matrix and the time increment h is based on Gerschgorin's circle theorem. The theorem states (Strang, 1980): *Every eigenvalue of $\mathcal{A}$ lies in at least one of the circles $C_1,\ldots,C_N$, where C_i has its center at the diagonal entry a_{ii} and its radius $r_i = \sum_{j\neq i}|a_{ij}|$ equal to the sum of the moduli of the elements along the rest of the row.* By scaling every row such that the absolute sum along any row is identical, according to this theorem all the circles will be coincident for equal mesh spacing, and they will be nearly coincident for unequal spacing (Underwood, 1983). Moreover, Gerschgorin's first theorem shows that the largest eigenvalue of $\mathcal{A}$ cannot exceed $\|\mathcal{A}\|_\infty$, which is the largest sum of the moduli of the elements along any row, i.e. $\mathcal{A}_{max} \leq \max_i \sum_{j=1}^{N}|a_{ij}|$. This gives a good estimate of the highest frequency ω_{max}. Using equation (3.30), this approach gives the following general expression for m_{ii}:

$$m_{ii} \geq \frac{1}{4} h^2 \sum_{j=1}^{N} \left| \mathcal{K}_{ij} \right|, \qquad (i = 1,.....,N\ ), \tag{3.32}$$

where $\mathcal{K}_{ij}$ are the elements of the stiffness matrix $\mathcal{K}$.

Underwood (1983) shows that the scaling produced by selecting m_{ii} from (3.32) will at least preserve and in general increase the ratio ω_0/ω_{max}, for faster convergence. Also, this way of selecting m_{ii} is not hindered by the variety of elements in the structural model.

This approach may be used for nonlinear problems as well, by substituting the tangential stiffness matrix ${}^t\mathcal{K}(u^n)$ in (3.32) (Park, 1977, Underwood, 1983). The elements of ${}^t\mathcal{K}(u^n)$ can be obtained at any time step n by numerical differentiation of $\mathcal{P}(u^n)$ (Underwood, 1983):

$${}^t\mathcal{K}(u^n) = -\frac{\partial \mathcal{P}(u^n)}{\partial u^n}. \tag{3.33}$$

However, for nonlinear problems, the fictitious mass matrix computed initially ($n = 0$) from (3.32) may not satisfy the condition of stability throughout the analysis, due to the stiffening or softening of the structure. Consequently, the elements of the fictitious mass matrix should be updated (Park and Underwood, 1980, Underwood and Park, 1980, Underwood, 1983), or computed at each time step (Zhang and Yu, 1989).

An approach proposed by Papadrakakis (1981) assumes $m_{ii} \sim \mathcal{K}_{ii}$. The stable time step is then determined from Gerschgorin's theorem. However, this approach is not suitable for partially wrinkled membrane structures, since the regions of very soft stiffness may lead to a singular stiffness matrix and thus to a singular mass matrix as well, the latter having to be inverted in the DR algorithm.

Choice of c

There are several approaches for determining the damping coefficient c, which according to (3.31) should be near its critical value for optimum convergence of the solution.

Day (1965) used a trial and error procedure to find suitable values for c. Other authors (Cassel, Kinsey and Stefton, 1968, Rushton, 1968a, Cassel, 1970, Frieze, Hobbs and Dowling, 1978) determine c from a numerical experiment, which consists of forming the fictitious mass matrix by using a certain approach, and then with $c = 0$, computing the response for a number of iterations. This number must be sufficient to observe the lowest natural frequency ω_0. The damping coefficient is then obtained from (3.31). Rushton (1968a), Frieze, Hobbs and Dowling (1978) and other authors determine a distinct damping coefficient for each intrinsic coordinate. Another alternative, due to Rushton (1968b), is to observe the variation of the total kinetic energy of the undamped system, again after determining the fictitious mass matrix. Since the kinetic energy varies at twice the fundamental frequency of the structure, ω_0 can be obtained and then the damping coefficient computed. The major disadvantage of these techniques is that as much computer time is required in finding ω_0 as is needed for solving the original problem. Bunce (1972) estimates the critical damping coefficient by using Rayleigh's quotient to evaluate the lowest natural frequency, and this approach is very common. Papadrakakis (1981) calculates a series of approximations to the dominant eigenvalue from $\lambda_{DR} = \|\boldsymbol{u}^{n+1} - \boldsymbol{u}^{n}\| / \|\boldsymbol{u}^{n} - \boldsymbol{u}^{n-1}\|$. When λ_{DR} has converged to an almost constant value, then this is the minimum eigenvalue needed to determine c.

For nonlinear problems, an adaptive method for obtaining c has been developed by Underwood (1979). It is based on estimating the lowest frequency from Rayleigh's quotient as $\omega_0^2 \leq \boldsymbol{u}^{\mathrm{T}} \boldsymbol{K} \boldsymbol{u} / \boldsymbol{u}^{\mathrm{T}} \mathcal{M} \boldsymbol{u}$ (Meirovitch, 1986). The damping matrix coefficient is then computed from (3.31), at each iteration as

$$c^n = 2\left\{\frac{(u^n)^T\, {}^{\ell}K^n u^n}{(u^n)^T \mathcal{M}^n u^n}\right\}^{1/2}, \tag{3.34}$$

where ${}^{\ell}K^n$ is a diagonal *local* stiffness matrix, with elements ${}^{\ell}\mathcal{K}_{ii}^n$ (no sum on i), given by

$${}^{\ell}\mathcal{K}_{ii}^n = [\mathcal{P}_i(u^{n-1}) - \mathcal{P}_i(u^n)] / h\dot{u}_i^{n-1/2}. \tag{3.35}$$

Equation (3.34) gives actually an estimate of the critical damping for the current deformation mode u^n, based on an estimate of the local tangent stiffness. This has the virtue that the lowest active mode will be found in the event that the fundamental mode is not participating. The use of (3.34) has proven to be very effective (Key, Stone and Krieg, 1981, Zhang and Yu, 1989), and it requires no unproductive iterations (Underwood, 1983).

A very different approach proposed by Cundall (1976), is to neglect viscous damping ($c = 0$), and to use instead *kinetic damping*. In this case the total kinetic energy of the structure is constantly monitored, and when an energy peak is detected, all the current velocities are set to zero. This approach has been successfully used for form-finding and static analysis of cable networks and membrane structures (Wakefield, 1986, Barnes and Wakefield, 1988, Lewis, 1989, Lewis and Shan, 1990).

3.2.7 DR Algorithms for Nonlinear Problems

A variety of DR algorithms are available for nonlinear problems (Papadrakakis, 1981, Underwood, 1983, Zhang and Yu, 1989). Papadrakakis' *automatic algorithm* is not suitable for the DR analysis of structures containing regions of very soft stiffness characteristics, for reasons already mentioned at § 3.2.6. However, the *adaptive DR algorithm* developed by Underwood (1983), as well as a version of it by Zhang and Yu

(1989), termed *modified adaptive DR algorithm* are of special interest in the context of the present work, since these algorithms are adaptable to the analysis of partially wrinkled membrane structures.

For the *adaptive method* the fictitious mass is computed from (3.32), with a time increment $\tilde{h} > h$, to provide a safety margin for stability. The iterations are then performed with h. Since the problem is nonlinear, $\mathcal{K}_{ij}$ in (3.32) must represent the tangential stiffness matrix (3.33), such that the stability requirements of the central difference time integrator are maintained (Park, 1977). The elements of ${}^{t}\mathcal{K}(\boldsymbol{u})$ are obtained by numerical differentiation of the internal force $\mathcal{P}$ at $t = 0$ ($n = 0$). The elements of the initial fictitious mass matrix may not satisfy the conditions for stability throughout the analysis, due to the stiffening or softening of the structure. The "perturbed apparent frequency" error measure (Park and Underwood, 1980, Underwood and Park, 1980, 1982) may be used to determine when the mass matrix should be updated, or a smaller time increment h should be chosen. The damping matrix coefficient is computed at each iteration from (3.34), employing the local stiffness matrix (3.35). The *adaptive DR algorithm* (Underwood, 1983) may be formally written as :

(I) $\boldsymbol{u}^0$ given; $\dot{\boldsymbol{u}}^0 = \boldsymbol{0}$; $n = 0$,

(II) compute $\mathcal{M}$ from (3.32) with $h = \tilde{h}$, where $\tilde{h} > h$ and $\mathcal{K}_{ij}$ is determined from (3.33),

(III) $\mathcal{R}^n = \mathcal{F}^n + \mathcal{P}(\boldsymbol{u}^n)$,

(IV) if $\mathcal{R}^n \cong \boldsymbol{0}$ stop, else continue,

(V) for $n = 0$, $\dot{\boldsymbol{u}}^{1/2} = \frac{h}{2}\mathcal{M}^{-1}\mathcal{R}^0$,

for $n \neq 0$, $\dot{\boldsymbol{u}}^{n+1/2} = \frac{(2-ch)}{(2+ch)}\dot{\boldsymbol{u}}^{n-1/2} + \frac{2h}{(2+ch)}\mathcal{M}^{-1}\mathcal{R}^n$, (3.36)

(VI) $\boldsymbol{u}^{n+1} = \boldsymbol{u}^n + h\dot{\boldsymbol{u}}^{n+1/2}$,

(VII) evaluate error and reform $\mathcal{M}$ if necessary;
repeat (III) – (VI),

(VIII) $n = n+1$,

(IX) compute damping matrix coefficient c^n from (3.34),
where ${}^{\ell}\mathcal{K}_{ii}^n$ is determined from (3.35),

(X) return to (III).

Since this algorithm is adaptive, the robustness of the DR method is increased considerably. This method has consistently produced good results (Underwood, 1983).

A *modified adaptive DR algorithm* is proposed by Zhang and Yu (1989). A few steps are added to Underwood's *adaptive DR algorithm*: the fictitious mass matrix is updated at each time step from (3.32), improving the convergence rate; the damping matrix coefficient is obtained from $c^n = 2[(\boldsymbol{u}^n)^{\mathrm{T}} \mathcal{P}(\boldsymbol{u}^n) / (\boldsymbol{u}^n)^{\mathrm{T}} \mathcal{M}^n \boldsymbol{u}^n]^{1/2}$, eliminating the need to calculate the local stiffness matrix from (3.35); the initial displacement vector $\boldsymbol{u}^0$ in the main program is determined from $u_i^0 = (u_i^* + u_i^{**}) / 2$ with $c = 0$ and an initial mass matrix is computed from (3.32), where u_i^* and u_i^{**} are the values of two neighboring but opposite peaks of the locus u_i. This modified adaptive method has been successfully applied to the analysis of elastic-plastic bending and wrinkling of circular plates (Zhang and Yu, 1989 Zhang, Yu and Wang, 1989). However, the computing time needed to obtain $\boldsymbol{u}^0$ is substantial, compared with the computing time needed to solve the original problem.

3.3 Spatial Discretization

3.3.1 Introduction

The DR algorithm has been developed from equation (3.5), which represents a spatial discretization of the PDE governing the transient response of a structure. Equation (3.5) may be obtained by applying a finite difference (Forsythe and Wasow, 1981) or finite element (Oden, 1972, Zienkiewicz, 1977) discretization technique. For a membrane structure, a spatial discretization of the global equation of motion (2.38) would lead to an equation of the form (3.5).

In the early stages of DR, central differences with interlacing meshes were used to approximate partial derivatives in space (Otter, 1965, Otter, Cassel and Hobbs, 1966). Rushton (1968a,b, 1969a,b,c, 1972) approximated spatial derivatives by central differences (without interlacing meshes) to solve plate problems. Finite elements in the context of DR were first employed by Lynch, Kelsey and Saxe (1968). The technique has been frequently used for form-finding and static analysis of lightweight tensile structures such as cable networks and membranes (Barnes, 1976, Lewis et al., 1984, Barnes and Wakefield, 1988, Lewis and Shan, 1990, Lewis and Gosling, 1993). Finite elements in the context of DR are likewise employed for solving plate and shell problems (Estefen and Harding, 1986, Eriksson, 1987, Marchertas, Kennedy and Pfeiffer, 1988, Sauve and Badie, 1993), as well as for other nonlinear structural analyses (Rericha, 1986, Kulak and Fiala, 1988, Rao and Shantaram, 1990, Sauve and Metzger, 1992). However, due to its simplicity, the method of central differences with or without interlacing meshes continued to be preferred by some authors (Alwar and Ramachandra Rao, 1973, Frieze, Hobbs and Dowling, 1978, Lim and Turvey, 1985, Turvey and Der Avanessian, 1986, 1990, Turvey and Lim, 1986, Zhang and Yu, 1989, Turvey and Osman, 1993).

Silling (1985, 1987, 1988a,b, 1989) used a spatial finite difference discretization technique based on Green's theorem, in the context of DR analysis of plane strain problems in nonlinear elasticity. Besides its simplicity, this method avoids the inconvenience of mapping techniques, being applicable to uniform as well as irregular types of meshes, which can be fitted to any shape of boundary.

3.3.2 Green's Theorem Differencing Method

The Green's theorem differencing method for the evaluation of spatial partial derivatives was developed by Wilkins (1964, 1969) in connection with elastic-plastic flow problems. The method is used for gradient approximations in a number of codes such as HEMP (Wilkins, 1964, 1969), STEALTH (Hoffman, 1975), PISCES (Hancock, 1976), TODDY (Swegle, 1978), CHIMP (Silling, 1985, 1987, 1988a, 1989). A description of this technique is given by Belytschko (1983) under the name "contour integral finite difference method". Herrmann and Bertholf (1983) present a detailed discussion on finite-difference approximations of gradients, including Green's theorem method. According to the authors the latter is to be preferred because of its simplicity.

The codes developed by Wilkins (1964) for elastic-plastic flow problems use the Cauchy stress tensor and perform differencing in the deformed configuration, whereas Silling's codes (Silling, 1985) which were designed for plane strain problems in nonlinear elasticity use the first Piola-Kirchhoff stress and perform all differencing in the reference configuration. The latter method is considered to be more convenient for the purposes of finite elasticity (Silling, 1987).

In this work, Green's theorem differencing method is adapted to finite elasticity problems concerned with deformations of membranes starting from plane reference configurations, evolving to curved deformed configurations in 3-D. The method may be readily adjusted to curved reference configurations as well. Further, the Piola stress

tensor $\boldsymbol{T}$ is employed, and differencing is performed in the plane reference configuration Ω.

The plane region Ω is discretized into a $Q \times S$ mesh of nodes. Quadrilateral non-uniform meshes are considered here, but the results can be extended to non-quadrilateral meshes as well. Each node is labeled by a pair of integer superscripts (k,l). The location of the node (k,l) in the reference configuration Ω is given by its position vector $\boldsymbol{x}^{k,l}$, or by its Cartesian coordinates $x_\alpha^{k,l}$, where $\alpha = 1, 2$. In the deformed configuration, the location of the node (k,l) at time step n is given by the time-dependent position vector $\boldsymbol{r}^{k,l,n} = \boldsymbol{x}^{k,l} + \boldsymbol{u}^{k,l,n}$, where $\boldsymbol{u}^{k,l,n}$ is the nodal displacement vector. The corresponding Cartesian coordinates are $r_i^{k,l,n}$, with $i = 1, 2, 3$.

The quadrilateral region formed from each set of four adjacent nodes represents a zone. Zones and zone centers are labeled by half-integers. In Fig. 3.1, zone $(k+1/2, l+1/2)$ may be identified with the shaded area. Certain quantities termed node-centered variables are associated with nodes, bearing the nodal label as superscript. These include position $\boldsymbol{x}^{k,l}$ and $\boldsymbol{r}^{k,l,n}$, displacement $\boldsymbol{u}^{k,l,n}$, velocity $\dot{\boldsymbol{u}}^{k,l,n}$, acceleration $\ddot{\boldsymbol{u}}^{k,l,n}$, fictitious nodal mass $m^{k,l}$, internal forces $\mathcal{P}^{k,l,n}$ due to the divergence of Piola stress tensor $(Div\boldsymbol{T})^{k,l,n}$, with components $T_{i\alpha,\alpha}^{k,l,n}$, and external forces $\mathcal{F}^{k,l}$ (or $\mathcal{F}^{k,l,n}$, if loaded in steps) such as body forces, point loads, or forces due to pressure acting on a membrane. Zone-centered variables are identified over zones, bearing the zonal label as superscript. These include the Piola stress tensor $\boldsymbol{T}^{k+1/2,l+1/2,n}$, the deformation gradient $\boldsymbol{F}^{k+1/2,l+1/2,n}$, and the real mass density $\rho^{k+1/2,l+1/2}$, which may be needed to calculate body forces.

A spatial discretization of the damped equation of motion of a structure at node (k,l) of the mesh may be written in the form:

$$m^{k,l}\ddot{\boldsymbol{u}}^{k,l,n} + cm^{k,l}\dot{\boldsymbol{u}}^{k,l,n} = \mathcal{F}^{k,l,n} + \mathcal{P}^{k,l,n}. \tag{3.37}$$

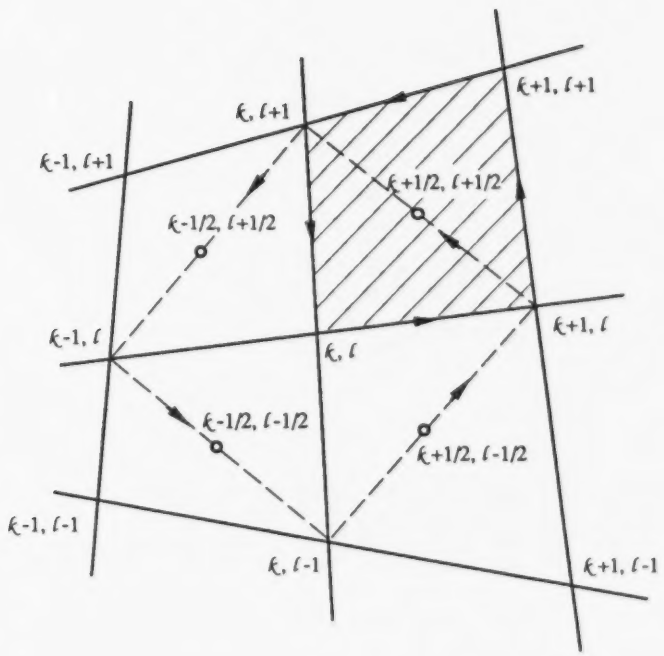

Fig. 3.1 Mesh for spatial discretization, with integration paths used in Green's theorem method for differencing gradient components

For a membrane, (3.37) may be obtained either by discretizing the global equation of equilibrium (2.29), and then transforming it into an equation of motion by artificially adding an acceleration term as well as a viscous damping term, or by discretizing the global equation of motion (2.38) and then adding viscous damping. The term $\iint_D T_{i\alpha,\alpha} dA$ in equations (2.29) or (2.38) can be approximated using Green's theorem (2.28). Substituting $\phi = T_{i\alpha}(x,t^n)$ in (2.28), and applying a one-point integration rule to the components $T_{i\alpha}$ of the Piola stress with ∂D taken to be the dashed quadrilateral path shown in Fig. 3.1, leads to the following difference formula

$$\begin{aligned} 2A^{k,l}T^{k,l,n}_{i\alpha,\alpha} = e_{\alpha\beta}\Big\{ & T^{k+1/2,l+1/2,n}_{i\alpha}(x^{k,l+1}_{\beta} - x^{k+1,l}_{\beta}) + T^{k-1/2,l+1/2,n}_{i\alpha}(x^{k-1,l}_{\beta} - x^{k,l+1}_{\beta}) \\ & + T^{k-1/2,l-1/2,n}_{i\alpha}(x^{k,l-1}_{\beta} - x^{k-1,l}_{\beta}) + T^{k+1/2,l-1/2,n}_{i\alpha}(x^{k+1,l}_{\beta} - x^{k,l-1}_{\beta})\Big\}. \end{aligned} \tag{3.38}$$

Here $A^{k,l}$ is the equivalent nodal area (Herrmann and Bertholf, 1983), equal to one half of the area enclosed by the dashed quadrilateral in Fig. 3.1, and given by

$$A^{k,l} = \frac{1}{4}\Big\{(x^{k-1,l}_2 - x^{k+1,l}_2)(x^{k,l+1}_1 - x^{k,l-1}_1) - (x^{k-1,l}_1 - x^{k+1,l}_1)(x^{k,l+1}_2 - x^{k,l-1}_2)\Big\}. \tag{3.39}$$

The left hand side in (2.28) is approximated by the product of $T_{i\alpha,\alpha}$ at the node (k,l) and the area contained within the dashed contour, which is twice the equivalent nodal area. On each of the four edges that comprise the boundary of the region, the contribution to the right hand side of (2.28) is approximated by setting the integrand equal to its value at the center of the zone. Thus, the stresses $T_{i\alpha}$ on the right hand side of (3.38) are zone-centered, and these in turn depend through the constitutive equations on the zone-centered components of the deformation gradient $F_{i\alpha}$. These latter components are obtained by applying Green's formula (2.28) with $\phi = r_i(x,t^n)$, to the shaded zone in Fig. 3.1. Here the contributions from the edges of the zone are approximated by setting the integrand equal to the average of its end-point values along

each zone edge. After some simplifications, this leads to the following difference formula for the zone-centered components of the deformation gradient at time step n:

$$F_{i\alpha}^{k+1/2,l+1/2,n} = \frac{e_{\alpha\beta}}{2A^{k+1/2,l+1/2}}\Big\{(x_\beta^{k,l+1}-x_\beta^{k+1,l})(r_i^{k+1,l+1,n}-r_i^{k,l,n}) \\ -(x_\beta^{k+1,l+1}-x_\beta^{k,l})(r_i^{k,l+1,n}-r_i^{k+1,l,n})\Big\}. \tag{3.40}$$

where $A^{k+1/2,l+1/2}$ is the area of the shaded zone, given by

$$A^{k+1/2,l+1/2} = \frac{1}{2}\Big\{(x_2^{k,l+1}-x_2^{k+1,l})(x_1^{k+1,l+1}-x_1^{k,l}) \\ -(x_1^{k,l+1}-x_1^{k+1,l})(x_2^{k+1,l+1}-x_2^{k,l})\Big\} \tag{3.41}$$

Herrmann and Bertholf (1983) indicate that the same difference approximations (3.38) or (3.40) may be obtained by using Taylor series expansions. Defining the mesh distortion parameters as

$$\xi_\alpha^{k+1,l+1;k-1,l-1} = \frac{1}{2}(x_\alpha^{k+1,l+1}+x_\alpha^{k-1,l-1})-x_\alpha^{k,l}; \\ \xi_\alpha^{k-1,l+1;k+1,l-1} = \frac{1}{2}(x_\alpha^{k-1,l+1}+x_\alpha^{k+1,l-1})-x_\alpha^{k,l}, \tag{3.42}$$

they show that the local truncation error arising from each of the difference approximations (3.38) and (3.40) is of order mesh size times the mesh distortion parameters. When the mesh distortions are very small, the difference expressions involve error terms which are third order in mesh size. However, when the mesh distortions are of the same order as the mesh size, then the error terms are of second order in the mesh size. Thus, for uniform rectangular meshes, the local truncation error is $O(\varepsilon^3)$ and for other types of meshes it is $O(\varepsilon^2)$, where ε is a typical zone width. Since the stress gradient difference operator acts on stresses found using the deformation gradient approximation, their truncation errors combine (Silling, 1988a).

Therefore, the local truncation error for the method is $O(\varepsilon^2)$ for uniform rectangular meshes and $O(\varepsilon)$ for other types of meshes.

3.3.3 Internal and external forces

The quantity $A^{k,l}T^{k,l,n}_{i\alpha,\alpha}$ in (3.38) may be interpreted as the i-th force component acting on the node (k,l) due to the internal stresses at time step n :

$$\mathcal{P}^{k,l,n}_i = A^{k,l}T^{k,l,n}_{i\alpha,\alpha}\,. \tag{3.43}$$

Using the right hand side in (3.38) gives

$$\begin{aligned}\mathcal{P}^{k,l,n}_i = \frac{e_{\alpha\beta}}{2}\Big\{&T^{k+1/2,l+1/2,n}_{i\alpha}(x^{k,l+1}_\beta - x^{k+1,l}_\beta) + T^{k-1,l+1/2,n}_{i\alpha}(x^{k-1,l+1}_\beta - x^{k,l+1}_\beta)\\ &+T^{k-1/2,l-1/2,n}_{i\alpha}(x^{k,l-1}_\beta - x^{k-1,l}_\beta) + T^{k-1/2,l-1/2,n}_{i\alpha}(x^{k+1,l}_\beta - x^{k,l-1}_\beta)\Big\}.\end{aligned} \tag{3.44}$$

To calculate the internal force $\mathcal{P}^{k,l,n}$, the zone-centered stress components $T_{i\alpha}$ are needed. These depend on the zone-centered components $F_{i\alpha}$ of the deformation gradient. In the DR algorithm, the position $r^{k,l,n}$ of each node in the deformed configuration is known from the previous time step, thus (3.40) may be employed to determine the zone-centered components of the deformation gradient. Further, equation (2.2b) gives the zone-centered components $C_{\alpha\beta}$ of the Cauchy-Green strain tensor. To simplify the notation, the superscripts representing the labels of the zone center and time step have been suppressed. The principal stretches λ, μ are then obtained as the roots of equation (2.15). These roots are always ordered such that $\lambda \geq \mu$. From $\boldsymbol{CL} = \lambda \boldsymbol{L}$ and $\boldsymbol{CM} = \mu \boldsymbol{M}$, the components L_α, M_α of the associated principal vectors of strain are:

$$L_1 = C_{12}\left[(\lambda^2 - C_{11})^2 + C_{12}^2\right]^{-1/2}, \quad L_2 = C_{12}\left[(\lambda^2 - C_{22})^2 + C_{12}^2\right]^{-1/2},$$
$$M_1 = C_{12}\left[(\mu^2 - C_{11})^2 + C_{12}^2\right]^{-1/2}, \quad M_2 = C_{12}\left[(\mu^2 - C_{22})^2 + C_{12}^2\right]^{-1/2}, \tag{3.45}$$

and these are chosen such that $\boldsymbol{L} \times \boldsymbol{M} = \boldsymbol{e}_3$, i.e. $L_\alpha M_\beta e_{\alpha\beta} = 1$. Equation (2.4) then gives l_i and m_i as:

$$l_i = \lambda^{-1} F_{i\alpha} L_\alpha, \quad m_i = \mu^{-1} F_{i\alpha} M_\alpha. \tag{3.46}$$

These are the components of the images of the of the principal vectors of strain on the tangent plane of the deformed surface. All these quantities characterizing the strain are zone-centered.

The Piola stress is then obtained from equation (2.25), where the relaxed strain energy $W_R(\boldsymbol{F})$ given by (2.53) is employed, in order to account for the possibility of wrinkling. The natural width in simple tension for isotropic, incompressible materials is considered in (2.53), i.e. $v(\lambda) = \lambda^{-1/2}$ and $v(\mu) = \mu^{-1/2}$. The ordering of the stretches implies that the second branch of the relaxed energy is operative whenever partial wrinkling is indicated. The third branch is never encountered. Then, the zone-centered Piola stress derived from the relaxed energy is

$$T_{i\alpha} = \begin{cases} w_\lambda l_i L_\alpha + w_\mu m_i M_\alpha; & \lambda > \mu^{-1/2}, \quad \mu > \lambda^{-1/2} \\ \hat{w}'(\lambda) l_i L_\alpha; & \lambda > 1, \quad \mu \le \lambda^{-1/2} \\ 0; & \lambda \le 1, \quad \mu \le 1, \end{cases} \tag{3.47}$$

and this delivers the node-centered divergence of the stress and respectively the internal force $\mathcal{P}_i^{k,l,s}$, according to equation (3.44).

For a membrane structure, the external forces may be point loads, body forces, such as gravity forces, or forces due to pressure loading. To calculate the gravity

forces, the real mass density of the membrane material is employed, but this type of force is very small compared to the internal forces arising as a consequence of even moderate strain.

In the case of uniform pressure loading, the external forces may be obtained by a spatial discretization of the term $\iint_D pnJdA$ in equation (2.29). Since the Jacobian $J = \lambda\mu$ and the unit normal $\boldsymbol{n} = \ell \times \boldsymbol{m}$ are zone centered, the integral $\iint_D pnJdA$ is approximated as a zone-centered external force due to pressure acting over the area of a zone:

$$\mathcal{F}_i^{k+1/2,\ell+1/2,n} = p\, n_i^{k+1/2,\ell+1/2,n} \lambda^{k+1/2,\ell+1/2,n} \mu^{k+1/2,\ell+1/2,n} A^{k+1/2,\ell+1/2}, \tag{3.48}$$

where $n_i = e_{ijk}\ell_j m_k$. Here e_{ijk} is the permutation symbol ($e_{ijk} = 1$ if (i, j, k) is a cyclic permutation of (1, 2, 3), $e_{ijk} = -1$ if (i, j, k) is an anti cyclic permutation of (1, 2, 3), and $e_{ijk} = 0$ if any two numbers of (i, j, k) are equal). Then, the node-centered external force due to uniform pressure loading is obtained as the average:

$$\mathcal{F}_i^{k,\ell,n} = \frac{1}{4}\left(\mathcal{F}_i^{k+1/2,\ell+1/2,n} + \mathcal{F}_i^{k-1/2,\ell+1/2,n} + \mathcal{F}_i^{k-1/2,\ell-1/2,n} + \mathcal{F}_i^{k+1/2,\ell-1/2,n}\right). \tag{3.49}$$

If a concentrated force $\tilde{\mathcal{F}}$ is acting at a point $\tilde{x}$ on the membrane, the mesh has to be arranged such that a nodal point $x^{k,\ell}$ coincides with the application point of the force. Then, the external force due to the point load at $x^{k,\ell}$ is

$$\mathcal{F}_i^{k,\ell,n} = \tilde{\mathcal{F}}_i. \tag{3.50}$$

The concentrated load may be applied in steps if necessary.

Having calculated the internal forces $\mathcal{P}_i^{k,\ell,n}$ and external forces $\mathcal{F}_i^{k,\ell,n}$ at node (k, ℓ) and time step n, the DR algorithm can be applied.

3.3.4 Boundary Conditions

Displacement boundary conditions on a part $\partial\Omega_\Gamma$ of the membrane boundary $\partial\Omega$ are easily enforced by arranging the mesh such that $\partial\Omega_\Gamma$ contains nodal points. The prescribed displacements are then imposed at the nodes lying on $\partial\Omega_\Gamma$. The deformation gradient at the center of the zones adjacent to $\partial\Omega_\Gamma$ is further obtained from equation (3.40), the internal forces at the internal nodes adjacent to $\partial\Omega_\Gamma$ are given by equation (3.44), and then the DR algorithm can be applied.

In the case of a traction boundary condition on $\partial\Omega \setminus \partial\Omega_\Gamma$, the mesh is also arranged such that the boundary contains nodal points. A phantom mesh is provided outside the boundary carrying zero densities and appropriate stresses derived from the boundary conditions, so that the calculations with the DR algorithm of velocities and positions of a boundary node become identical to those for an interior node (Herrmann and Bertholf, 1983). If AOB in Fig. 3.2 is a traction boundary, the added phantom mesh is represented by the dashed lines.

For a traction-free boundary AOB, the zone-centered stresses in the phantom mesh shown in Fig. 3.2 are set equal to zero:

$$T_{i\alpha}^{k+1/2,\ell+1/2,n} = 0,$$
$$T_{i\alpha}^{k+1/2,\ell-1/2,n} = 0. \tag{3.51}$$

Also, node $(k, \ell+1)$ is set coincident with node (k, ℓ). Equation (3.44) gives the internal force at node (k, ℓ) on the boundary, and then the DR algorithm may be applied.

If AOB in Fig. 3.2 has a prescribed boundary stress, then appropriate average values of the boundary stress acting over AO and OB are considered at the zone centers $(k+1/2, \ell+1/2)$ and $(k+1/2, \ell-1/2)$. Again node $(k, \ell+1)$ is set coincident with node (k, ℓ)

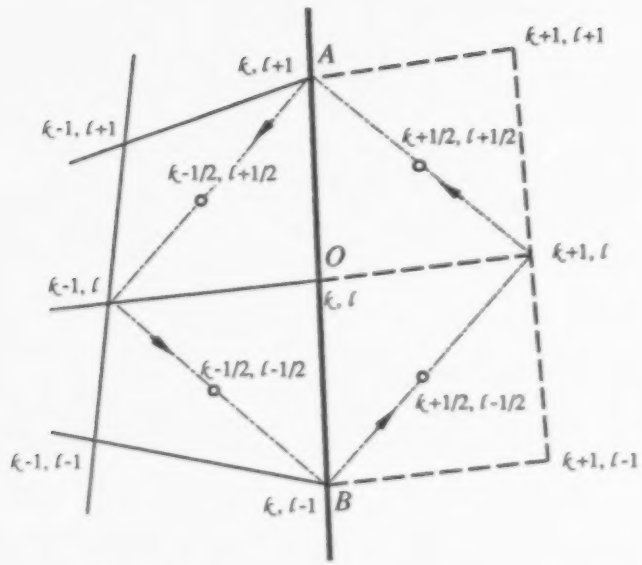

Fig. 3.2 Phantom mesh at boundary

and equation (3.44) gives now the force at node (k, l) due to internal stresses as well as boundary tractions.

3.4 Adaptive DR Method for Analysis of Membranes

An adaptive DR method is presented here, which has been especially developed for the static analysis of elastic membranes undergoing finite deformations. The algorithm accounts for the possibility of partial wrinkling of the membranes by employing the relaxed strain energy density, introduced in § 2.4. Isotropic membranes are considered.

This adaptive technique is based on the Dynamic Relaxation method, inheriting its advantages of simplicity, tenacity, robustness and reliability. Being an explicit vector method, there is no need to manipulate or store matrices, so complicated problems may be solved using a microcomputer. The algorithm is designed for problems starting from plane reference configurations and evolving to arbitrarily curved deformed configurations in 3D. However, it may be readily adapted to curved reference configurations. Green's theorem differencing method has been employed for the spatial discretization. Besides its simplicity, this method avoids the inconvenience of mapping techniques, being applicable to uniform as well as irregular meshes, which can be fitted to any shape of boundary. Regarding the stability of the equilibrium solution, Silling (1988a) has remarked that equilibria obtained by the DR method may be considered as asymptotically dynamically stable, since they do not spontaneously decay to other configurations.

According to the DR methodology, the global equilibrium equation of the membrane (2.29) is first discretized in space and then transformed into the equation of a damped motion of the form (3.5) or (3.38), by artificially introducing an acceleration

as well as a viscous damping term. Fictitious mass density and mass proportional damping are used. Equation (3.5) is then explicitly integrated in time by using the central difference time integrator (3.16). The problem being nonlinear, stability and convergence of the solution are ensured by updating the iteration parameters at each time step. This is the reason for terming the method *adaptive*, since the information generated during the computation is used to modify system parameters in order to maintain optimum convergence. Thus, the elements of the fictitious mass matrix m_{ii}^n are evaluated at each iteration from Gerschgorin's circle theorem, such as to satisfy the stability condition (3.30) for the central difference time integrator (see equation (3.32), derived for m_{ii}). The stiffness matrix $\mathcal{K}_{ij}$ in (3.32) is replaced by the current tangential stiffness matrix ${}^t\mathcal{K}_{ij}^n$ which is computed at each time step by numerical differentiation of the internal force $\mathcal{P}^n$ (see equation (3.33)). The differentiation does not have to be particularly accurate, as only an estimate is being sought (Underwood, 1983). The summation in (3.32) is performed with the differentiation, so provisions for storing a matrix are not required. The damping coefficient c^n is also evaluated at each iteration, by estimating the lowest participating frequency from Rayleigh's quotient and using the expression (3.31) for critical damping (see equation 3.34 derived for c^n). The local stiffness matrix ${}^t\mathcal{K}_{ii}^n$ in (3.34) is computed from (3.35) at each time step, by numerical differentiation of the internal force $\mathcal{P}^n$.

To start the DR algorithm, the initial conditions $\boldsymbol{u}^0$ and $\dot{\boldsymbol{u}}^0$ are required at step (I), ($t = 0,\ n = 0$). The expression of the strain energy density $w(\lambda,\ \mu)$ of the material is also needed. Further, an arbitrary time increment h has to be chosen, which is maintained constant during the iteration process. However, a time increment $\tilde{h} > h$ has to be used at step (VIII) in the computation of the elements m_{ii}^n of the mass matrix, in order to provide a safety margin for stability. At step (II) the zone centered variables characterizing the deformation and strain are computed. Next, the algorithm checks for wrinkling and computes the Piola stress by choosing the appropriate branch of the

relaxed strain energy $w_R(\lambda^n,\mu^n)$ (step (III)). The internal and external forces $\mathcal{P}^n$ and $\mathcal{F}^n$ are computed at steps (IV) and (V), and their sum gives the residual $\mathcal{R}^n$ at step (VI). If the residual is close to zero (i.e. $\max_i |\mathcal{R}_i^n| < \varepsilon = 10^{-6}$ for example), the solution $\boldsymbol{u}$ is considered to approximately satisfy the equilibrium equation (3.3), and the program stops. If this is not the case, the elements of the fictitious mass matrix are computed at step (VIII) and if $n \neq 0$ the damping coefficient is computed at step (IX). At steps (X) and (XI) the velocity and displacement vectors are obtained using the central difference time integrator, and the next iteration starts with step (II). Displacement boundary conditions are enforced at step (I) and (XI), whereas traction boundary conditions are enforced at step (IV).

To simplify the notation, the superscripts representing labels of nodes or labels of zone centers have been omitted. However, for the computations occurring at steps (II) and (III), which involve zone centered variables, this has been specified. At these steps, the subscripts i and α refer to the orthonormal bases $\{\boldsymbol{e}_i\}$ and $\{\boldsymbol{e}_\alpha\}$. For the remaining steps, computations involve node-centered variables, but to avoid repetition this has not been mentioned. Instead, a subscript i referring to the $(1,\ldots\ldots,N)$ nodal degrees of freedom of the structure has been used in the steps involving scalar equations, but this has been specified. Formally, this adaptive DR algorithm may be written as:

(I) initial conditions:

$\boldsymbol{u}^0$ given; $\dot{\boldsymbol{u}}^0 = \boldsymbol{0}$; $n = 0$,
$w(\lambda, \mu)$ given;
choose $h, \bar{h}$; $(\bar{h} > h)$,

(II) compute zone-centered quantities :

deformation gradient $\boldsymbol{F}^n$ from (3.40),
Cauchy-Green strain $\boldsymbol{C}^n$ from (2.2b),
principal stretches λ^n, μ^n from (2.13), order $\lambda^n \geq \mu^n$,
principal vectors of strain $\boldsymbol{L}^n, \boldsymbol{M}^n$; $\boldsymbol{l}^n, \boldsymbol{m}^n$ from (3.45) and (3.46),

(III) check for wrinkling; compute zone centered Piola stress T^n:

if $\lambda^n > (\mu^n)^{-1/2}$, $\mu^n > (\lambda^n)^{-1/2}$, tense zone;

$$w_R(\lambda^n, \mu^n) = w(\lambda^n, \mu^n),$$

$$T^n_{i\alpha} = w^n_\lambda \, l^n_i L^n_\alpha + w^n_\mu \, m^n_i M^n_\alpha,$$

if $\lambda^n > 1$, $\mu^n \le (\lambda^n)^{-1/2}$, wrinkled zone;

$$w_R(\lambda^n, \mu^n) = \hat{w}(\lambda^n),$$

$$T^n_{i\alpha} = \hat{w}'(\lambda^n) l^n_i L^n_\alpha,$$

if $\lambda^n \le 1$, $\mu^n \le 1$, slack zone;

$$w_R(\lambda^n, \mu^n) = 0,$$

$$T^n_{i\alpha} = 0, \qquad i = 1, 2, 3; \quad \alpha = 1, 2,$$

(IV) compute internal forces $\mathcal{P}^n$ from (3.44),

(V) compute external forces $\mathcal{F}^n$ if any;
for pressure loading use (3.48) and (3.49),

(VI) compute residual $\mathcal{R}^n = \mathcal{F}^n + \mathcal{P}^n$, (3.52)

(VII) if $\mathcal{R}^n \equiv \mathbf{0}$ stop, else continue,

(VIII) compute elements of fictitious mass matrix $\mathcal{M}^n$:

$$m^n_{ii} = \frac{1}{4}\tilde{h}^2 \sum_{j=1}^{N} \left| {}^t\mathcal{K}^n_{ij} \right|, \qquad i = 1, \ldots\ldots, N, \text{ (no sum on } i\text{)},$$

$$n = 0, \quad {}^t\mathcal{K}^0_{ij} = \mathcal{P}^0_i / u^0_j,$$

$$n \neq 0, \quad {}^t\mathcal{K}^n_{ij} = (\mathcal{P}^n_i - \mathcal{P}^{n-1}_i) / h\dot{u}^{n-1/2}_j,$$

(IX) compute damping coefficient ($n \neq 0$):

$$c^n = 2\left\{\frac{(u^n)^T\, {}^{\ell}K^n u^n}{(u^n)^T \mathcal{M}^n u^n}\right\}^{1/2},$$

$${}^{\ell}\mathcal{K}_{ii}^n = (\mathcal{P}_i^n - \mathcal{P}_i^{n-1}) / h\dot{u}_i^{n-1/2}, \quad \text{(no sum on } i\text{)},$$

(X) compute velocity at time step $n+1/2$:

$$n = 0, \quad \dot{u}_i^{1/2} = \frac{h}{2}(m_{ii}^0)^{-1}\, \mathcal{R}_i^0,$$

$$n \neq 0, \quad \dot{u}_i^{n+1/2} = \frac{(2-ch)}{(2+ch)}\dot{u}_i^{n+1/2} + \frac{2h}{(2+ch)}(m_{ii}^n)^{-1}\, \mathcal{R}_i^n,$$

$$i = 1,\ldots\ldots,N, \quad \text{(no sum on } i\text{)},$$

(XI) compute displacement at time step $n+1$:

$$u^{n+1} = u^n + h\dot{u}^{n+1/2},$$

(XII) $n = n+1$, return to (II).

If the square root at the step (IX) is greater than $2/h$, then it is set to a value less than $2/h$, since step (VIII) gives $\omega_{\max} \leq 2/h$. Furthermore, if the argument of the square root at the same step is not positive, c^n is set to zero. This is required for problems which traverse an unstable region (Underwood, 1983).

A simpler, non-adaptive but still efficient version of this algorithm is obtained by omitting steps (VIII) and (IX). Real mass density is used for the computation of the elements of the diagonal mass matrix, and a stable time increment is obtained by visualizing the behavior of the solution. To evaluate the critical damping coefficient, the variation of the total kinetic energy of the undamped motion of the system is observed. Since the kinetic energy varies at twice the fundamental frequency of the

system, an estimate of the lowest natural frequency can be obtained. Then, a damping coefficient which ensures rapid convergence can be computed from (3.31). This version does not require the formation of the tangential and local stiffness matrices. For the solution of a variety of problems with different boundary conditions, adapting the code for the computation of the stiffness matrices to the geometry of the boundary is a very time consuming operation. However, if a commercial software package should ever be developed from this program, a subroutine could be generated to perform the adaptation automatically, by using the input data describing the geometry of the problem.

Chapter 4

DR Solutions to Membrane Problems

4.1 General Considerations

A variety of boundary value problems were solved by applying the adaptive DR method as well as its non-adaptive version, presented in § 3.4. Two strain energy functions for incompressible rubber-like materials were used in the applications: the neo-Hookean strain energy and Ogden strain energy.

For the neo-Hookean material, the strain energy per unit of initial volume has the form (Pipkin, 1986a):

$$U(\lambda_1,\lambda_2,\lambda_3)=\frac{1}{2}\tilde{G}(\lambda_1^2+\lambda_2^2+\lambda_3^2-3), \tag{4.1}$$

where the λ_i are the principal stretches and $\tilde{G}$ is a positive constant with dimensions force/area (the shear modulus for infinitesimal strain). Incompressibility requires that $\lambda_3=1/\lambda_1\lambda_2$. For a membrane with a thickness h in the undeformed state, the corresponding strain energy per unit initial area may be approximated by setting $\lambda_1=\lambda$, $\lambda_2=\mu$. Then $\lambda_3=1/\lambda\mu$, and the strain energy becomes

$$w(\lambda,\mu)=\frac{1}{2}G(\lambda^2+\mu^2+\lambda^{-2}\mu^{-2}-3), \tag{4.2}$$

where $G=\tilde{G}h$. A diagram representing the original neo-Hookean strain energy as a function of λ and μ is shown in Fig. 4.1a.

In the wrinkled regions, where $\lambda>1,\ \mu\le v(\lambda)\equiv\lambda^{-1/2}$ or $\mu>1,\ \lambda\le v(\mu)\equiv\mu^{-1/2}$, the strain energy in uniaxial tension $\hat{w}(\lambda)$, respectively $\hat{w}(\mu)$ is given by

$$\hat{w}(x)=w(x,x^{-1/2})=\frac{G}{2}(x^2+2x^{-1}-3). \tag{4.3}$$

The relaxed neo-Hookean strain energy $w_R(\lambda,\mu)$ is then constructed according to (2.53), the result being represented in Fig. 4.1b. This relaxed energy has the property that equilibrium states automatically furnish the global minimum of the potential energy, for a certain class of boundary value problems (Haseganu and Steigmann, 1994b).

For deformations involving stretches larger than some moderate values, the experimental results do not support neo-Hookean predictions, and another more suitable strain energy should be employed. In the case of membranes subjected to pressure loading, Ogden energy is preferred since it is known to furnish good quantitative agreement with experiments, over a large range of stretch values (Ogden, 1984).

For the Ogden material, the strain energy function per unit initial volume has the form (Ogden, 1984):

$$U(\lambda_1,\lambda_2,\lambda_3)=\tilde{G}\sum_{r=1}^{3}g_r(\lambda_1^{\alpha_r}+\lambda_2^{\alpha_r}+\lambda_3^{\alpha_r}-3)/\alpha_r, \tag{4.4}$$

where $\alpha_1=1.3,\quad \alpha_2=5.0,\quad \alpha_3=-2.0;$

$g_1=1.491,\quad g_2=0.003,\quad g_3=-0.0237.$

Setting $\lambda_1=\lambda,\ \lambda_2=\mu$ and taking $\lambda_3=1/\lambda\mu$, the associated membrane energy (i.e. strain energy per unit initial area) may be approximated as

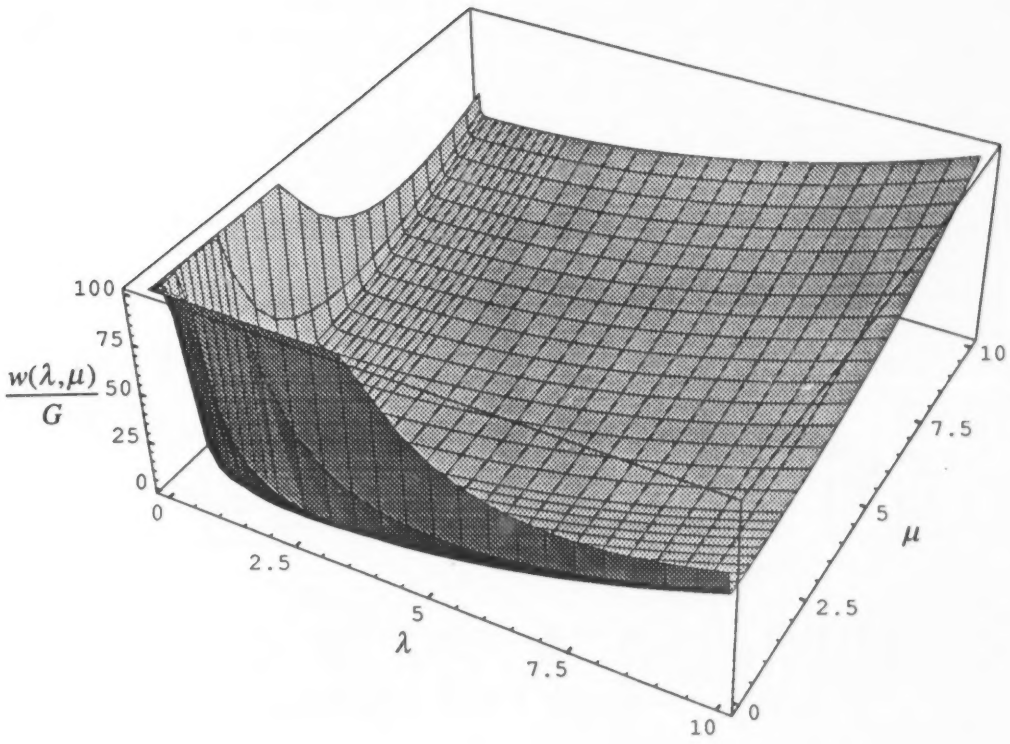

Fig. 4.1a Original neo-Hookean strain energy function,
for $0.02 \leq \lambda, \mu \leq 10.0$

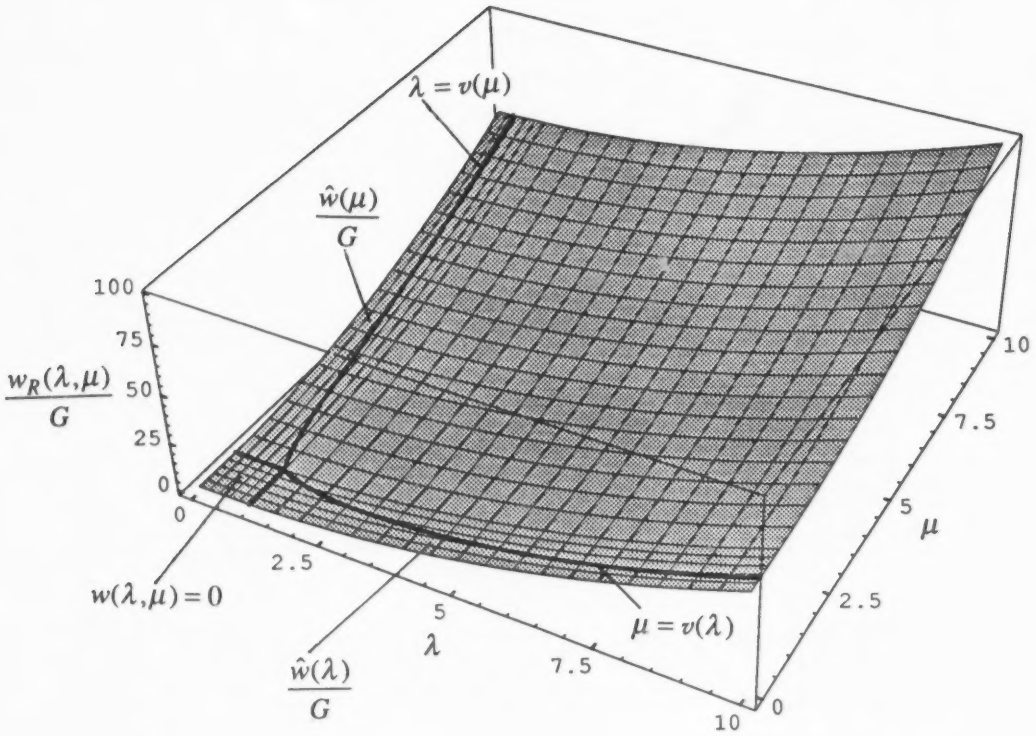

Fig. 4.1b Relaxed neo-Hookean strain energy function,
for $0 \le \lambda, \mu \le 10.0$

$$w(\lambda,\mu) = G\sum_{r=1}^{3} g_r[\lambda^{\alpha_r} + \mu^{\alpha_r} + (\lambda\mu)^{-\alpha_r} - 3]/\alpha_r, \tag{4.5}$$

where again $G = \tilde{G}h$. This is represented in Fig. 4.2a.

As in the previous case, in the wrinkled regions, where $\lambda > 1$, $\mu \le v(\lambda) \equiv \lambda^{-1/2}$ or $\mu > 1$, $\lambda \le v(\mu) \equiv \mu^{-1/2}$, the strain energy in uniaxial tension $\hat{w}(\lambda)$, respectively $\hat{w}(\mu)$, is given by

$$\hat{w}(x) = w(x, x^{-1/2}) = G\sum_{r=1}^{3} g_r(x^{\alpha_r} + 2x^{-\alpha_r/2} - 3)/\alpha_r. \tag{4.6}$$

The relaxed Ogden strain energy $w_R(\lambda,\mu)$ is then constructed according to (2.53). A graphical representation is shown in Fig. 4.2b.

A comparison between Fig. 4.1a and Fig. 4.2a, as well as between Fig. 4.1b and Fig. 4.2b shows that at stretches larger than some moderate values, the Ogden material gives much larger values of the strain energy per unit initial area than the neo-Hookean material (for the same λ and μ).

Planar as well as 3D deformations of the membranes were considered, starting in all cases from a plane reference configuration. Square, rectangular, circular-annular, and square-annular geometrical shapes of the membrane were analyzed, along with hybrid shapes such as square sheet with centrally located circular hole, and rectangular sheet with a slot.

Displacement boundary conditions as well as mixed displacement/null-traction boundary conditions were used.

In some of the problems certain axes of symmetry are readily apparent, but no prior assumption was made about the symmetry of the solution. In this respect, consideration was given to Silling's observations on the asymmetries that may develop when non-relaxed strain energies are used, symmetry axes notwithstanding (Silling, 1988b). However, it has been found that the solutions obtained using the relaxed energy *do*

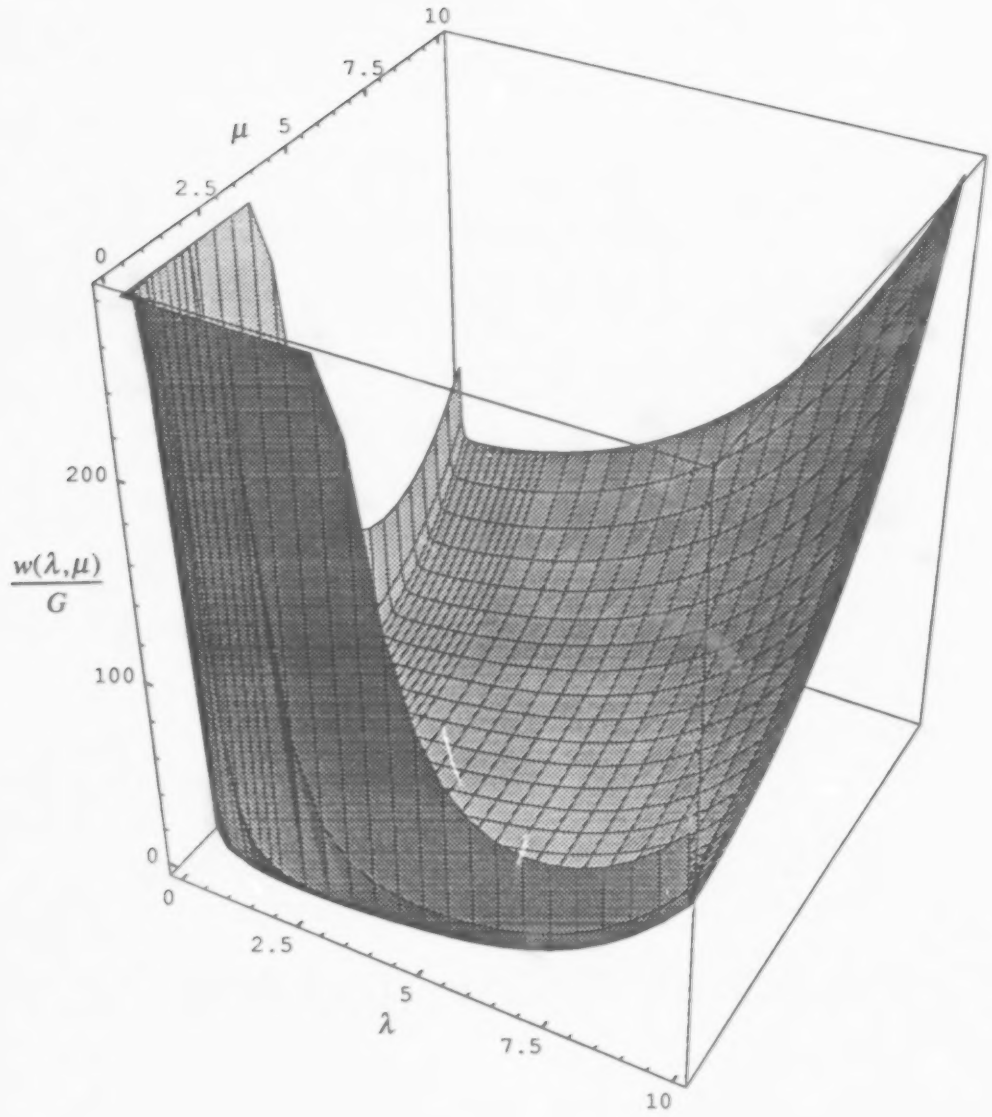

Fig. 4.2a Original Ogden strain energy function,
for $0.02 \le \lambda, \mu \le 10.0$

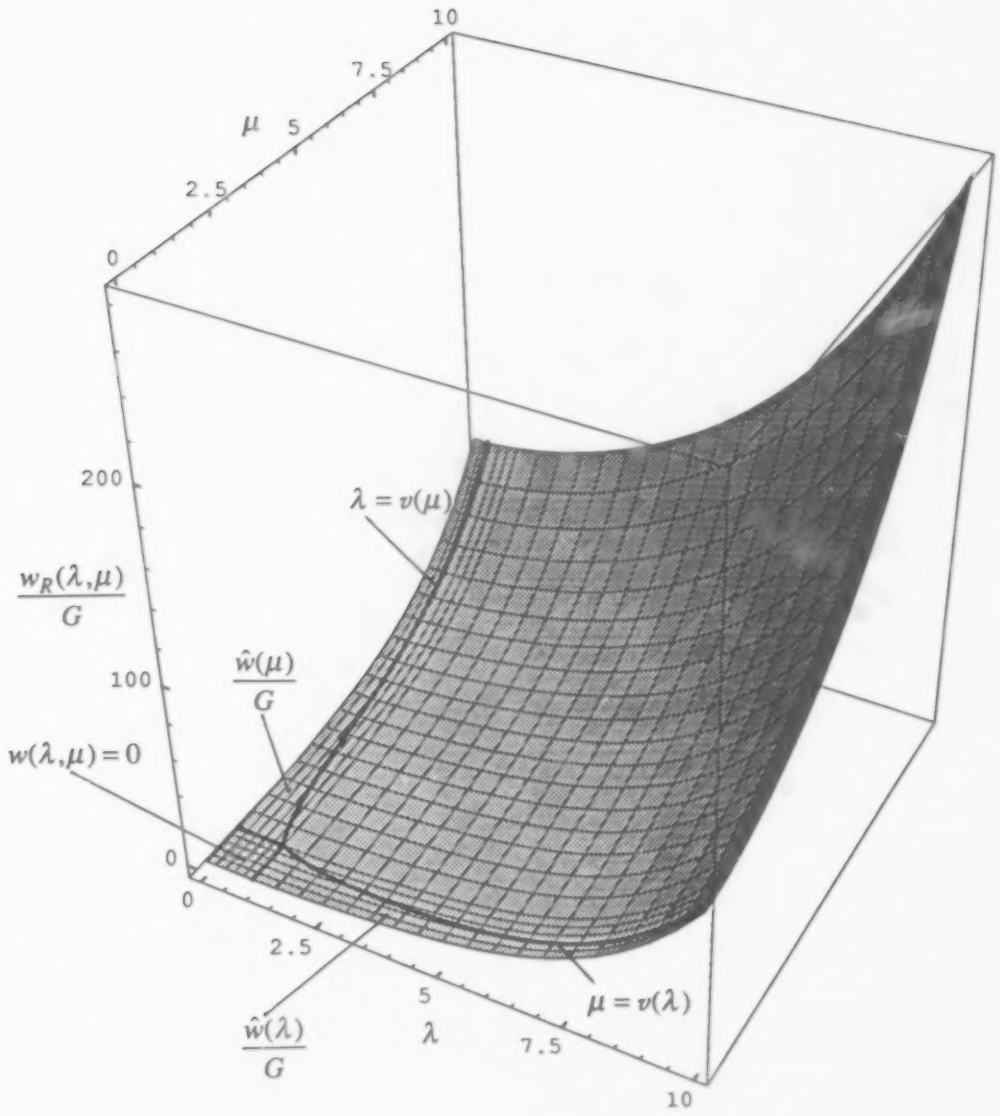

Fig. 4.2b Relaxed Ogden strain energy function,
for $0 \le \lambda, \mu \le 10.0$

exhibit symmetry. Moreover, the equilibria appear to be wholly insensitive to variations in the initial data. In contrast, equilibria are highly sensitive to these data when the original (non-relaxed) energy is used.

Cases of zero distributed loading, uniform pressure loading and loading by concentrated forces were studied.

Stability and convergence of the DR solution $\boldsymbol{u}$ to the solution $\tilde{\boldsymbol{u}}$ of the equilibrium equation (3.1) have been ensured by an adequate choice of the iteration parameters, as described in § 3.4.

The magnitude of the spatial discretization error of the method is given by the local truncation error. As shown in § 3.3.2, this is of $O(\varepsilon^2)$ for uniform rectangular meshes and $O(\varepsilon)$ for other types of meshes, where ε is a typical zone width. Graded rectangular interlacing meshes were used for most of the applications. For a few applications uniform rectangular interlacing meshes were considered to be more suitable. A refinement of the mesh is usually carried out until convergence of the solution is obtained. However, in all the applications the mesh has been refined beyond the needs of the convergence of the DR solution, especially in the zones where wrinkling occurred.

To reduce the rounding errors introduced during the computation, double precision has been exclusively employed.

Comparing the two methods, adaptive versus non-adaptive, the efficiency in terms of CPU time is superior for the adaptive method, since the optimum convergence conditions are satisfied at each time step. However, in terms of programming time, the non-adaptive version is by far more efficient, since it does not require the adaptation of the code for the computation of the stiffness matrices to the mesh and the geometry of the boundary of every particular problem; this is a very time consuming and labor-intensive operation. Since both methods yield approximately the same DR solution - within reasonable limits of accuracy - the non-adaptive version has been preferred in most cases.

A non-dimensional form of the algorithm (3.52) was used. This was obtained by non-dimensionalizing equation (3.3) by a force scale consisting of the product of the

material constant G in the expression of the strain energy and a characteristic length, specific for each problem. The numerical value of the constant G was obtained from $G = \tilde{G}h$. For a thickness of the membrane $h = 0.1\,\text{mm}$ and a shear modulus for infinitesimal strain $\tilde{G} = 4\,\text{kg}/\text{cm}^2 \cong 4\times10^5\,\text{N}/\text{m}^2$ (Varga, 1966), the resulting G is 40 N/m..

The DR solution was considered reasonably accurate if the residual at step (VII) of the algorithm (3.52) satisfied $\max_i \left|\mathcal{R}_i^n\right| < \varepsilon$, where $\varepsilon = 10^{-6}$ was chosen in the computations.

4.2 Neo-Hookean Membranes Subjected to Displacement Boundary Conditions

4.2.1 Simple Shear of Square Membrane

A unit square Ω of a membrane is considered as the reference configuration. The boundary $\partial\Omega$ is subjected to the planar simple shear deformation $\boldsymbol{x} \to \boldsymbol{r}(\boldsymbol{x}) = \tilde{\boldsymbol{F}}\boldsymbol{x}$, where $\tilde{\boldsymbol{F}} = \Delta + \gamma \boldsymbol{e}_1 \otimes \boldsymbol{e}_2$, and $\gamma = 1/\sqrt{3}$; thus the shear angle is $\pi/6$. The relaxed energy is defined in such a way that in the interior of the region Ω, the homogeneous deformation with gradient $\tilde{\boldsymbol{F}}$ minimizes the energy absolutely. This deformation is trivially in equilibrium. Using the relaxed energy, it is found that the entire membrane is wrinkled, with a total strain energy E/G = 0.5438. The same results are obtained by using the adaptive DR method, regardless of the degree of mesh refinement or the choice of initial conditions. For a uniform rectangular 21 x 21 mesh, the reference configuration is shown in Fig. 4.3a, and the deformed configuration in Fig. 4.3b. The trajectories of tensile stress are represented by dashed lines at zone-centered points, indicating wrinkling over the entire membrane. The principal stretches obtained from the

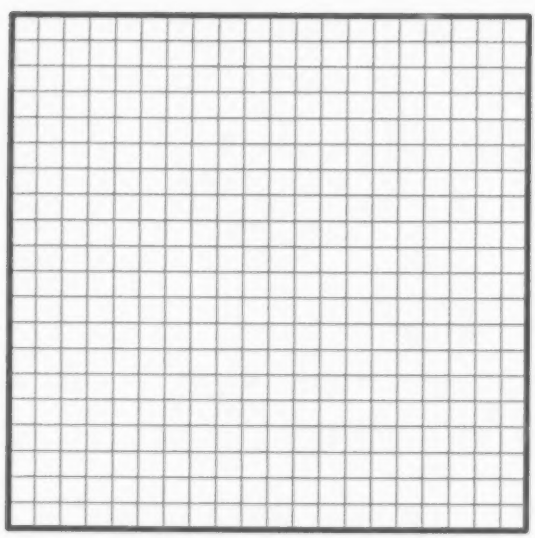

Fig. 4.3a Square membrane; meshed reference configuration

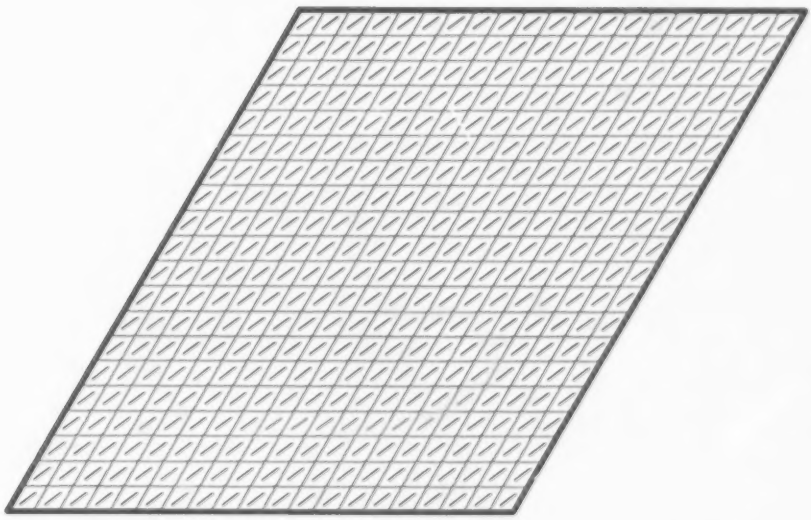

Fig. 4.3b Square membrane in simple shear; deformed configuration

computation are $\lambda = 1.33$ and $\mu = 0.75$.

A strong sensitivity to initial data is found in the same boundary value problem when the original strain energy is employed. If purely planar initial conditions are chosen, with no transverse displacements, then homogeneous equilibria with deformation gradient $\tilde{F}$ are always obtained. The associated stress has a compressive principal value, so the deformation is unstable with respect to out-of-plane perturbations, but such perturbations are never generated as the solution advances in time. The total equilibrium energy is found to be $E/G = 0.6667$. In contrast, when the initial data contain non-zero transverse displacement components, the equilibria obtained appear to be weakly dependent on their nodal variations. In such cases the solutions exhibit a strong dependence on the mesh, the deformed surfaces being corrugated or wrinkled, and the characteristic wave length of the wrinkles decreasing with mesh refinement. Successive refinement yields equilibria whose total energies approach the relaxed energy from above. For example, a 26 x 26 uniform rectangular mesh yields a total energy ranging from 0.5527 to 0.5529, depending on the choice of initial data. The equilibrium stress has compressive and tensile components that are comparable in magnitude. For a 51 x 51 uniform mesh, the total equilibrium energy is 0.5484, with minor fluctuations due to variations in initial data. In this case, the tensile principal stress is several orders of magnitude larger than the compressive component. A cross section through the deformed mesh is shown in Fig. 4.4.

Thus it appears that when the original energy is used, successive mesh refinement furnishes equilibria whose energies tend to the relaxed energy, provided that the initial data include transverse displacements. The equilibria exhibit a wrinkly structure that is reminiscent of the minimizing sequences constructed in section 2.4. These results support Ball's conjecture (Ball 1984) that minimizing sequences may be realized, to some degree of approximation, by the dynamics (see also Swart and Holmes, 1992).

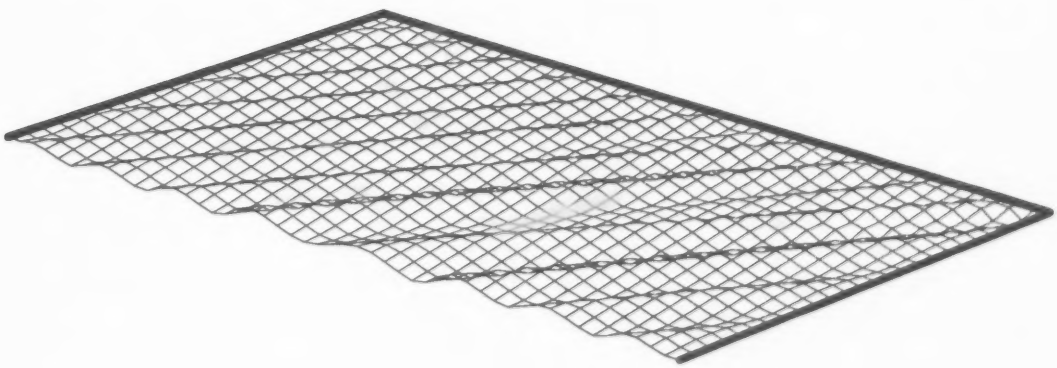

Fig. 4.4 Mesh dependent wrinkling
for membranewith original, unrelaxed strain energy
and boundary subjected to a simple shear deformation

4.2.2 Plane Twisting of Annular Membranes

The problem of twisting an annular membrane bounded by concentric circles was considered by Reissner (1938) in his original formulation of the mathematical theory of tension fields. A similar problem was reconsidered much later by Stein and Hedgepeth (1961) and Mikulas (1964). Li and Steigmann (1993) recently extended the analysis of this problem to finite deformations for a certain class of strain energy functions.

A neo-Hookean annular membrane bounded by concentric circles is considered first. The graded mesh shown in Fig. 4.5a was used. The ratio of the radii of the internal and external circular boundaries was taken to be 0.5. Holding the external boundary fixed, the inner boundary is rotated counterclockwise through an angle of 5°. The deformed configuration of the mesh is represented with continuous lines in Fig. 4.5b. The dashed lines at the zone centered points of the mesh layers adjacent to the inner boundary indicate the trajectories of tensile stress in the wrinkled part of the membrane. The extent of the wrinkled region can be also seen in Fig. 4.5c, where the mesh has been removed for clarity. The membrane is tense elsewhere. The maximum principal stretch in the solution was 1.13, and occurred at the zone-centered points situated on a circle immediately adjacent to the inner boundary.

A similar problem was solved for an annular membrane with square boundaries. The ratio of the sides of the interior square to the exterior square is 0.35. The graded rectangular mesh shown in Fig. 4.6a was used. As in the previous case, the exterior boundary is fixed and the interior boundary is rotated counterclockwise through an angle of 5°. The deformed mesh is shown in Fig. 4.6b, where the tension trajectories in the wrinkled region are also indicated. The membrane is tense elsewhere, as in the previous example. The DR method cannot be used to detect the expected stretch singularities at the corners of the inner square, because the stretches are evaluated at zone-centered points. The largest computed stretch is 1.17 and occurs at the zone-centered points adjacent to the four corners of the inner square.

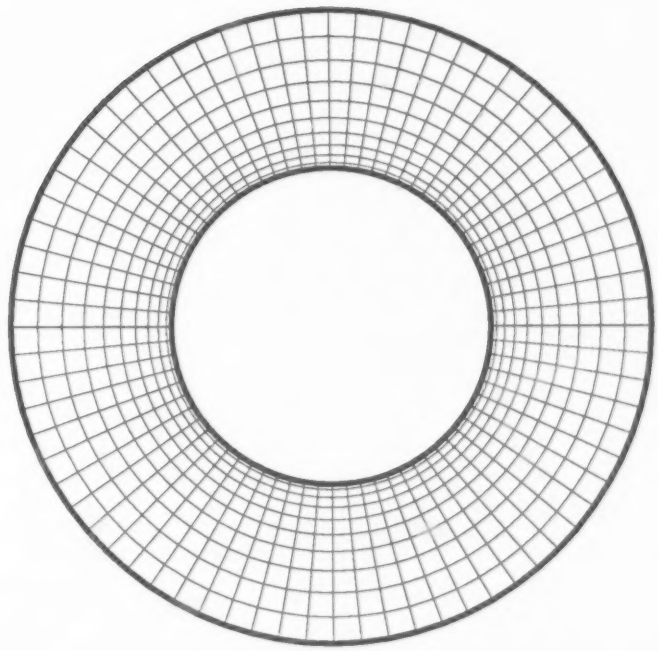

Fig. 4.5a Circular annular membrane; meshed reference configuration

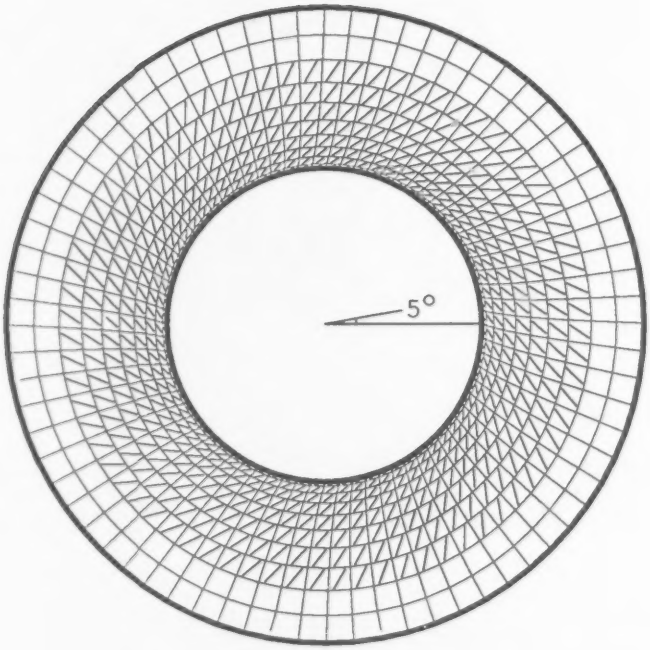

Fig. 4.5b Plane twisting of circular annular membrane;
deformed configuration

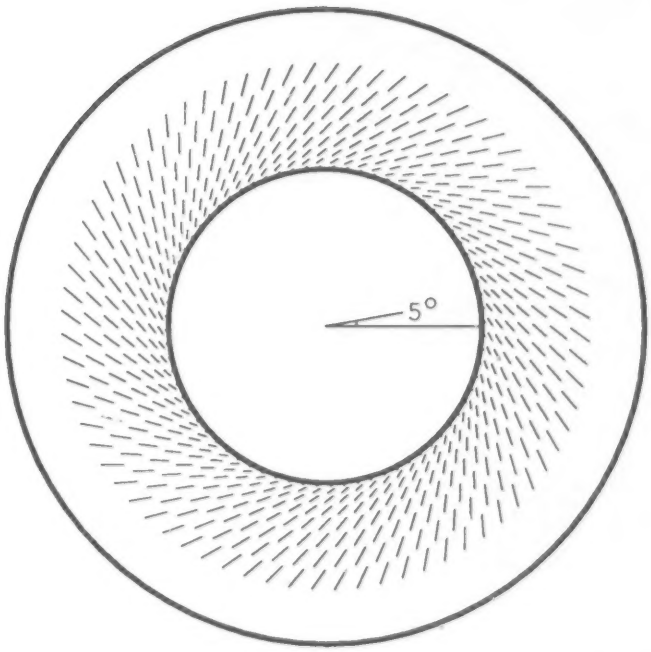

Fig. 4.5c Plane twisting of circular annular membrane; deformed configuration, mesh removed

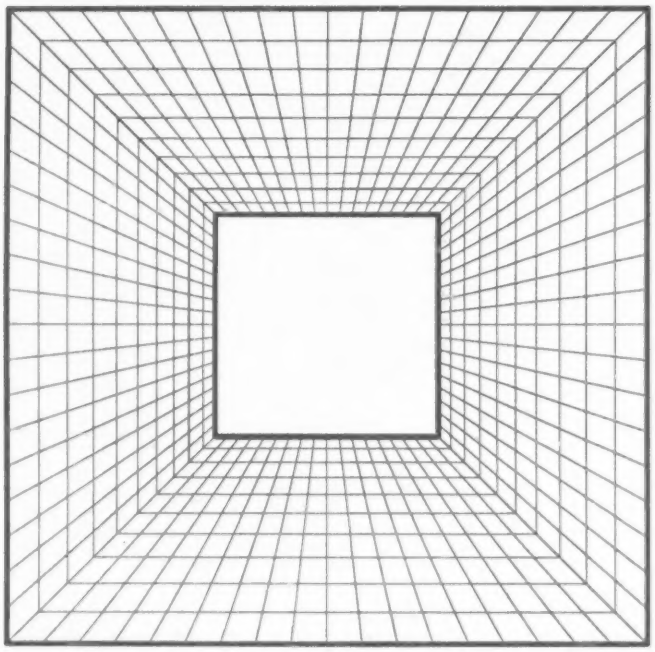

Fig. 4.6a Square annular membrane; meshed reference configuration

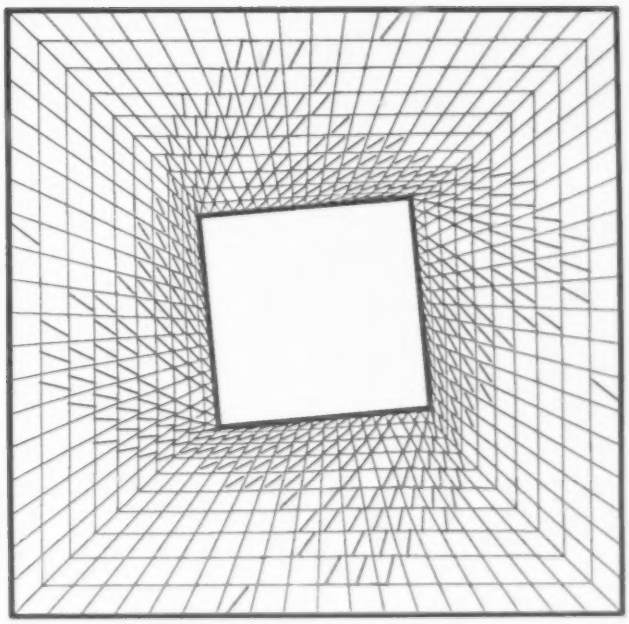

Fig. 4.6b Plane twisting of square annular membrane; deformed configuration

4.2.3 Combined Twist and Lateral Deflection of Annular Membranes

The circular annular membrane with the ratio of the radii of the internal and external boundaries of 0.5, and with the meshed reference configuration shown in Fig. 4.5a is considered. Holding the external boundary fixed, the ratio of the radii is reduced to 0.25. This intermediate deformed configuration is represented in Fig. 4.7a. Wrinkling occurs in a zone immediately adjacent to the inner boundary. The radial tension trajectories indicate the extent of the wrinkled region. Fig. 4.7b shows the deformed configuration with the mesh removed for clarity. Next, the inner boundary is displaced vertically by an amount equal to the radius of the external boundary. As can be seen in Fig. 4.7c, the extent of the wrinkled region decreased. This is followed by a counterclockwise rotation of the inner boundary through an angle of 90°. The deformed configuration of the mesh is shown in Fig. 4.7d, the tension trajectories indicating an increase in the width of the wrinkled region. The membrane is tense elsewhere. It was found that the extent of wrinkling increased with the increase in rotation angle and diminished with increasing lateral displacement. This behavior is in qualitative agreement with the analysis of Roxburgh, Steigmann and Tait (1993), in which axisymmetry was assumed at the outset, and a more refined strain energy function was used.

The maximum principal stretch computed increased from 1.82, in the solution represented in Fig. 4.7a, to 3.39 for the solution in Fig. 4.7c, and finally to 3.98 for the solution in Fig. 4.7d. It occured in all three cases on the circle of zone-centered points immediately adjacent to the inner boundary. The last two values are outside the range for which the neo-Hookean material furnishes quantitative agreement with experimental data on rubber. For less severe deformations the stretches obtained are within this range. Nevertheless, the solution exhibited in Fig. 4.7d is useful for studying some qualitative aspects of the problem and for verifying the numerical method. In particular, one of the analytical results known from tension-field theory is that stress trajectories form families

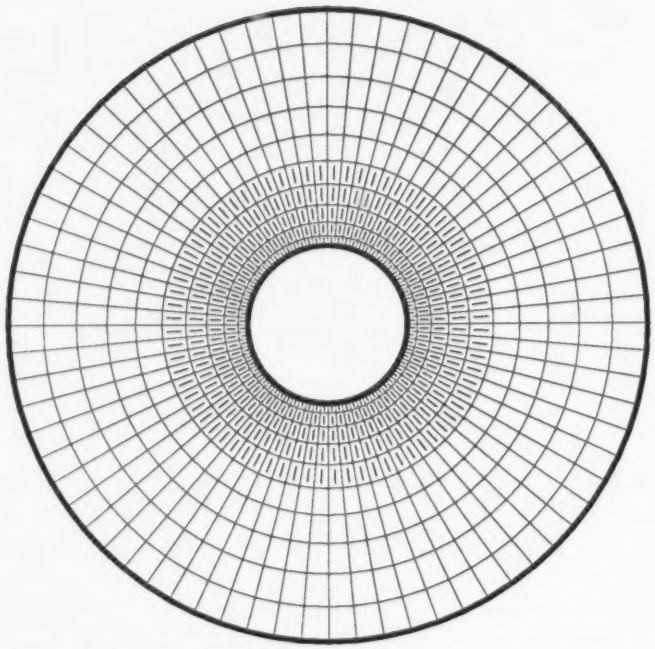

Fig. 4.7a Circular annular membrane; radial displacement and reduction in circumference of inner boundary; intermediate deformed configuration

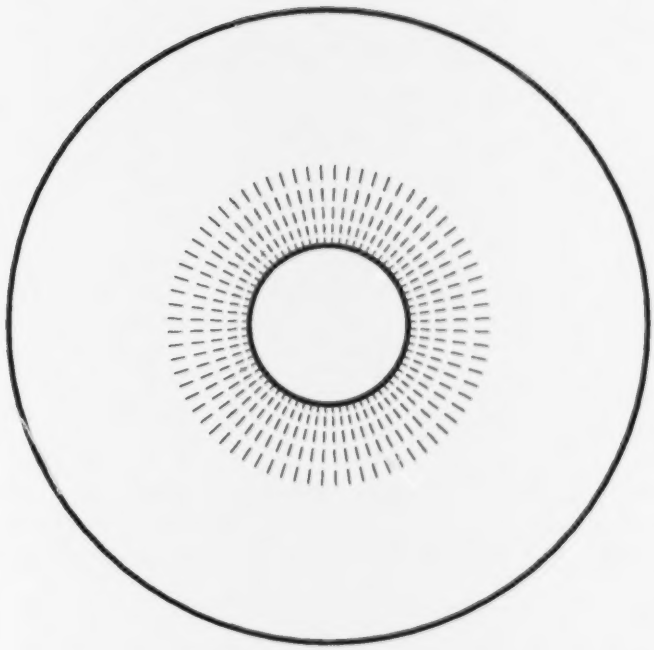

Fig. 4.7b Circular annular membrane; radial displacement and reduction in circumference of inner boundary; intermediate deformed configuration, mesh removed

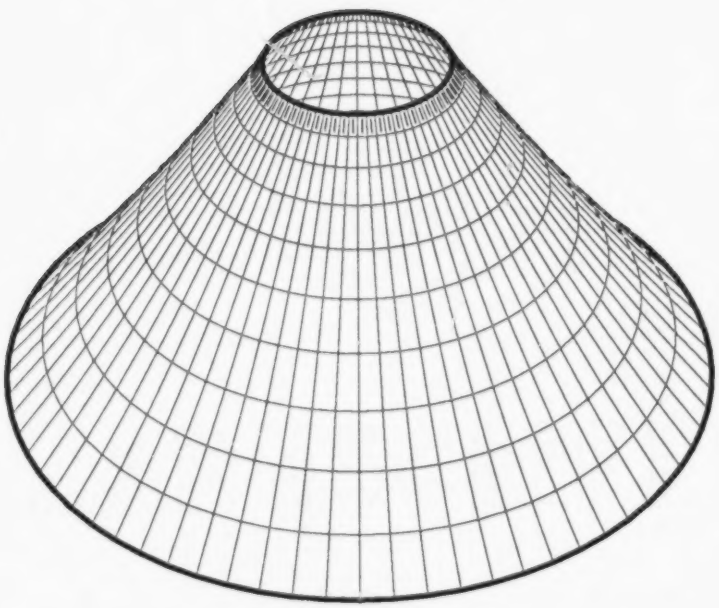

Fig. 4.7c Combined radial displacement and lateral deflection
of circular annular membrane; intermediate deformed configuration

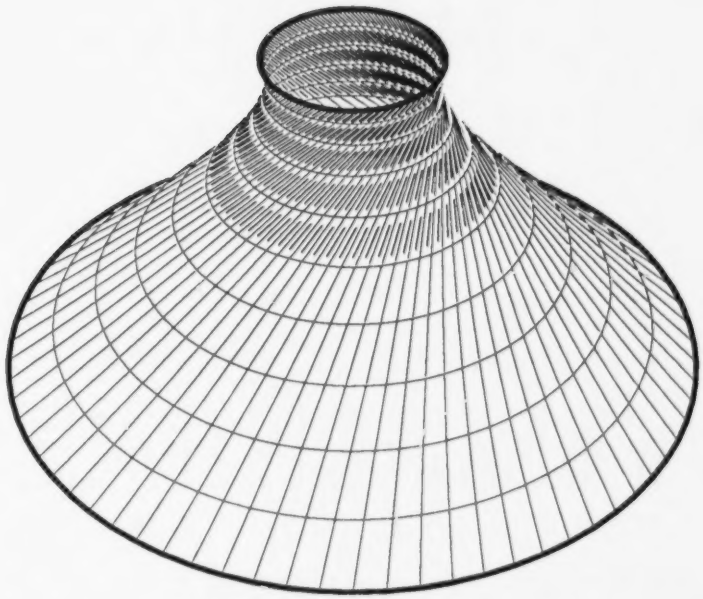

Fig. 4.7d Combined radial displacement, lateral deflection and twist of circular annular membrane; final deformed configuration

of straight lines on the deformed surface, independent of the form of the strain energy (Steigmann, 1990). For axisymmetric deformations, the surface must then be a sector of a single-sheet hyperboloid of revolution wherever it is wrinkled. The computed results conform to this requirement.

Another analytical result pertains to the variation of the stretch λ along a stress trajectory as a function of radius r in the reference configuration. According to this result the implicit relation (Steigmann, 1990)

$$r^2 = [a / f(\lambda)]^2 + (b / \lambda)^2, \tag{4.7}$$

is valid in the wrinkled region, where a and b are constants and $f(\lambda) = \hat{w}'(\lambda)$ is the stress-stretch relation in uniaxial tension. To use this relation, the values of λ are substituted on the extreme inner and outer circles of zone-centered points delimiting the wrinkled region. Then (4.7) yields two equations for the constants a^2 and b^2, and the relation between r^2 and λ may be plotted. This is given by the solid curve in Fig. 4.8, where r has been non-dimensionalized by the radius of the external boundary. By construction, the extreme zone-centered values are located at the endpoints of the analytical curve. The three intermediate values shown in Fig. 4.8 are taken from the computed solution at the remaining zone-centered points. The results indicate an acceptable degree of accuracy in the representation of the spatial variation of λ, despite the relative coarseness of the mesh.

For the annular membrane with square boundaries, the mesh in the reference configuration is shown in Fig. 4.6a. In this case the exterior boundary is fixed, the interior square is rotated counterclockwise through an angle of 90°, and simultaneously displaced vertically by an amount equal to one-half of the side of the outer boundary. The deformed mesh is shown in Fig. 4.9, where the tension trajectories in the wrinkled regions are also indicated. The membrane is tense elsewhere, as in the previous example.

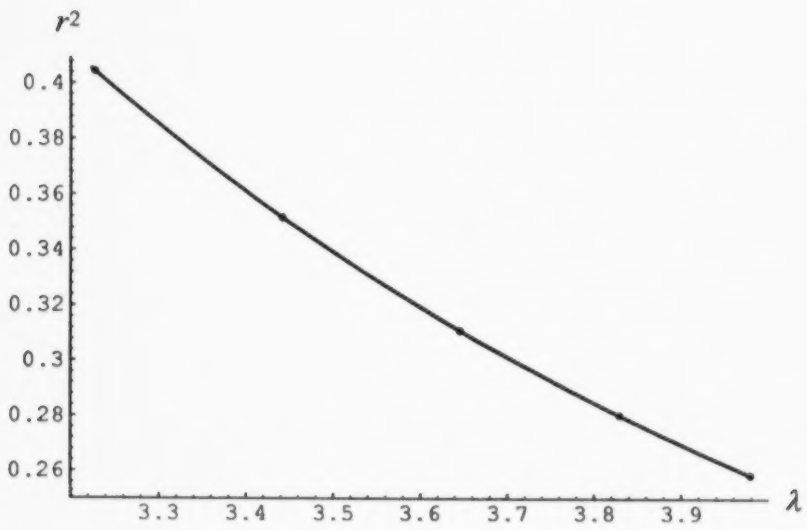

Fig. 4.8 Variation of stretch λ along a tension trajectory with initial radius r

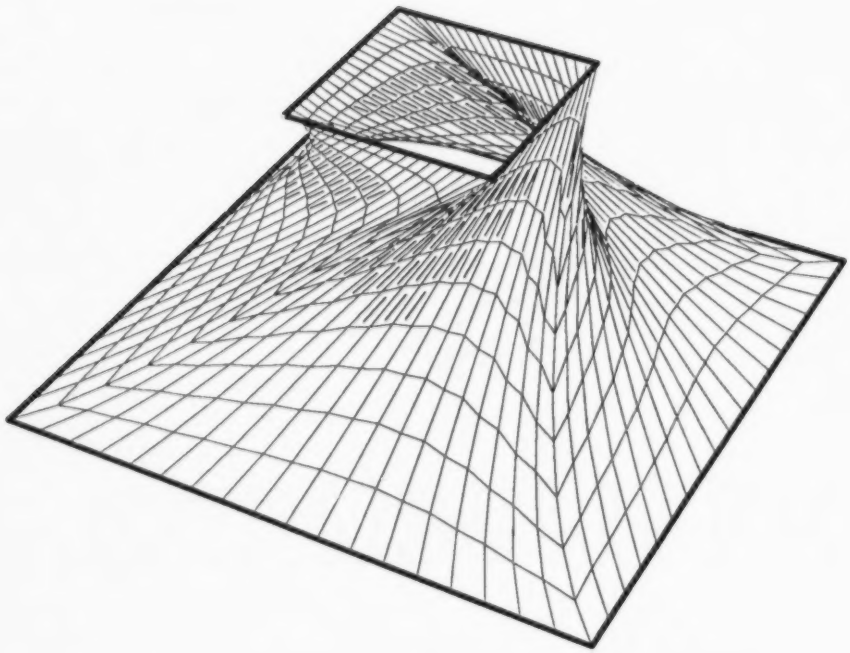

Fig. 4.9 Combined twist and lateral deflection of square annular membrane; deformed configuration

Although no detailed analytical results are available for comparison in this case, it is observed that the tension trajectories again form families of straight lines, as required by the analytical theory. As mentioned in § 4.2.2, the adaptive DR method cannot be used to detect the expected stretch singularities at the corners of the inner square, because the stretches are evaluated at zone-centered points. The largest computed stretch is 5.63 and occurs at the zone-centered points nearest the four corners of the inner square.

4.3 Neo-Hookean Membranes Subjected to Mixed Displacement/ Null Traction Boundary Conditions

4.3.1 Combined Stretching and Shearing of Rectangular Membrane with Traction-Free Lateral Boundaries

The plane deformation involving combined stretching and shearing of a rectangular strip with ratio of height to length of 0.370 is investigated. The lateral boundaries are traction-free. The meshed reference configuration is represented in Fig. 4.10a. The sheet is first deformed by holding the lower boundary fixed and displacing the upper boundary normal to itself so that the perpendicular distance between the boundaries increases by 20%, to 0.444. Holding this distance constant, the upper boundary is then translated to the right until the chord connecting the left endpoints of the boundaries forms an angle of 30° with the vertical. The deformed mesh is shown in Fig. 4.10b. The dashed lines again indicate trajectories of tensile stress in the wrinkled region, which nearly covers the entire membrane. The tense regions are confined to thin layers near the traction-free boundaries and to small zones at the lower left and upper right corners. The

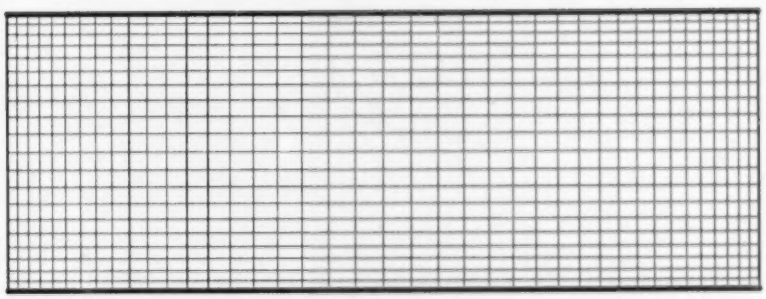

Fig. 4.10a Rectangular membrane with traction-free lateral boundaries; reference configuration

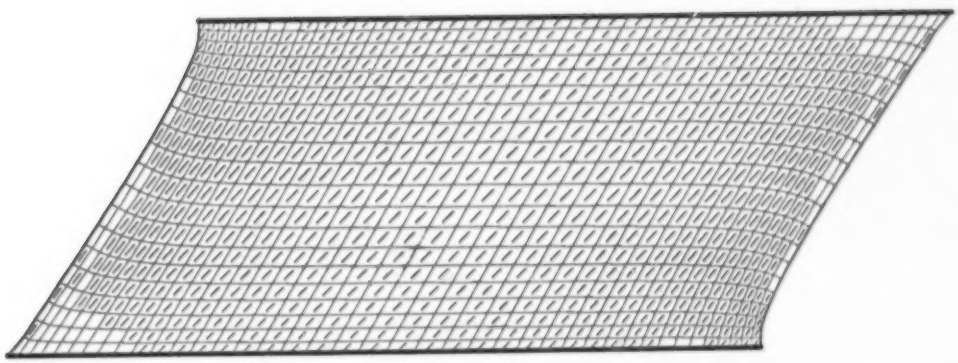

Fig. 4.10b Combined stretching (20% of height) and shearing (30°) of rectangular membrane with traction-free lateral boundaries; intermediate deformed configuration

largest computed stretch is 2.38 and occurs at the zone-centered points, closest to these corners.

Next, the perpendicular distance between the upper and lower boundaries is adjusted to 0.481 (representing a 30% increase of the initial value), while holding the chord angle fixed. The result is that wrinkling in the interior of the sheet is suppressed (Fig. 4.10c). This effect is similar to the competing influences of twist and transverse displacement observed in the annular membrane. The maximum computed stretch of 2.53 is located as previously at the zone centered points adjacent to the lower left and upper right corners.

Then, the chord angle is increased to 45° without altering the spacing between the boundaries. As expected, this substantially increases the extent of wrinkling. In this latest configuration the maximum stretch is 3.29 and occurs at the same location as in the previous two cases (Fig. 4.10d).

Finally, the case of shearing with no prestretch is considered. The upper boundary is translated to the right until the cord forms an angle of 30° with the vertical, while the length of the chord is maintained constant. The deformed configuration is represented in Fig. 4.10e. The wrinkled zone has the shape of a parallelogram, covering the main part of the membrane. Two triangular-shaped slack regions can be identified at the upper left and lower right corners. The presence of two narrow tense regions immediately adjacent to the lower third of the left traction-free boundary, respectively to the upper third of the right traction-free boundary is also noticed. To distinguish these, single dashes are used at the centers of the zones to indicate stress trajectories in the wrinkled regions and crosses to indicate the principal stress directions in tense regions. The slack regions do not contain markings of either type. Details of the deformation near the left traction-free boundary are shown in Fig. 4.10f. The largest computed stretch is 1.826, and occurs in the tense regions, at the zone-centered points closest to the lower left and upper right corners.

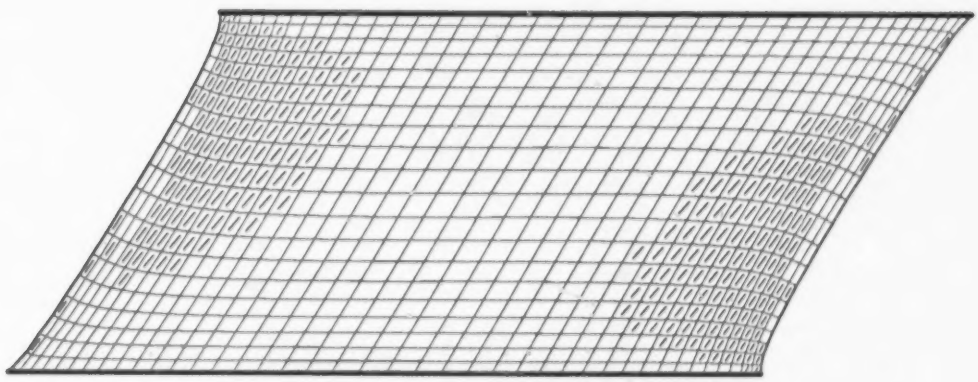

Fig. 4.10c Combined stretching (30% of height) and shearing (30°) of rectangular membrane with traction-free lateral boundaries; intermediate deformed configuration

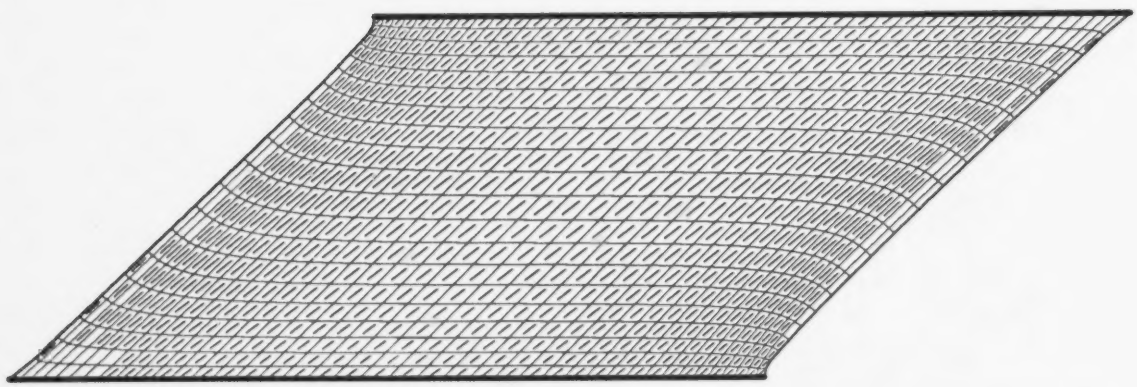

Fig. 4.10d Combined stretching (30% of height) and shearing (45°) of rectangular membrane with traction-free lateral boundaries; final deformed configuration

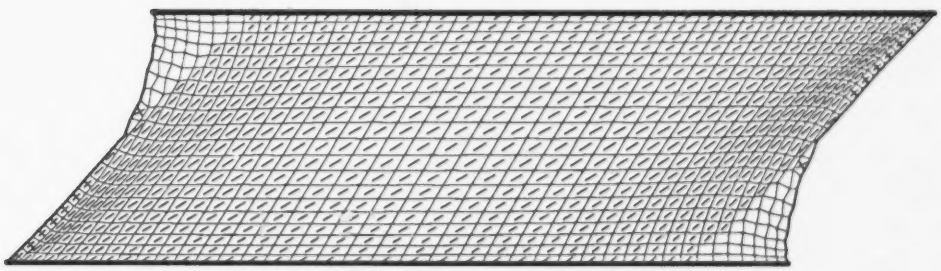

Fig. 4.10e Shearing (30°) with no prestretch of rectangular membrane with traction-free lateral boundaries; deformed configuration

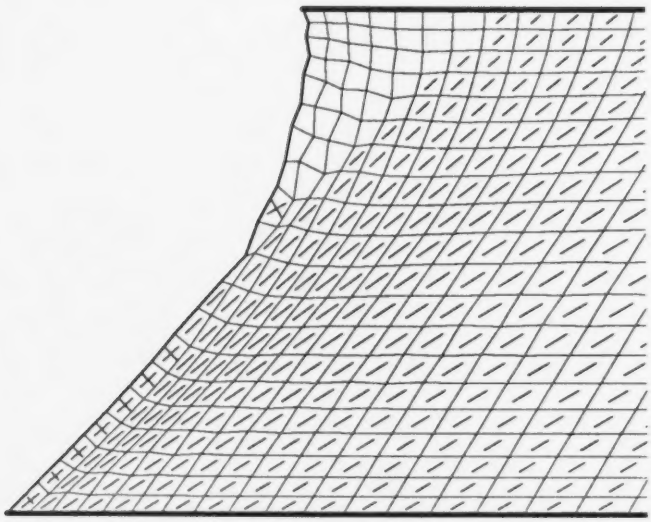

Fig. 4.10f Shearing (30°) with no prestretch
of rectangular membrane with traction-free lateral boundaries;
details of deformation in the proximity of the left free boundary

4.3.2 Shearing of Square Sheet with Traction-Free Circular Hole

The plane deformation induced by shearing of a square sheet with a traction-free circular central hole (Fig. 4.11a) is studied. The ratio of the hole diameter to the side of the square is 0.20. The sheet is deformed by mapping points $\boldsymbol{x}$ on the boundary onto the parallelogram described by $\boldsymbol{r}(\boldsymbol{x}) = \tilde{\boldsymbol{F}}\boldsymbol{x}$, where $\tilde{\boldsymbol{F}}$ is a simple shear with $\gamma = 1/\sqrt{3}$. Were it not for the presence of the hole, the minimum-energy deformation of the sheet would have the uniform gradient $\boldsymbol{F}(\boldsymbol{x}) = \tilde{\boldsymbol{F}}$, $\boldsymbol{x} \in \Omega$, and the deformed configuration for this homogeneous deformation would be as shown in Fig. 4.3b, which indicates complete wrinkling.

However, in the presence of the hole, the deformation is highly non-homogeneous, consisting of a complicated distribution of tense, wrinkled and slack (stress-free) regions. As in the previous case, single dashes are used at the centers of the zones to indicate stress trajectories in the wrinkled regions and crosses to indicate the principal stress directions in tense regions. The membrane is slack in regions that do not contain markings of either type. The deformed mesh together with the distribution of the tense, wrinkled and slack regions are represented in Fig. 4.11b, whereas Fig. 4.11c shows a mapping of this distribution onto the meshed reference configuration. In the present problem, the slack regions are confined to the immediate vicinities of the extreme ends of the deformed hole boundary. These can be seen more clearly in Fig. 4.11d. It should be noted that the relative lengths of the dashes are dictated by the mesh spacing and do not indicate the intensities of stress or strain. The maximum principal stretch λ in the sheet was 1.89 and occurred at zone-centered points about half way along the major axis of the hole. This can be seen in the contour plot in Fig. 4.11e, representing contour lines of equal λ. The localized slack regions near the extreme endpoints of the hole can be identified by being bounded by the contour line with $\lambda = 1.03$. The presence of these slack regions was also confirmed by experiments on a thin rubber sheet (see § 5, Fig. 5.3b).

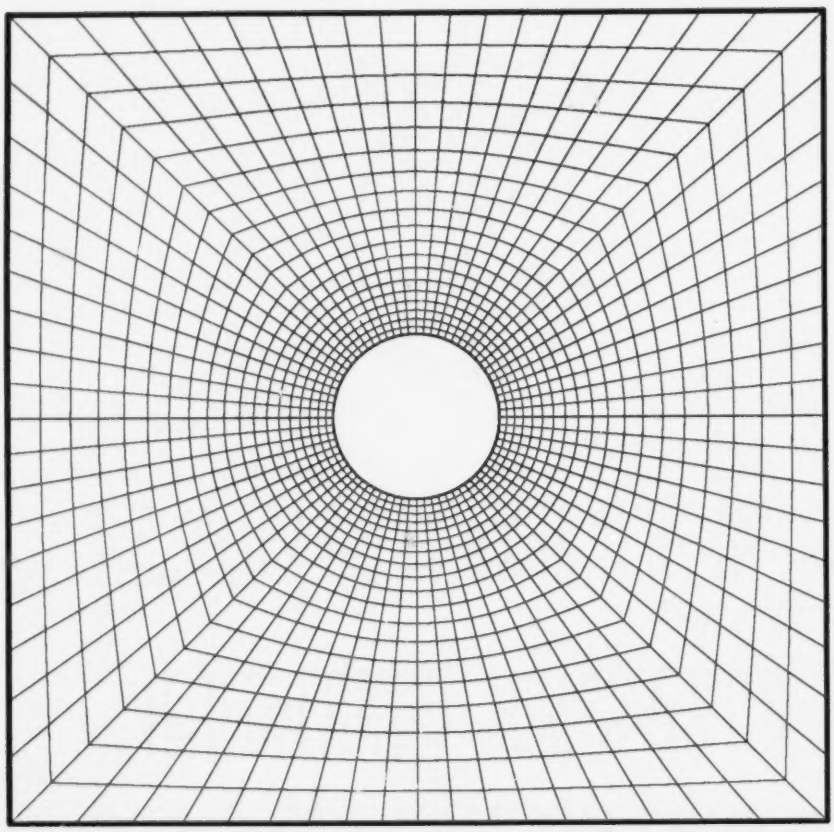

Fig. 4.11a Square sheet with circular hole; reference configuration

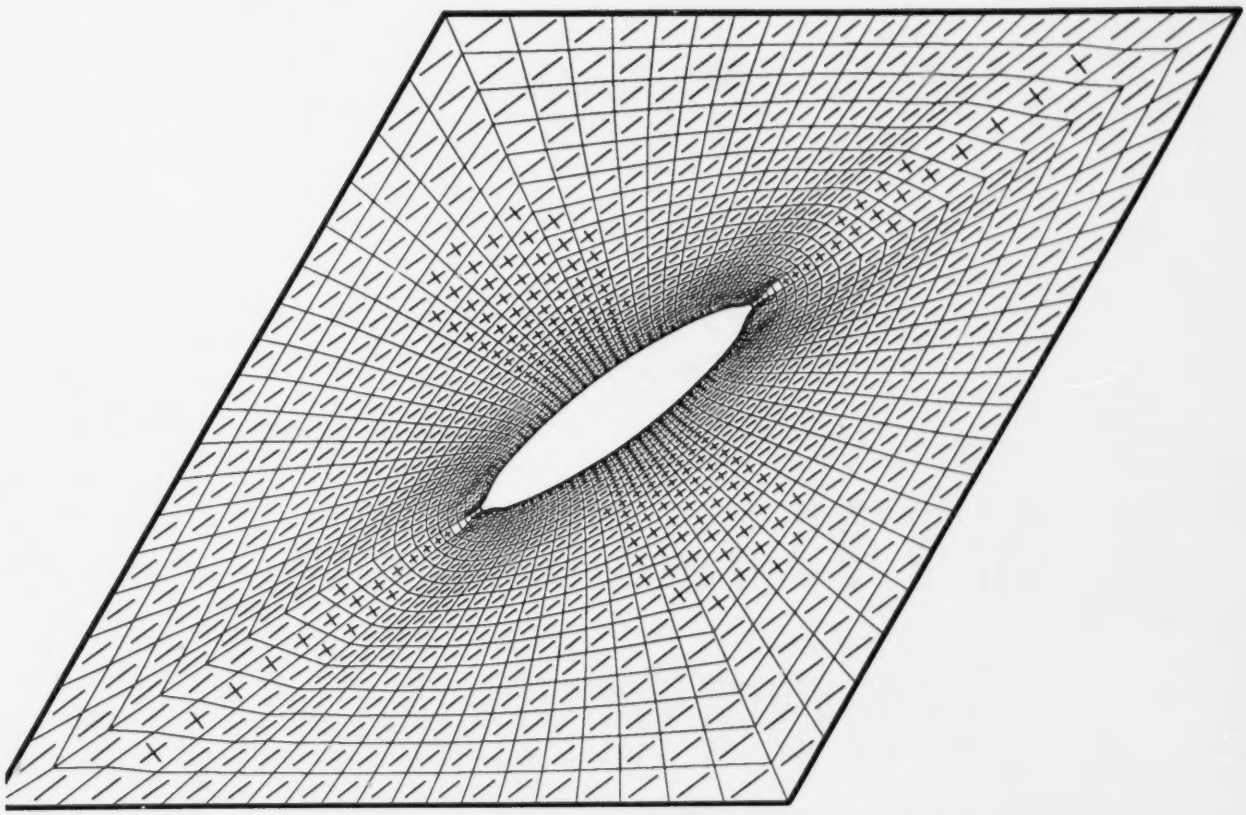

Fig. 4.11b Shearing of square sheet with traction-free circular hole; deformed configuration

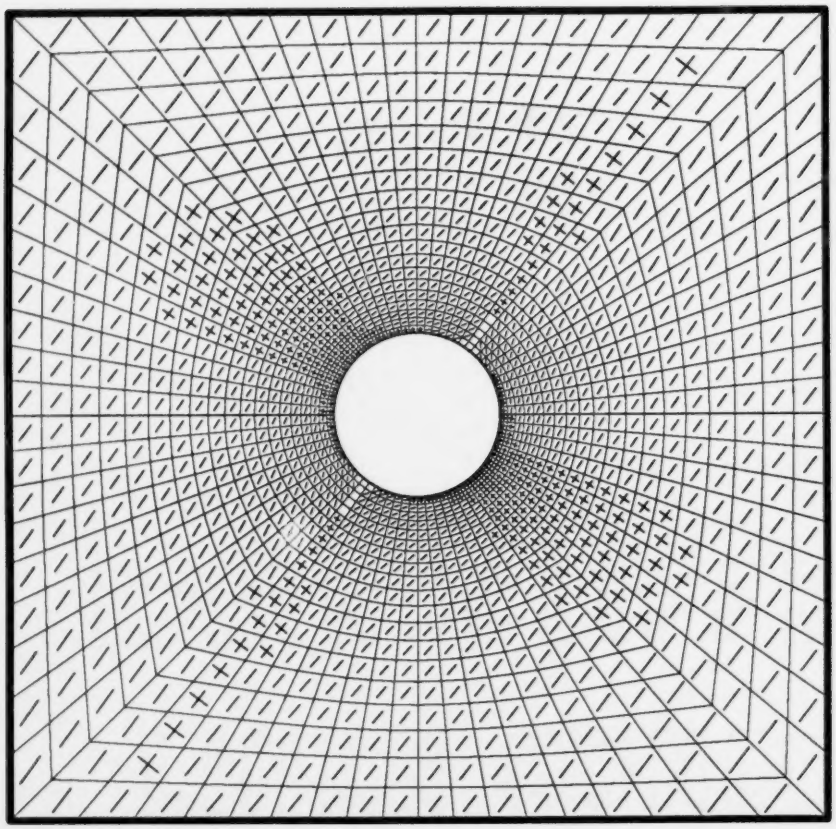

Fig. 4.11c Distribution of tense, wrinkled and slack regions mapped onto meshed reference configuration of square sheet with traction-free circular hole subjected to shearing

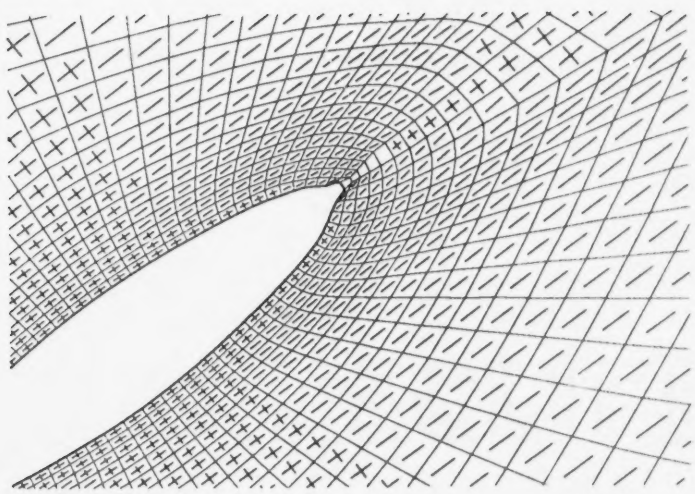

Fig. 4.11d Shearing of square sheet with traction-free circular hole; details of deformation around the hole

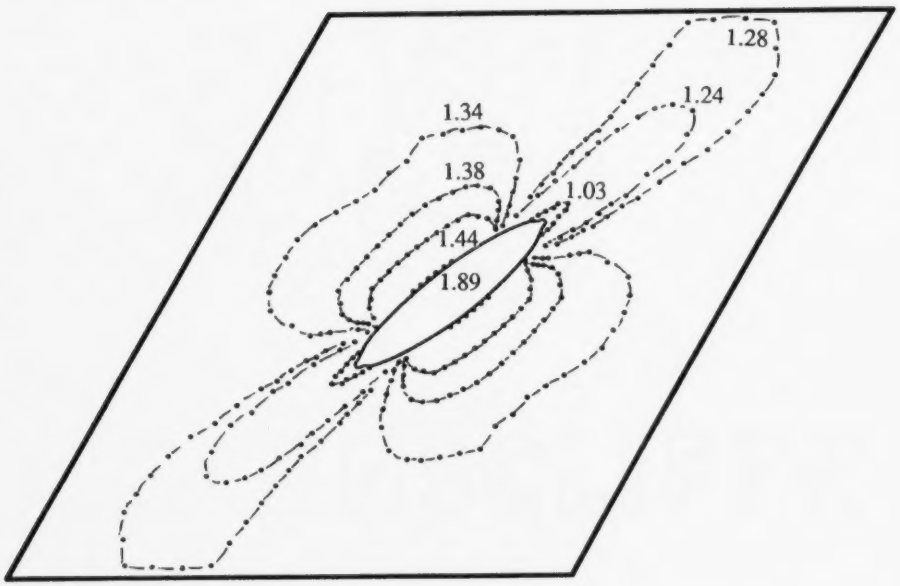

Fig. 4.11e Contour plot representing lines of equal principal stretch λ on deformed configuration of square sheet with traction-free circular hole

4.3.3 Stretching of Rectangular Sheet with Traction-Free Slot

A rectangular sheet containing a traction-free slot with semi-circular ends subjected to stretching is considered. All dimensions are scaled by the height of the rectangle in the reference configuration. The length of the base is 1.3 and the distance between the centres of the semi-circles at the ends of the slot is 0.3. The radii of these semi-circles are 0.015. The meshed reference configuration is shown in Fig. 4.12a. The parts of the mesh above and below the slot consist of rectangular regions with mesh spacings that vary abruptly from one region to the next. The transition from one region to another is accomplished by collapsing nodal points to form an interpolation layer with triangular zones. These layers are not shown in the figure.

The sheet is deformed by extending the lateral sides to a length of 1.2 and contracting the lower and upper sides to a length of 1.17 each. In the absence of the slot, the sheet would be homogeneously wrinkled with the tension trajectories oriented parallel to the lateral sides. The deformed mesh in the presence of the slot is shown in Fig. 4.12b. Four narrow zones of localized mesh distortion are observed in laterally opposed pairs near the ends of the slot.

Figure 4.12c shows the distributions of tense, wrinkled and slack regions in the entire sheet. The mesh has been removed for clarity. The narrow zones of distortion correspond to highly stressed wrinkled regions. The stress then decays in the transition to triangular slack regions above and below the slot. The results of the analysis indicate that the membrane is tense at the extreme endpoints of the slot. The maximum principal stretch occurs there and is equal to 2.23. The details of the solution in the vicinity of the slot can be seen in Fig. 4.12d. The presence of the slack regions was also confirmed by experiments on slotted rubber sheets.

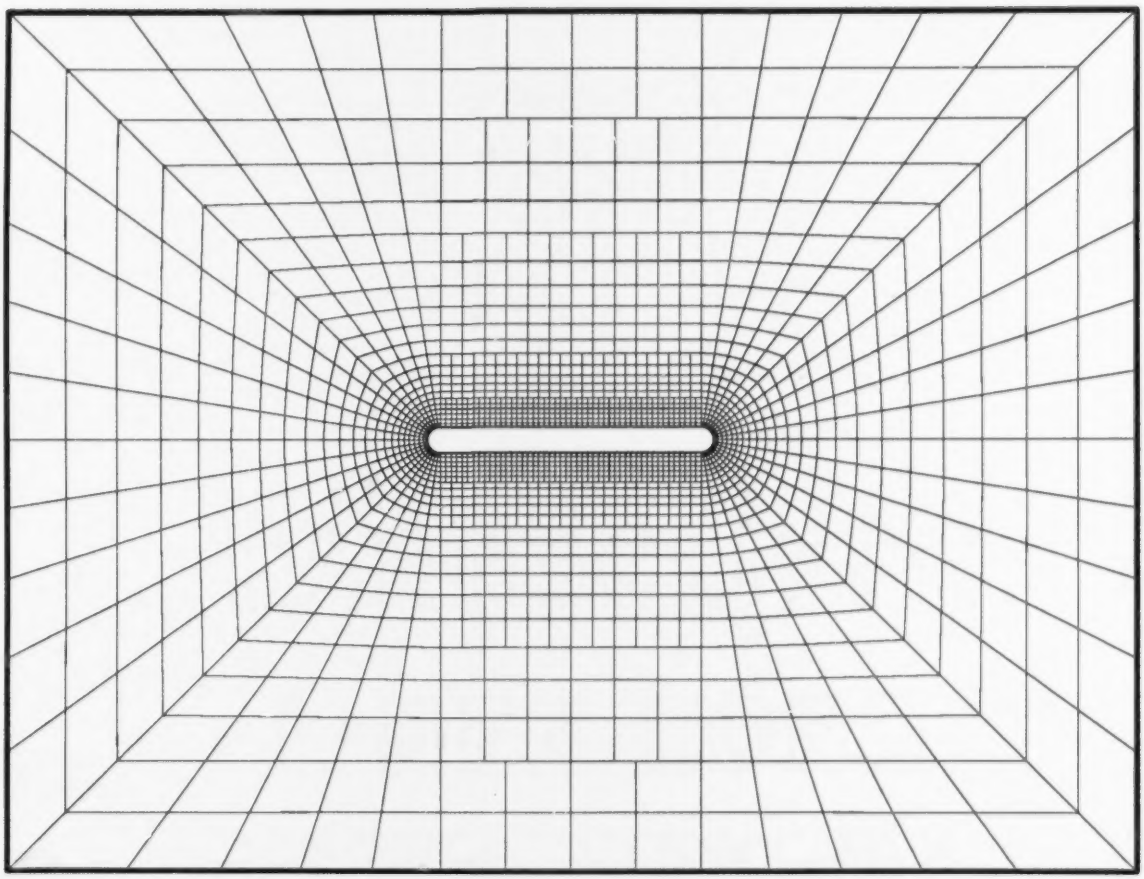

Fig. 4.12a Rectangular sheet with traction-free slot;
meshed reference configuration

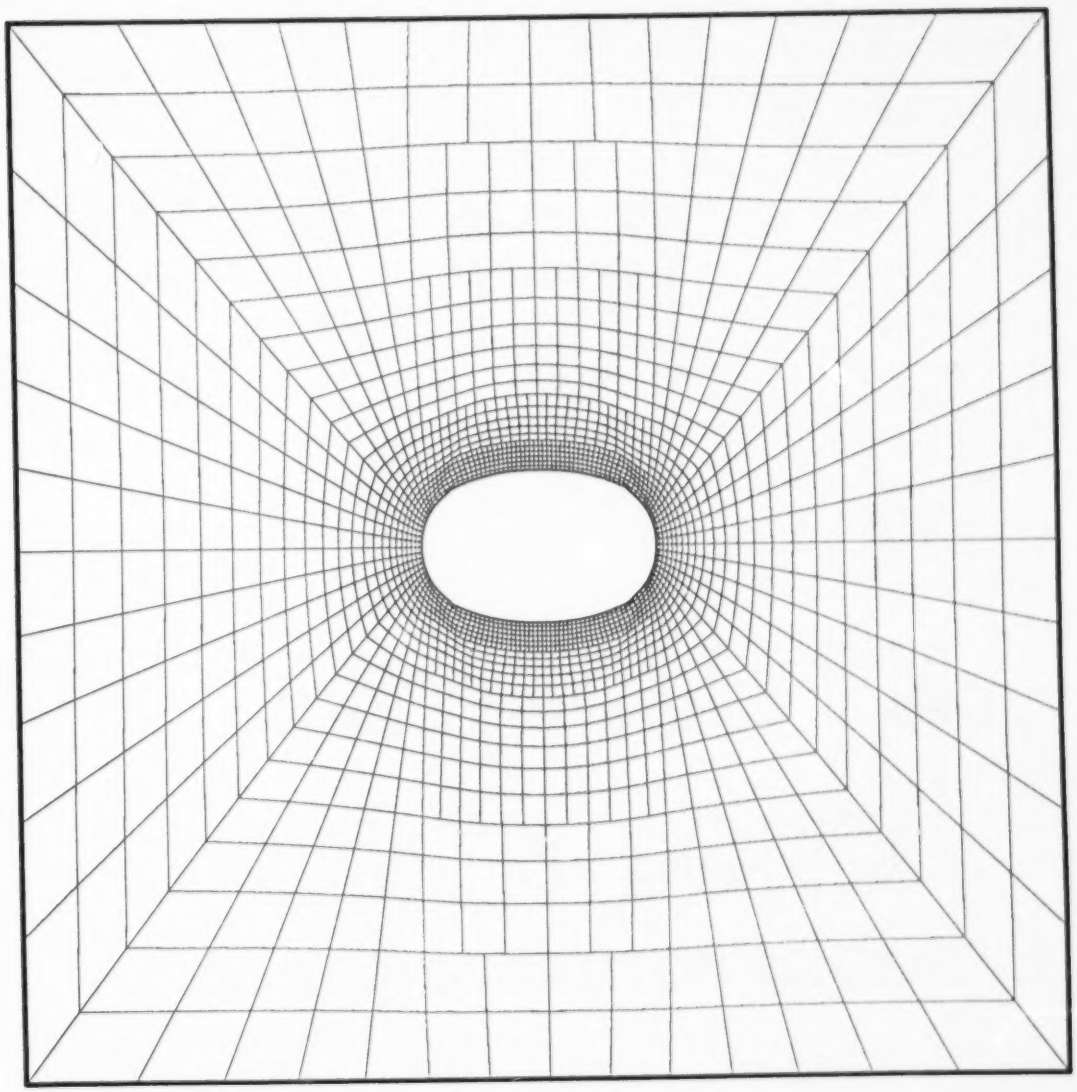

Fig. 4.12b Stretching of rectangular sheet with traction-free slot; deformed mesh

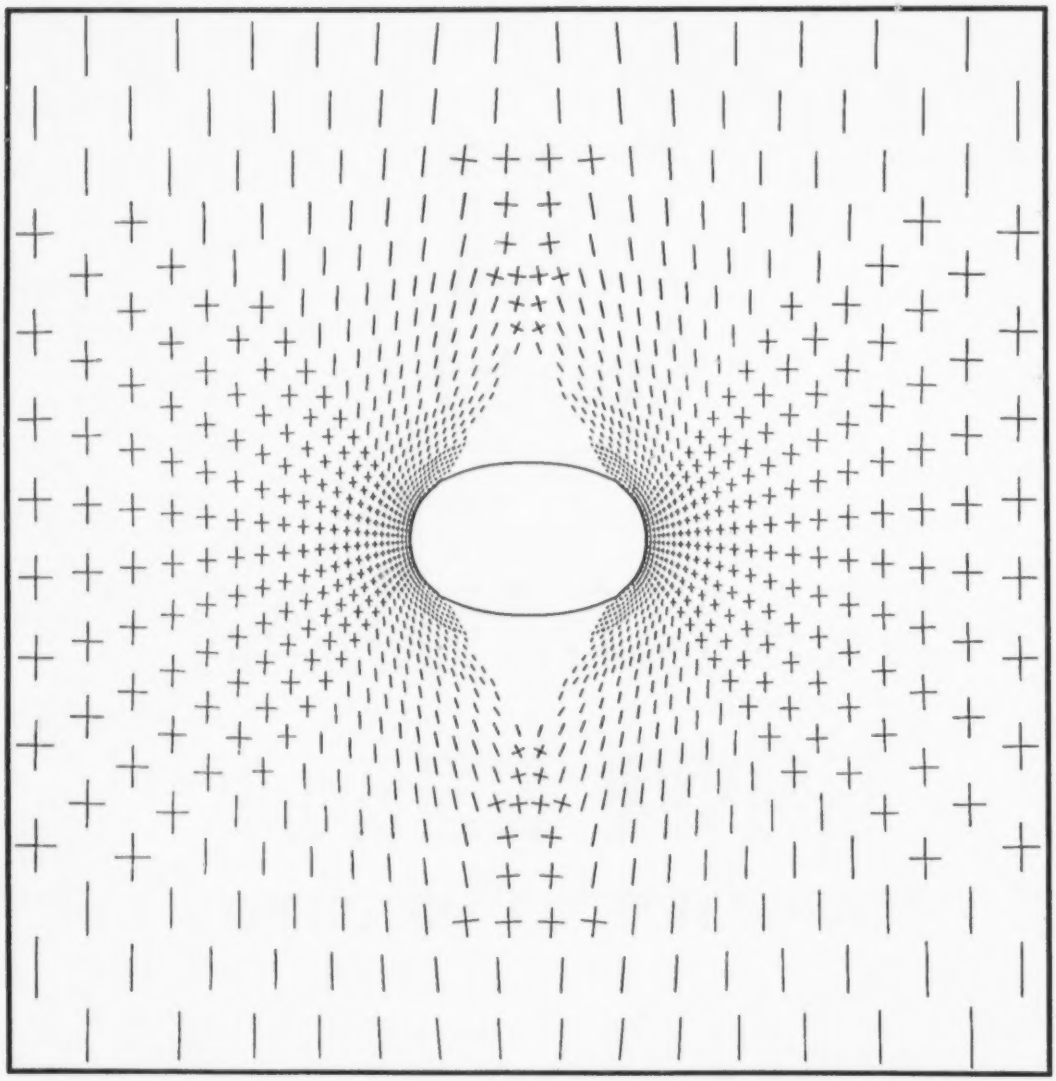

Fig. 4.12c Stretching of rectangular sheet with traction-free slot; distribution of tense, wrinkled and slack regions, mesh removed

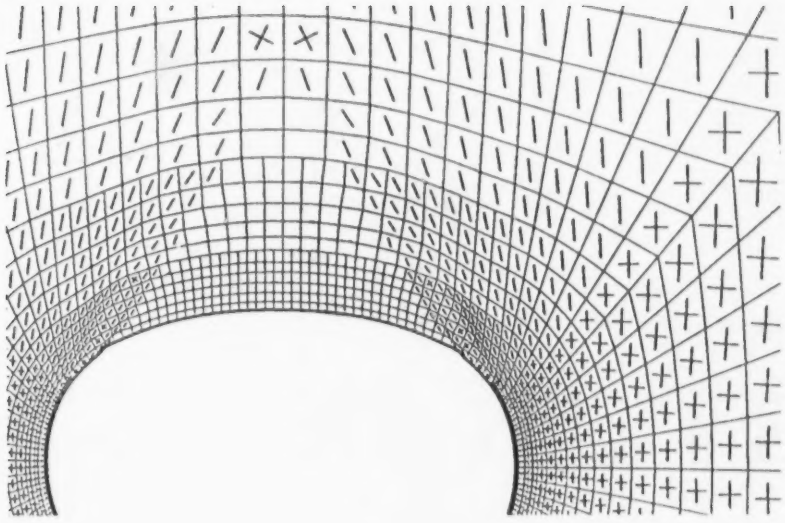

Fig. 4.12d Stretching of rectangular sheet with traction-free slot; details of deformation near slot

4.4 Neo-Hookean and Ogden Membranes Subjected to Uniform Pressure and Displacement Boundary Conditions

4.4.1 Square Neo-Hookean Membrane Subjected to Simple Shear and Uniform Lateral Pressure

The unit square membrane with meshed reference configuration represented in Fig. 4.3a, is first subjected to a planar simple shear deformation as described in § 4.2.1. The shear angle is 30°. The deformed configuration shown in Fig. 4.3b indicates that the entire membrane is wrinkled, the deformation being homogeneous. Next, the membrane is subjected to a uniform non dimensional pressure of 2.0. Fig. 4.13a shows the deformed configuration, where wrinkling is still present, the deformation being highly non-homogeneous. A top view of the deformed configuration is represented in Fig. 4.13b. This gives a better image of the change from the homogeneous deformation in Fig. 4.3b, to the actual non-homogeneous deformation due to pressurization. The tension trajectories are represented as previously by dashed lines at zone-centered points, showing the existence of two small wrinkled regions situated at the opposite obtuse corners. The rest of the membrane is tense, the wrinkling here being suppressed as a consequence of the pressurization; however the associated principal directions of stress are not represented this time, since slack regions are not present. The maximum stretch is 1.515 and occurs at the centers of the zones immediately adjacent to the middle of the lateral sides forming the boundary. Increasing the shear angle to 45° and maintaining the same uniform pressure, an extension of the wrinkled zones occurs, as can be seen in the top view in Fig. 4.13c. This latter deformation is accompanied by an increase in the maximum stretch to 1.738.

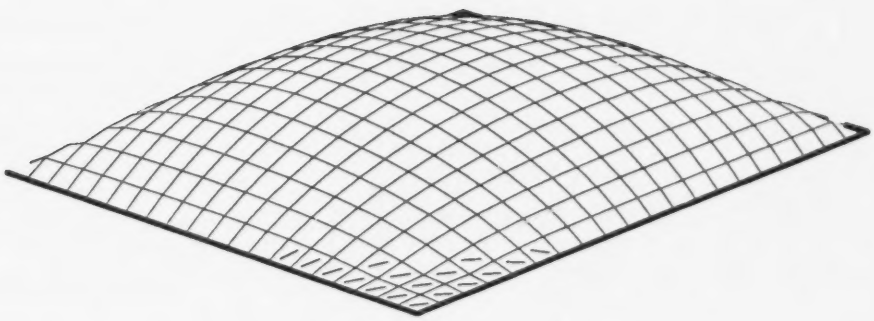

Fig. 4.13a Combined shear and pressurization of square membrane; deformed configuration for shear angle of 30^{0}

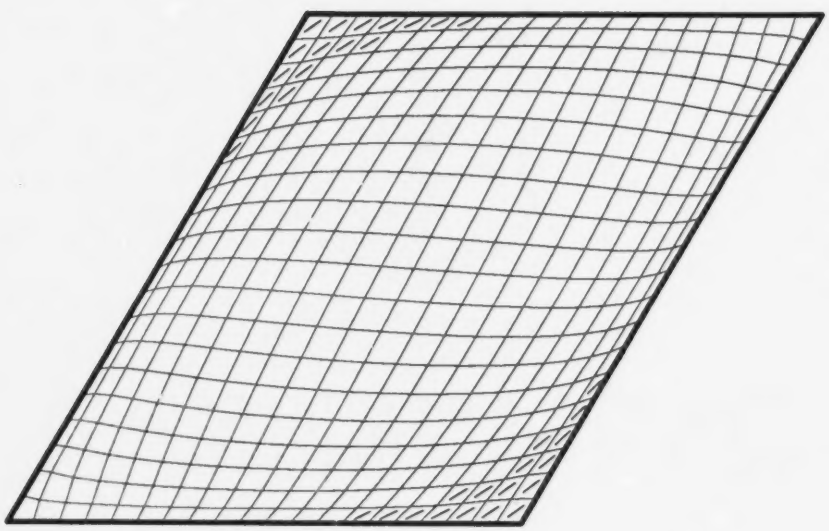

Fig. 4.13b Combined shear and pressurization of square membrane; deformed configuration for shear angle of 30°, top view

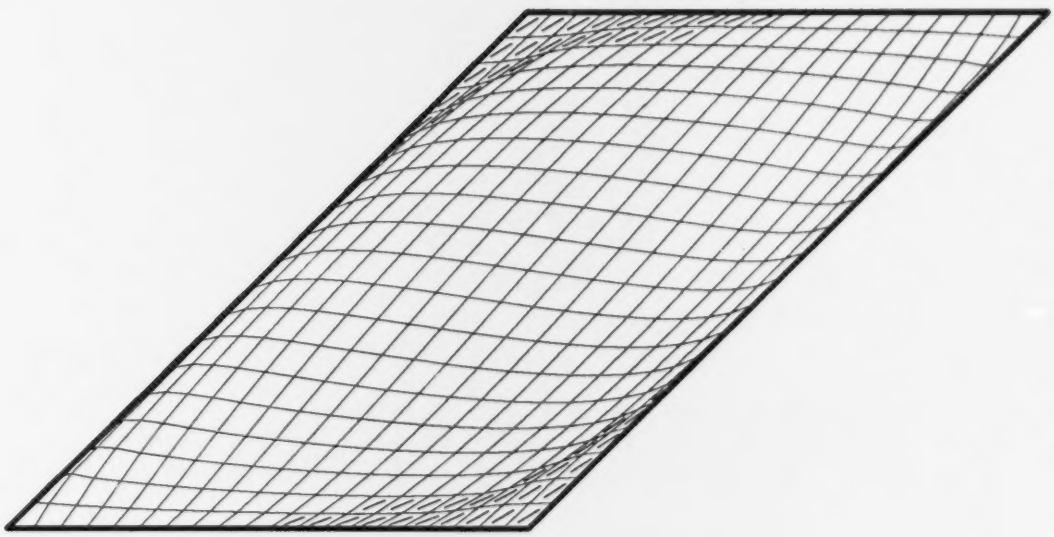

Fig. 4.13c Combined shear and pressurization of square membrane; deformed configuration for shear angle of 45°, top view

4.4.2 Circular Ogden and Neo-Hookean Membranes Subjected to Uniform Pressure Combined with the Reduction in Length of Boundary Circumference

A circular membrane with unit radius subjected to uniform pressure and displacement boundary conditions is analyzed. The meshed reference configuration is represented in Fig. 4.14a. The Ogden material is used first. The membrane is subjected to a uniform non dimensional pressure equal with 1.0, and at the same time the radius of the boundary is decreased to 0.8 of its initial value, leading to a 20% reduction in the length of circumference. Fig. 4.14b shows the deformed configuration, which is axisymmetric. Wrinkling occurs in a region of constant width immediately adjacent to the boundary, the tension trajectories being represented as usual by dashed lines at zone-centered points. The rest of the membrane is tense, and the principal directions of stress are not shown in the tense region. The maximum stretch λ is 1.15 and occurs at the zone centered points immediately adjacent to the apex of the deformed surface.

Maintaining the boundary fixed, the pressure is increased to 2.0. The axisymmetric deformation is shown in Fig. 4.14c. A decrease in the width of the wrinkled region is noticed. The maximum stretch increases to 1.44, and occurs at the same location as previously.

Next, the radius of the boundary is decreased to 0.5 of its initial value, and the uniform pressure is maintained equal with 2.0. The corresponding deformed configuration is shown in Fig. 4.14d, and it is no longer axisymmetric. Radial, partially wrinkled folds may be observed in the region adjacent to the boundary. The maximum stretch has the same location as previously, its value being 1.25.

In the following examples, the radius of the boundary is maintained at 0.5 of its initial value, and the pressure is increased in steps. Cross sections through the meridians of the deformed configurations obtained for numerical values of the non dimensional pressure $\tilde{p}$ of 1.0, 2.0, 2.5, 2.675, 2.6775, 3.0 and 3.5 are represented

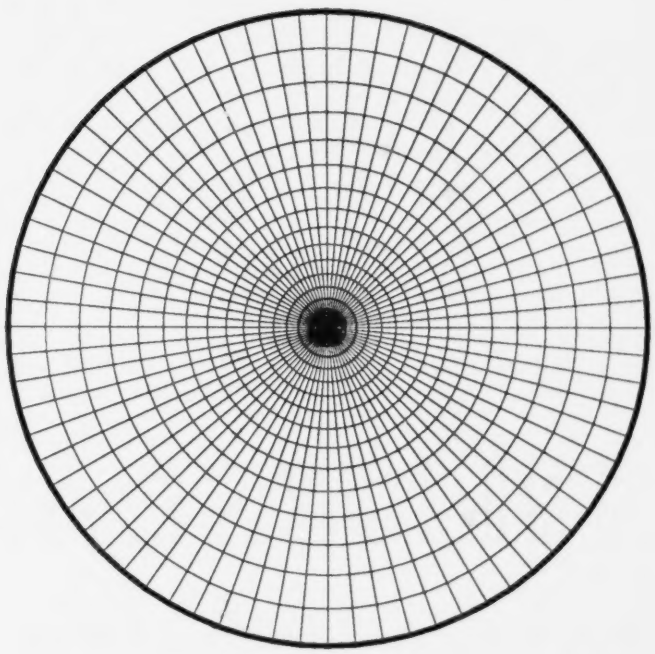

Fig. 4.14a Circular membrane; meshed reference configuration

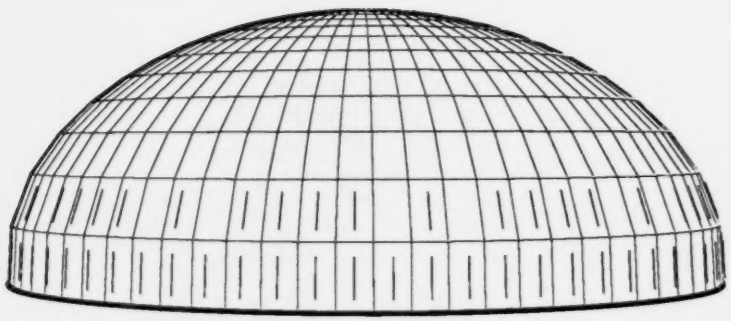

Fig. 4.14b Circular Ogden membrane
subjected to a non dimensional pressure of 1.0
combined with a 20% reduction in the length of boundary circumference

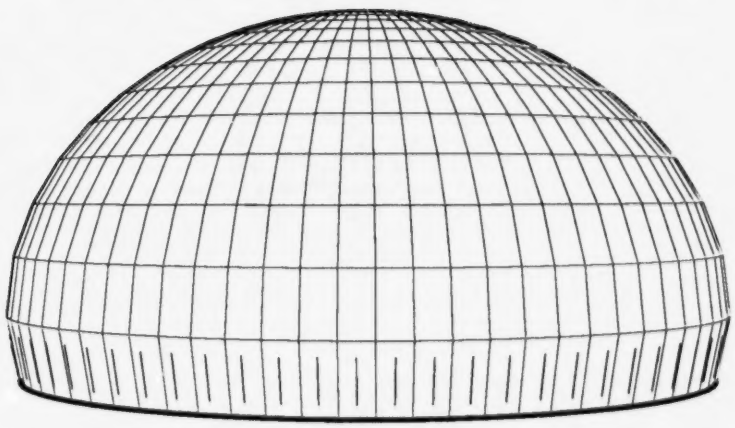

Fig. 4.14c Circular Ogden membrane
subjected to a non dimensional pressure of 2.0
combined with a 20% reduction in the length of boundary circumference

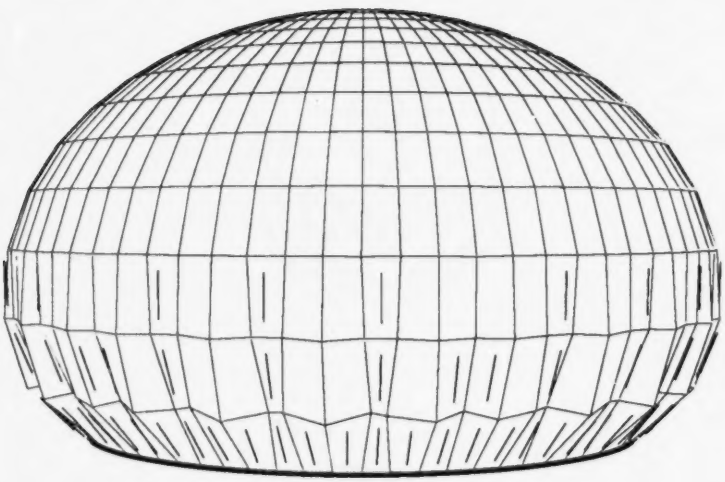

Fig. 4.14d Circular Ogden membrane
subjected to a non dimensional pressure of 2.0
combined with a 50% reduction in the length of boundary circumference

in Fig. 4.15. The corresponding maximum stretches λ are: 1.11, 1.25, 1.44, 1.77, 9.38, 10.20 and 11.36, respectively. These occur at the zone centered points immediately adjacent to the apex of the deformed surface. Comparing the cross sections for the pressures 2.675 and 2.6775, it is observed that for an increase in pressure of only 0.93%, a considerable expansion in the volume enclosed by the deformed configuration and the horizontal plane occurs. As expected, a substantial growth in the maximum stretch λ from 1.77 to 9.38, representing a 429.94% increase is found. This behavior is characteristic of bifurcation observed in spherical membranes with Ogden strain energies subjected to controlled pressure, where for a critical value of the pressure there is more than one equilibrium solution (Ogden, 1984). At this pressure, the solution "snaps through" from the smaller to the larger volume. In spherical equilibria, the variation of the pressure versus the stretch (or the volume) exhibits an increase to a maximum, a decrease to a minimum and again an increase. For large enough pressures, the computed configurations are nearly spherical, so qualitatively similar behavior is expected. In particular, DR does not pick up the unstable branch on which descending pressure accompanies increasing stretch or volume. Since these are DR solutions, it is concluded that in the class of dynamics and initial conditions considered, the solutions obtained for pressures above the critical value are asymptotically dynamically stable. It is also found that partial wrinkling is present in all solutions below the critical pressure, whereas above this pressure no wrinkling is observed.

Next, a circular membrane of neo-Hookean material is analyzed. The dimensions and the meshed reference configuration are the same as for the Ogden membrane. The radius of the membrane is reduced from its initial value of 1.0 to 0.5. Maintaining the boundary fixed, the pressure is increased in steps. Cross sections through the meridians of the deformed configurations obtained for numerical values of the non dimensional pressure $\tilde{p}$ of 1.0, 2.0, 2.5 and 2.612 are shown in Fig. 4.16a. The corresponding maximum stretches λ are: 1.11, 1.27, 1.55 and 1.84 respectively. These occur as in the

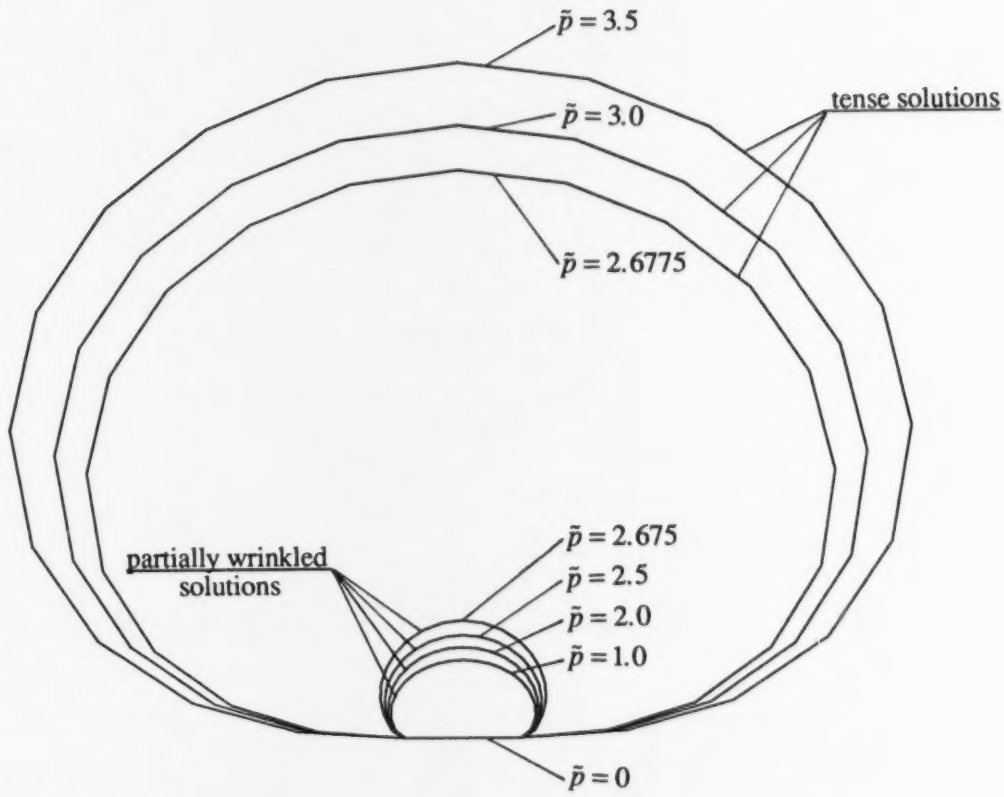

Fig. 4.15 Cross-sections through meridian of deformed configurations of circular Ogden membrane for different numerical values of pressure

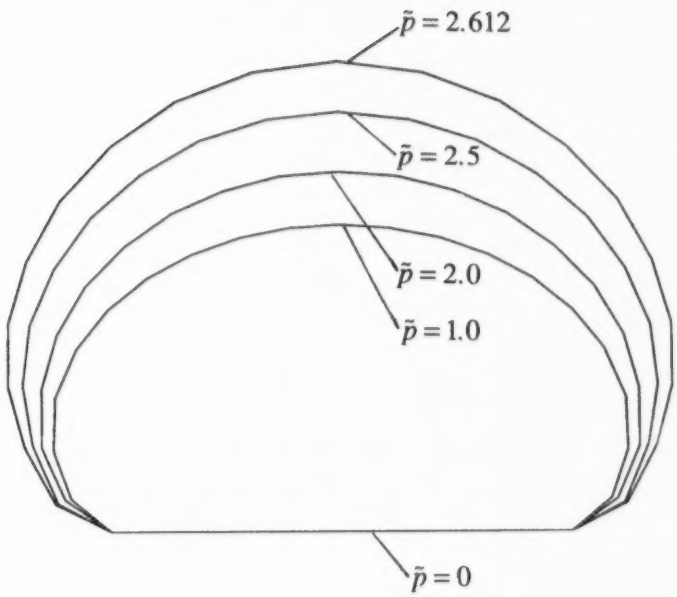

Fig. 4.16a Cross-sections through meridian of deformed configurations of circular neo-Hookean membrane for different numerical values of pressure

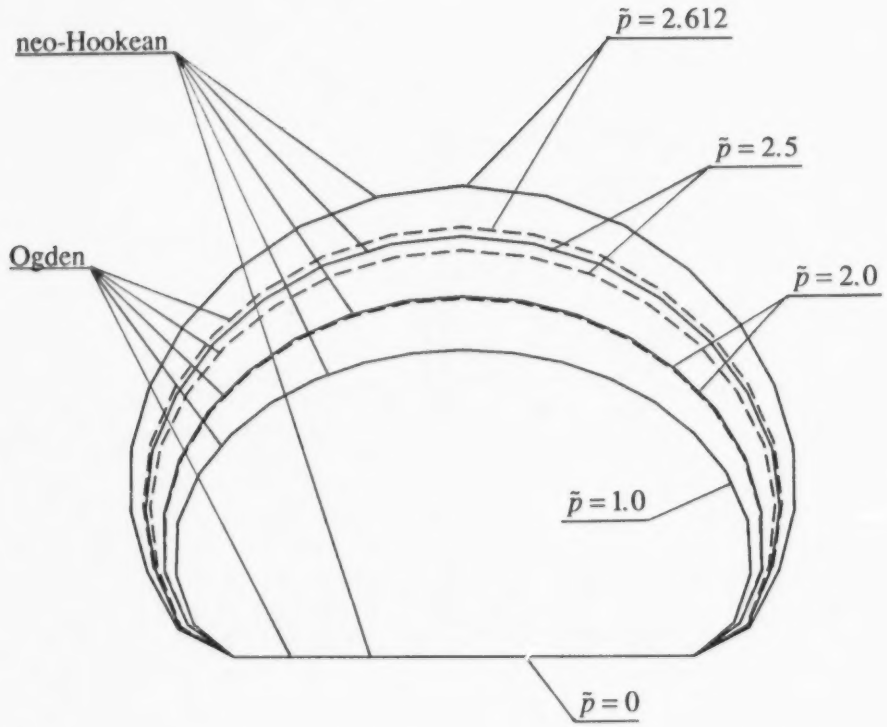

Fig. 4.16b Comparison of cross-sections through meridian of deformed configurations of circular neo-Hookean and Ogden membranes, for the same numerical values of pressure

previous case at the zone centered points immediately adjacent to the apex of the deformed surface. All solutions exhibit partial wrinkling in a zone adjacent to the boundary, the width of the region decreasing with the increase in pressure. No solutions are obtained beyond the pressure of 2.612. Thus, with increasing pressure, the neo-Hookean material exhibits a different behaviour than the Ogden material: the variation of pressure versus stretch shows only an increase toward a maximum, beyond of which no solutions exist. At low pressures (≤ 1.0), both materials deliver the same solutions. For pressures greater than 1.0, the neo-Hookean material gives larger principal stretches λ. The difference in λ between the neo-Hookean and Ogden material increases with increasing pressure. This can be observed in Fig. 4.16b, showing a comparison between the cross sections through the meridians of the deformed configurations of both neo-Hookean and Ogden membranes, for the numerical values of the non dimensional pressure $\tilde{p}$ of 1.0, 2.0, 2.5 and 2.612. The corresponding maximum principal stretches for the neo-Hookean material are 1.11, 1.27, 1.55 and 1.84, as mentioned above, whereas for the Ogden material these are 1.11, 1.25, 1.44 and 1.56.

4.5 Ogden Membranes Subjected to Point Loads, Uniform Pressure and Displacement Boundary Conditions

4.5.1 Circular Membrane Subjected to a Central Point Load

A circular membrane with unit radius subjected to a vertical, central point load and displacement boundary conditions is analyzed. The meshed reference configuration is represented in Fig. 4.14a. The boundary of the membrane is maintained fixed and the concentrated force is oriented upwards and has a non-dimensional intensity of 0.25.

The analytical formulation of a similar problem (Li and Steigmann, 1994) shows that the larger principal stretch is singular at the point of application of the force. However, the present model can be used to describe the associated deformation, since the concentrated force is applied at a node of the mesh, whereas the stretches are evaluated at zone centered points, where they remain finite.

The deformed configuration is shown in Fig. 4.17a. It is axisymmetric and completely tense. The largest computed principal stretch λ is 6.94, and is located at the zone centered points immediately adjacent to the central node, where the force is applied.

Next, the lateral (vertical) displacement of the central node caused by the previously applied force is maintained constant, no force is applied, and the radius of the boundary is decreased from its initial value of 1.0 to 0.8, leading to a 20% reduction in the length of the circumference of the boundary circle. (The intensity of the point load needed to produce the imposed displacement at the central node can be easily computed.) The resulting deformed configuration is shown in Fig. 4.17b, and is axisymmetric, with wrinkling present in the lower 2/3 of the lateral surface of the cone. It can be observed that the stress trajectories form straight lines on the deformed surface, as predicted by tension field theory. The largest computed principal stretch λ is 5.76, and is located at

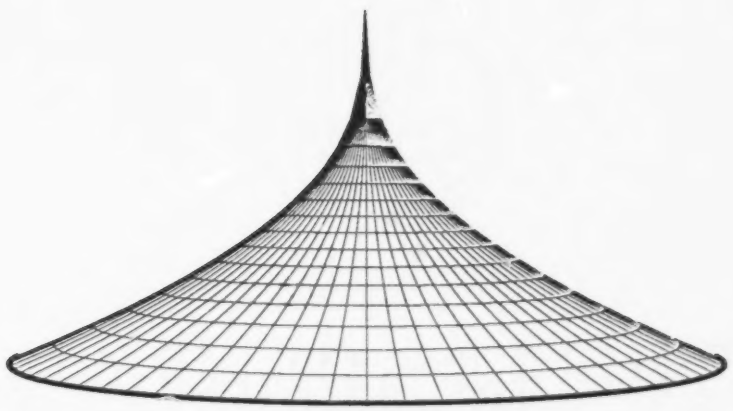

Fig. 4.17a Circular Ogden membrane subjected to a central vertical point load; deformed configuration.

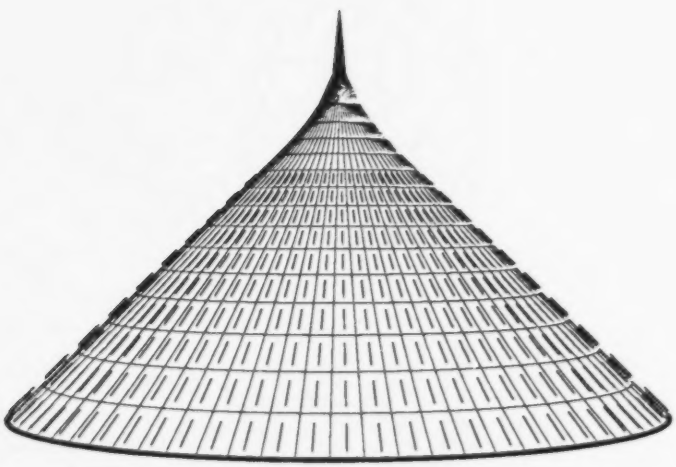

Fig. 4.17b Circular Ogden membrane subjected to a central vertical point load, combined with a 20% recuction in the length of circumference of boundary; deformed configuration

the zone centered points immediately adjacent to the central node, where the displacement is prescribed.

4.5.2 Circular Membrane Subjected to Uniform Pressure and a Central Point Load

The circular membrane with unit radius and meshed reference configuration represented in Fig. 4.14a is next subjected to uniform pressure, a central vertical point load, directed downwards and different displacement boundary conditions.

First, the numerical value of the non-dimensional uniform pressure is set equal to 1.0 and a concentrated force of intensity 0.4 is applied at the central node. The boundary is maintained fixed. The deformed configuration is represented in Fig. 4.18a. The frontal view of a central cross section through the deformed membrane (Fig. 4.18b) shows the details of deformation of the region adjacent to the application point of the force. The deformed configuration is axisymmetric and no wrinkling is indicated. The largest computed principal stretch λ is 6.35, and is located at the zone centered points immediately adjacent to the central node, where the concentrated force is applied.

Next, the lateral (vertical) displacement of the central node caused by the previously applied force is maintained constant, no force is applied except for the uniform pressure which is kept equal to 1.0, and the radius of the boundary is decreased from its initial value of 1.0 to 0.8, leading to a 20% reduction in the length of the circumference of the boundary circle. (The magnitude of the concentrated force needed to produce the imposed lateral deflection at the central node can be easily computed.) Fig. 4.18c shows the frontal view of a central cross section through the deformed configuration. The deformation is axisymmetric and wrinkling is present in the region adjacent to the boundary. The maximum computed principal stretch λ is 6.46, and is located at the zone

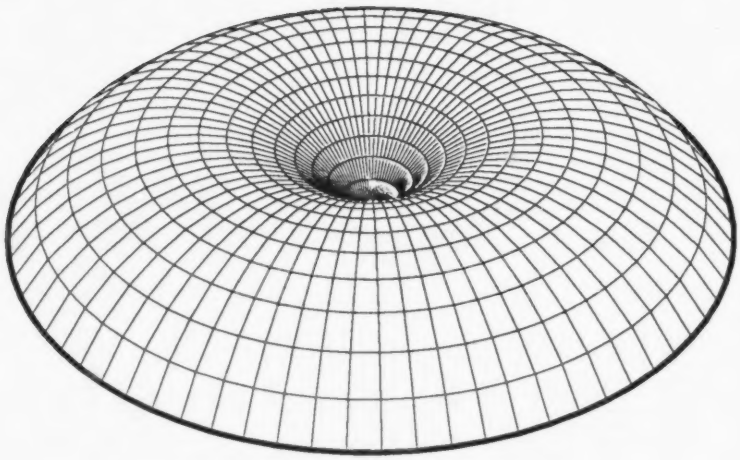

Fig. 4.18a Pressurized circular membrane
subjected to a central vertical point load directed downwards

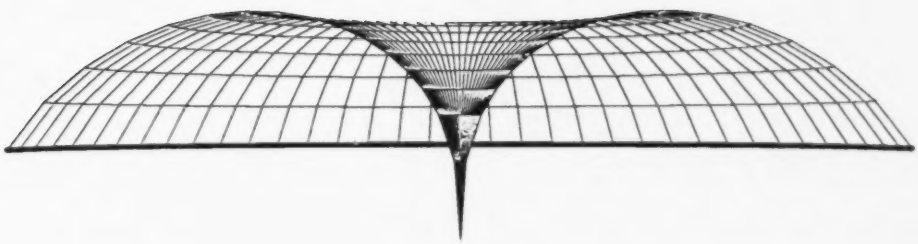

Fig. 4.18b Cross section through pressurized circular membrane subjected to a central vertical point load directed downwards

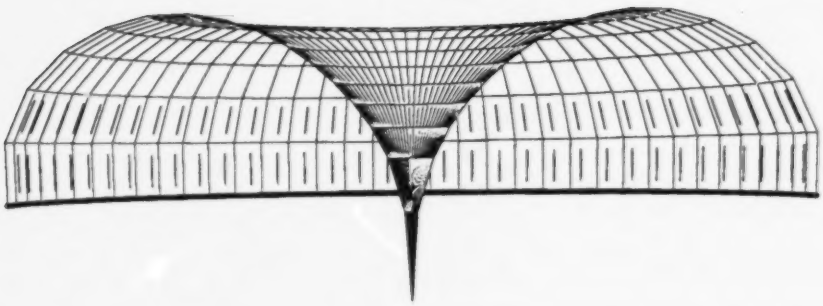

Fig. 4.18c Cross section through pressurized circular membrane subjected to a central vertical point load directed downwards, combined with a 20% reduction in the length of boundary circumference

centered points immediately adjacent to the central node, where the displacement is prescribed.

An unexpected response of the membrane is obtained by further reducing the radius of the boundary to a value of 0.5, while maintaining the pressure and the lateral displacement of the central node at their previous values. The resulting deformation is no longer axisymmetric. An oblique view, a top and a frontal view of the deformed configuration are represented in Fig. 4.19a, b, and c respectively. The oblique and the frontal view of a central cross section through a meridian of the deformed configuration show details of the deformation (Fig. 4.19d, e, and f). A combination of fine, medium and large wrinkles is observed. The maximum computed principal stretch λ is 5.9, and occurs at the zone centered points immediately adjacent to the central node, where the displacement is prescribed.

The numerical results reveal a periodic non-axisymmetric structure in the deformation, corresponding to pleats in the membrane. These are reminiscent of the pneumatic hinges observed in flexure of pressurized membrane tubes (Lukasiewicz and Glockner, 1984-1985). The computed deformation contains regions of self penetration of the membrane which would not occur in practice. The model does not preclude this possibility, and that is why this occurs in the solution. To model this behaviour properly, the effects of self contact would need to be taken into consideration. However, this is beyond the scope of the present work.

In an experimental study on spherical membranes subjected to vertical concentrated loads, Szyszkowski and Glockner (1987b) observed a change in the wrinkling pattern, from a large number of regularly distributed small wrinkles present during the initial stages of deformation, to a wrinkled area dominated by a few 'large' wrinkles appearing at advanced stages of deformation. The authors explained the difference in wrinkling patterns as a consequence of the small, but finite real bending stiffness existing in the membrane material. The numerical results obtained with the present model show the development of such a change in the wrinkling pattern, from the uniformly distributed

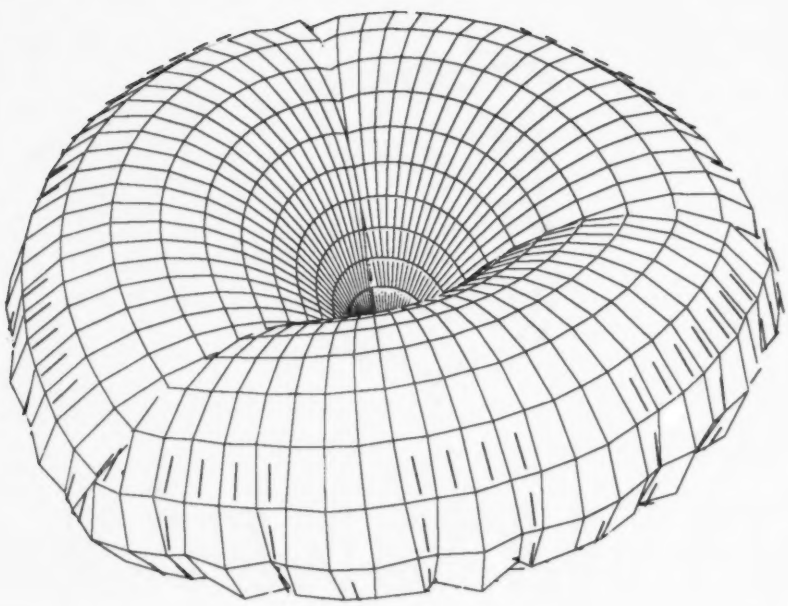

Fig. 4.19a Pressurized circular membrane subjected to a central vertical point load directed downwards, combined with a 50% reduction in the length of boundary circumference

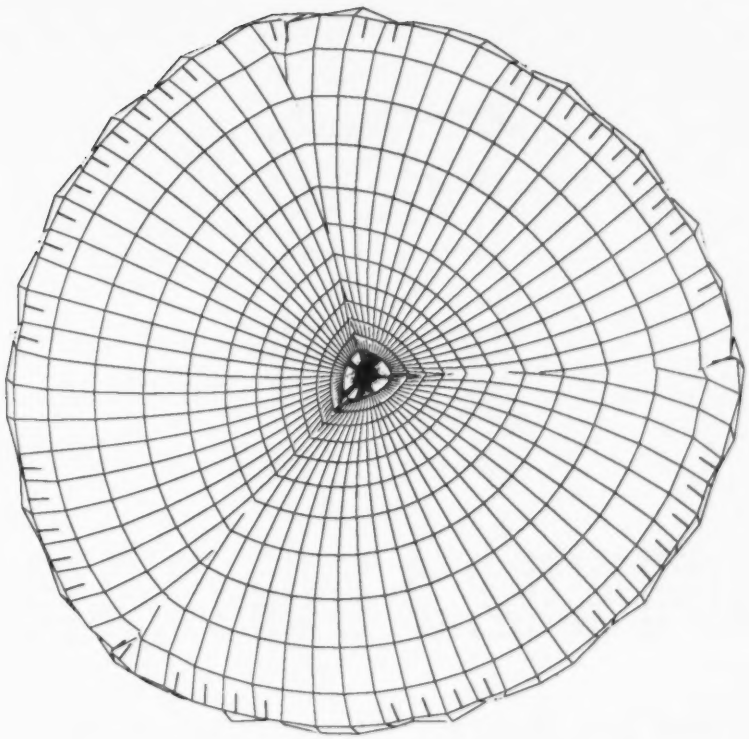

Fig. 4.19b Pressurized circular membrane subjected to a central vertical point load directed downwards, combined with a 50% reduction in the length of boundary circumference; top view

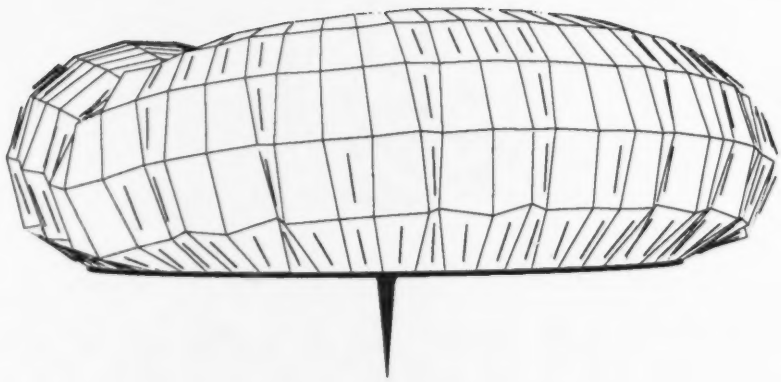

Fig. 4.19c Pressurized circular membrane subjected to a central vertical point load directed downwards, combined with a 50% reduction in the length of boundary circumference; frontal view

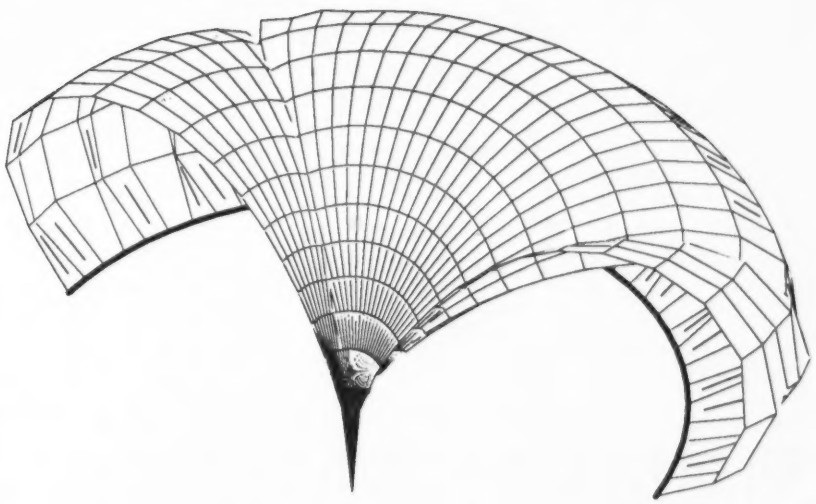

Fig. 4.19d Cross section through pressurized circular membrane subjected to a central vertical point load directed downwards, combined with a 50% reduction in the length of boundary circumference; oblique view

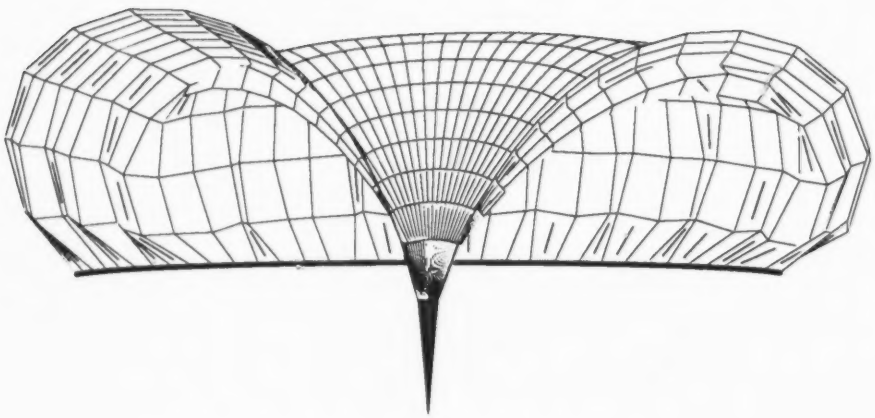

Fig. 4.19e Cross section through pressurized circular membrane subjected to a central vertical point load directed downwards, combined with a 50% reduction in the length of boundary circumference; frontal view

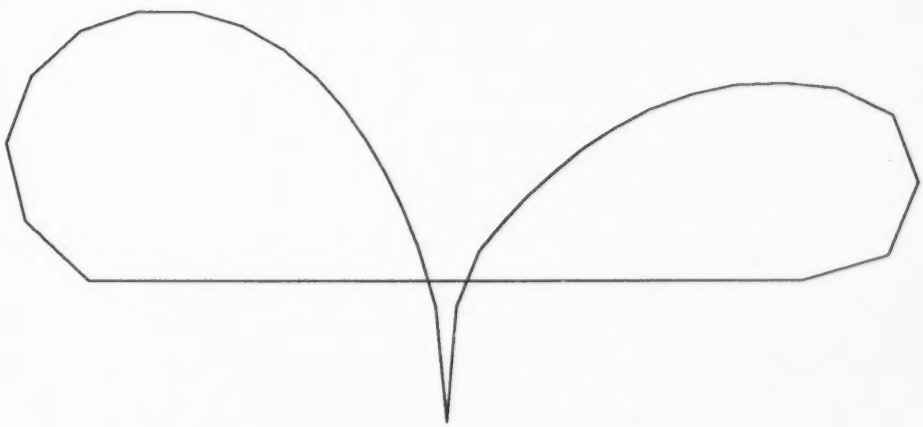

Fig. 4.19f Meridian of pressurized circular membrane subjected to a central vertical point load directed downwards, combined with a 50% reduction in the length of boundary circumference; frontal view

wrinkles in Fig. 4.18c, corresponding to the initial stages of wrinkling, to the three large dominating wrinkles in Fig. 4.19a,b, corresponding to an advanced stage of deformation. However, the model used for these computations does not account for the bending stiffness of the membrane.

These serendipitous findings regarding self contact of the membrane, a condition rarely encountered in elasticity, should generate additional interest in tension field theory.

Chapter 5

Experimental Models

A number of experimental models were constructed for the analysis of the real behaviour of the membranes. Planar as well as 3D deformations of the membranes were considered, starting in all cases from plane reference configurations. Although some of the geometries of the models are slightly different from those used in the numerical analysis, the qualitative response obtained with these models confirms the predictions of the numerical method.

First, a quadrilateral wooden frame is used as a support for the membranes. The frame is composed of four equal-length bares, articulated together at their extremities. A thin polyethylene sheet of square or rectangular shape is attached to the support in certain ways, ensuring the required boundary conditions.

Fig. 5.1a shows the reference configuration of a square sheet having all four margins attached to the frame. Displacement boundary conditions are imposed by deforming the square frame into a rhombus. The lateral bares, initially in a vertical position, are each rotated clockwise through an angle of 30° about the axes passing through the lower hinges, perpendicular to the plane of the membrane, while the inferior bar is maintained fixed in a horizontal position. The upper bar has a circular translation. As a consequence, the shearing of the membrane occurs in conditions close

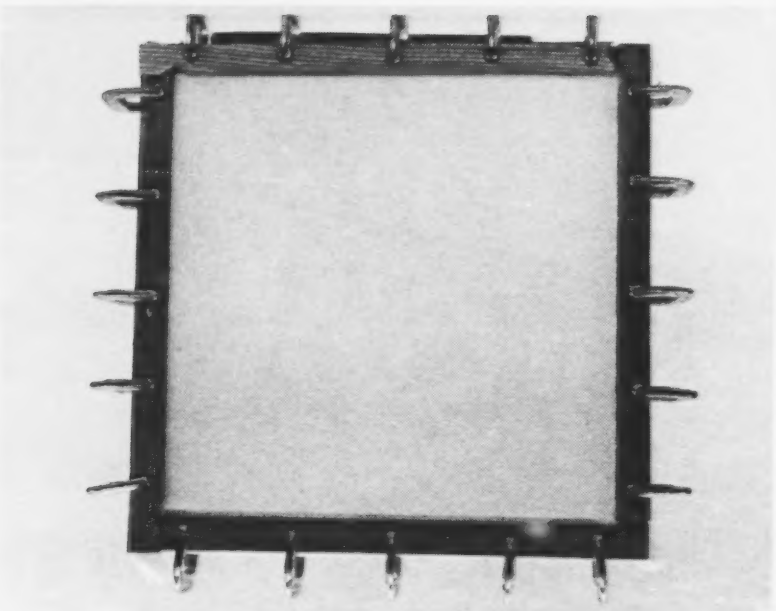

Fig. 5.1a Experimental model of square membrane;
initial configuration

to those of the numerical example at § 4.2.1, where a homogeneous deformation due to simple shear was analyzed. The deformed configuration obtained with this experimental model is shown in Fig. 5.1b. Since the bending stiffness of the membrane is very small, a high number of small height wrinkles can be observed. This is a homogeneous deformation, the trajectories of tensile stress coinciding with the crests of the wrinkles. Comparing this deformation to the one in Fig. 4.3b (§ 4.2.1), obtained with the numerical model, a very good qualitative agreement is observed.

The next model consists of a rectangular membrane with traction-free lateral boundaries and displacement boundary conditions imposed on the lower and upper sides by attaching them to the corresponding bares of the frame. The reference configuration is represented in Fig. 5.2a. As in the previous case, the frame is deformed into a rhombus, the lateral sides being each rotated clockwise through an angle of 30° (measured from the vertical). The deformed configuration in Fig. 5.2b shows a non-homogeneous deformation. A parallelogram shaped wrinkled region covers most of the membrane surface. Two triangular slack regions that bulge out of plane are located at the upper left and lower right corners, and two narrow tense regions can be identified immediately adjacent to the upper third of the right traction-free boundary, respectively to the lower third of the left traction-free boundary. Although the ratio of height to length of the membrane is different from the one used in the numerical example at § 4.3.1, a very good qualitative agreement is observed when comparing the deformed configuration in Fig. 5.2b obtained with the experimental model, to the one in Fig. 4.10e,f obtained with the numerical method.

Another experimental model is shown in Fig. 5.3a, and represents the reference configuration of a square membrane with a traction-free central, circular hole. As in the previous two examples, the membrane is sheared by deforming the square frame into a rhombus, the lateral sides being again rotated through an angle of 30°. Displacement boundary conditions are imposed on all four membrane margins which

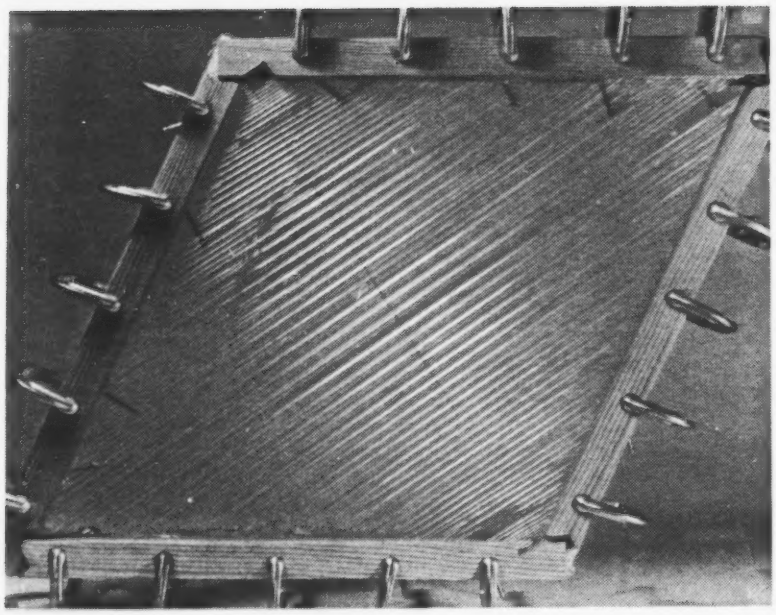

Fig. 5.1b Experimental model of square membrane
subjected to shearing

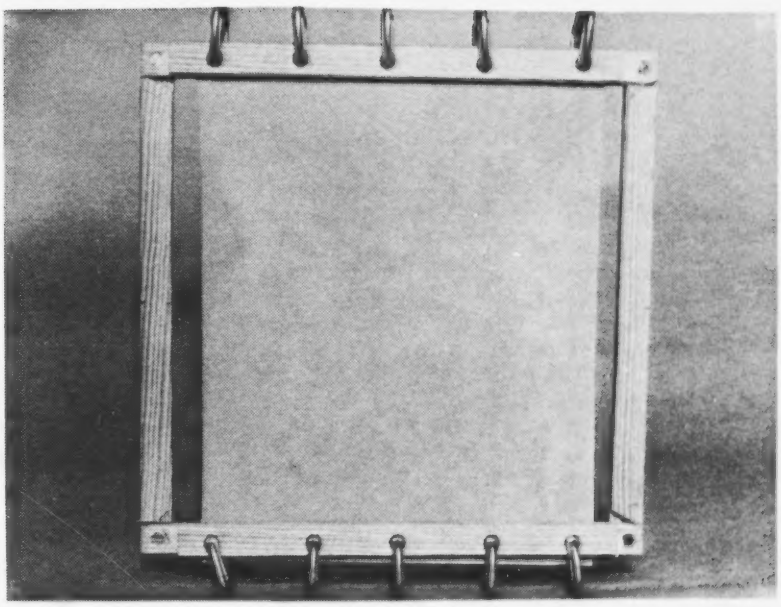

Fig. 5.2a Experimental model of rectangular membrane
with traction-free lateral boundaries; initial configuration

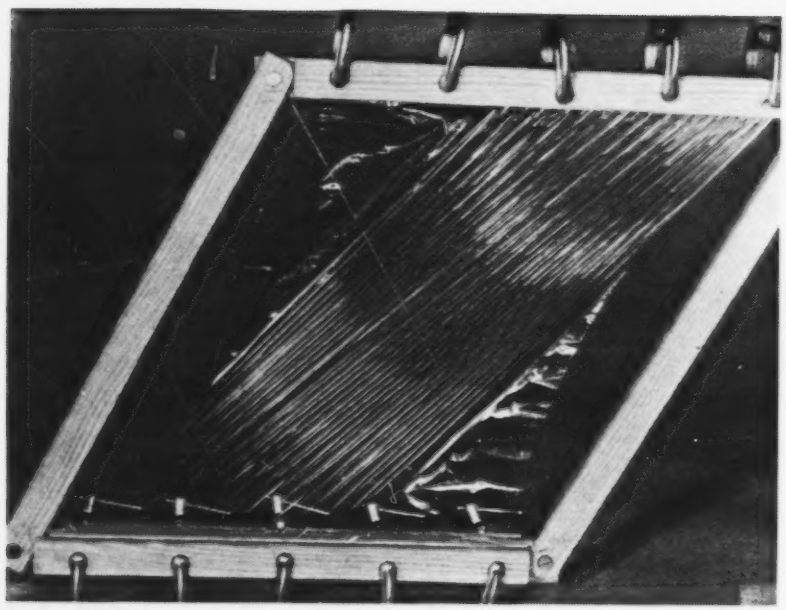

Fig. 5.2b Experimental model of rectangular membrane with traction-free lateral boundaries subjected to shearing

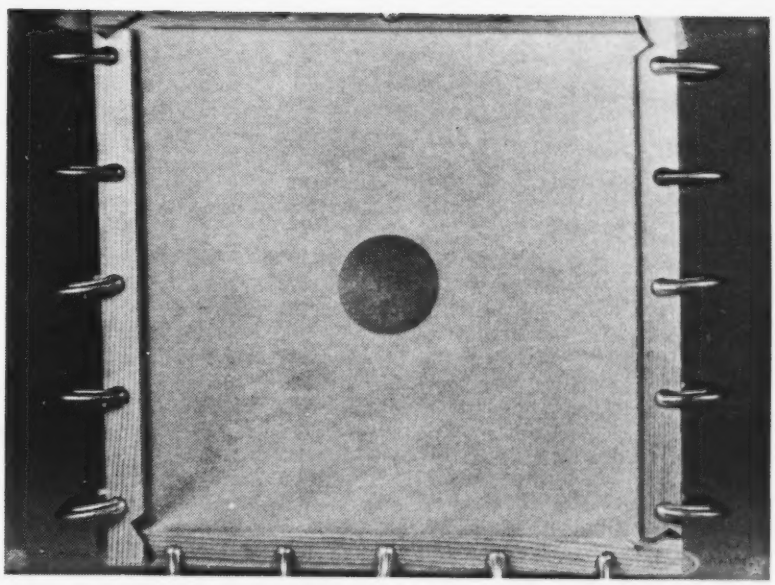

Fig. 5.3a Experimental model of square membrane
with traction-free circular hole; initial configuration

are attached to the frame, while the circular hole remains traction-free. The deformed configuration in Fig. 5.3b consists of a combination of tense, wrinkled and slack regions. Were it not for the presence of the hole, the deformation would be homogeneous, as shown in Fig. 5.1b. However, in the presence of the hole the deformation is highly non-homogeneous. The circular hole deforms into an ellipse, while two cone-shaped slack regions that bulge out of plane appear at the extremities of the hole. Four tense regions can be easily identified, the rest of the membrane being wrinkled. A very good qualitative agreement is observed when comparing the deformed configuration in Fig. 5.3b, obtained with the experimental model, to the one in Fig. 4.11b,d (§ 4.3.2), obtained with the numerical method.

Next, an experimental model is constructed by attaching the external boundary of an annular membrane to a circular plexiglass frame, while the internal boundary is attached to an aluminum hub mounted at the center of the annulus. The hub can be rotated with respect to a central axis, perpendicular to the plane of the membrane, leading to a plane deformation. As well, it can be displaced out of plane, parallel to itself, causing a 3D deformation of the membrane. In this case a thin latex rubber sheet is used. The ratio of the radii of the inner and outer circular boundaries of the membrane is 0.25. The reference configuration is represented in Fig. 5.4a. Displacement boundary conditions are enforced on both internal and external boundaries by maintaining the circular frame fixed, while rotating the hub counterclockwise through an angle of 5°. As can be seen in Fig. 5.4b, a tension field forms in an annular region immediately adjacent to the hub, the rest of the membrane being tense. By increasing the rotation angle to 20°, the extent of the wrinkled region increases (Fig. 5.4c). The trajectories of tensile stress are in both cases straight lines. These findings are in accordance with the results of the numerical analysis obtained with DR (§ 4.2.2), as well as with the results of Li and Steigmann (1993). It appears that the bending stiffness of the rubber sheet is greater than the bending stiffness of the

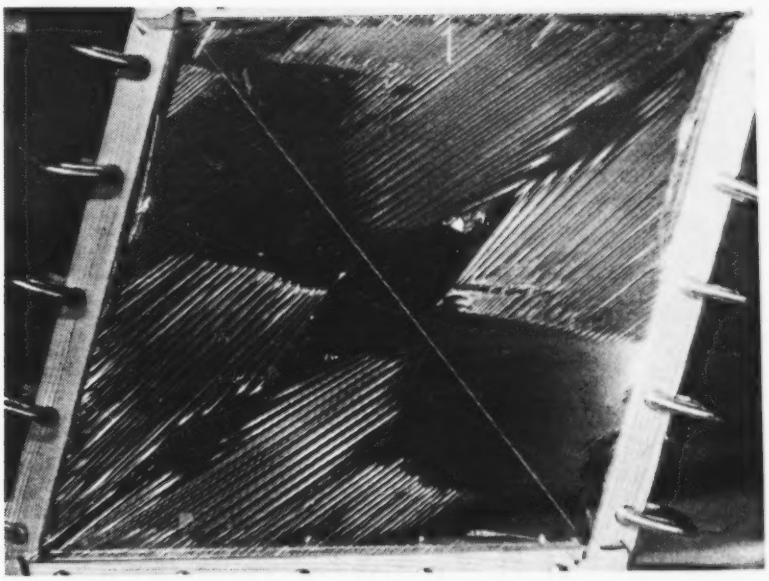

Fig. 5.3b Experimental model of square membrane
with traction-free circular hole subjected to shearing

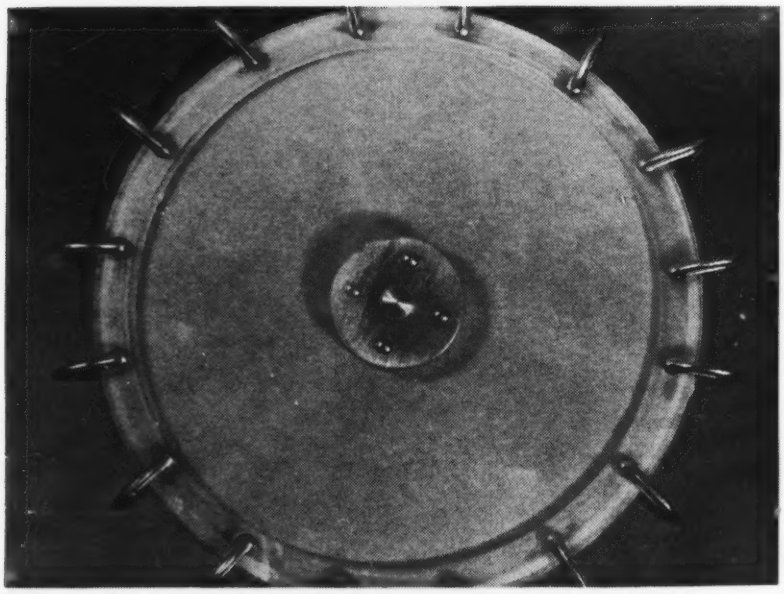

Fig. 5.4a Experimental model of circular annular membrane;
initial configuration

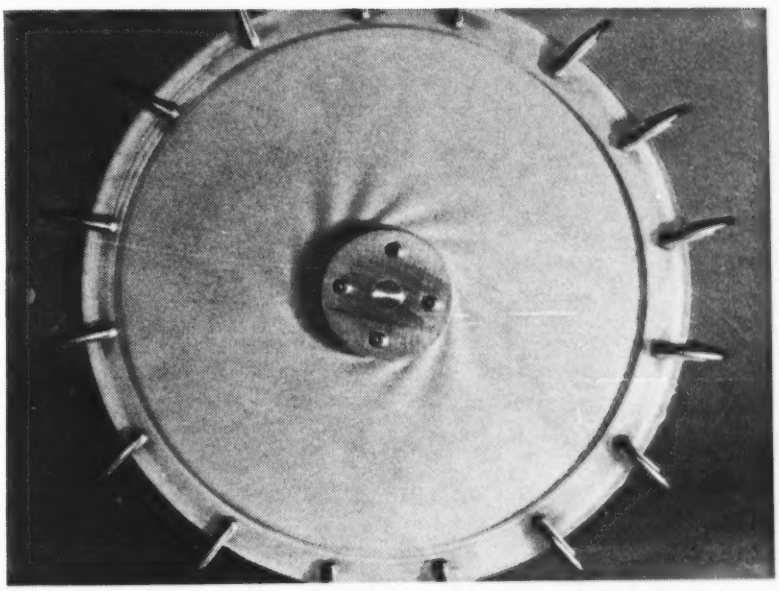

Fig. 5.4b Experimental model of circular annular membrane subjected to plane twisting (5°)

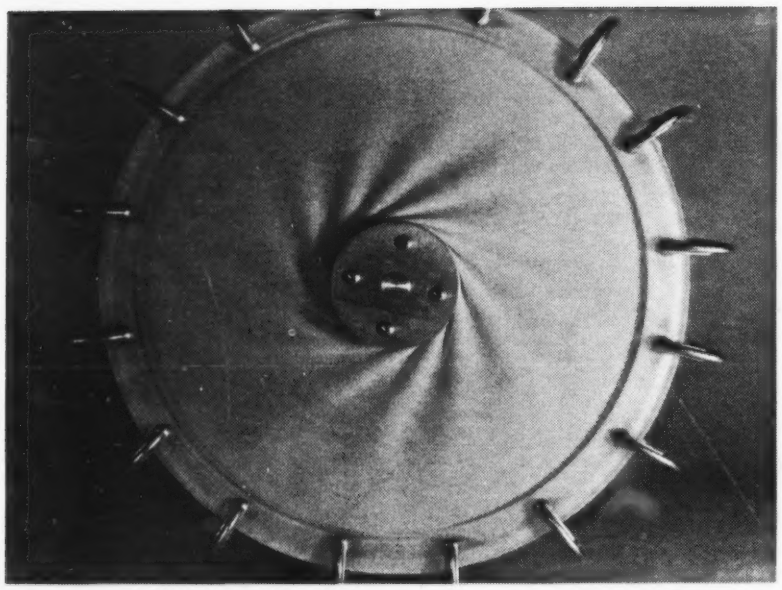

Fig. 5.4c Experimental model of circular annular membrane subjected to plane twisting (20°)

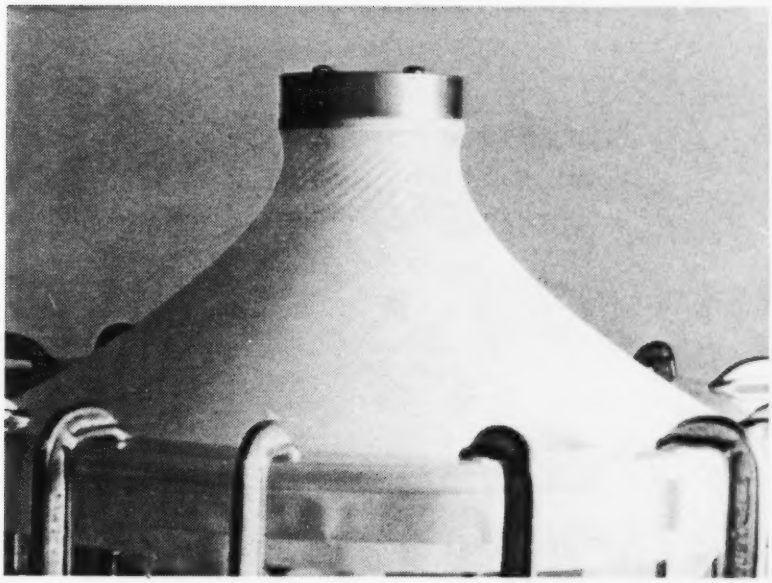

Fig. 5.4d Experimental model of circular annular membrane subjected to combined lateral deflection and twisting (90°)

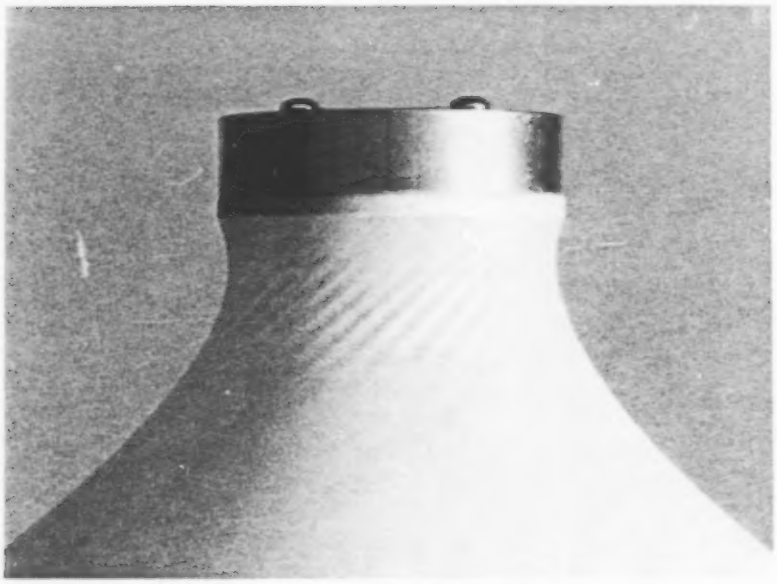

Fig. 5.4e Experimental model of circular annular membrane subjected to combined lateral deflection and twisting (90°); details of deformation near hub

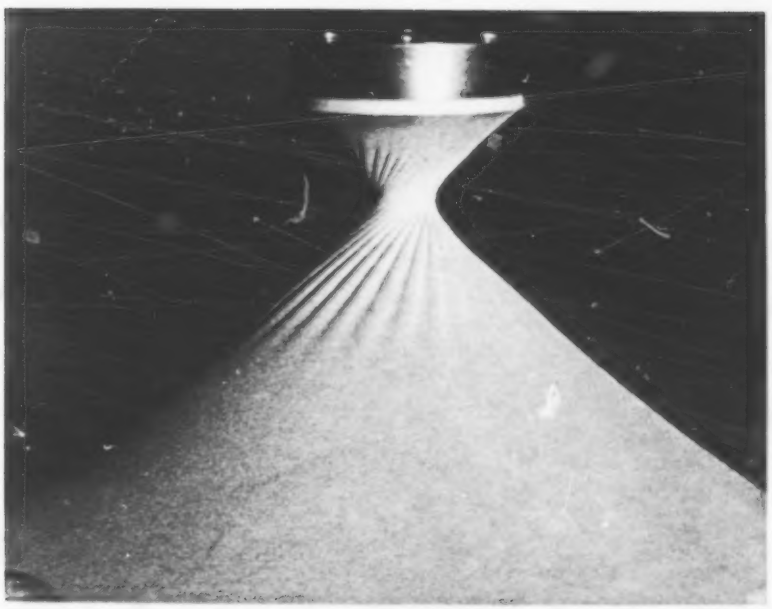

Fig. 5.4f Experimental model of circular annular membrane subjected to combined lateral deflection and twisting (180°)

polyethylene sheet, since fewer wrinkles of larger height are observed in the tension field of the deformed membrane when rubber is used, than in the case of polyethylene. However, a difference in thickness of the two membranes may also influence the results, the rubber membrane being thicker than the polyethylene one.

Finally, a 3D deformation of the annular membrane is obtained by rotating the hub through an angle of 90°, while simultaneously displacing it out of plane an amount equal with the outer radius of the annulus. The deformed configuration is shown in Fig. 5.4d and Fig. 5.4e. A wrinkled region appears in the vicinity of the hub, the trajectories of tensile stress forming again straight lines. This can also be observed in Fig. 5.4f, where the rotation angle was increased to 180°. This is in accordance with the analytical result known from tension field theory, which requires that stress trajectories form families of straight lines on the deformed surface (Steigmann, 1990). For axisymmetric deformations, the surface must then be a sector of a single-sheet hyperboloid of revolution wherever it is wrinkled. This can be particularly well observed in Fig. 5.4f. Although the present experimental model does not permit the reduction in circumference of the inner boundary, a comparison of the deformed configuration in Fig. 5.4.d obtained with the experimental model for combined rotation and lateral displacement of the membrane, and the one in Fig.4.7d, obtained with the numerical model for the case of combined twist and lateral deflection with reduction in circumference of the inner boundary (§ 4.2.2), shows a good qualitative agreement of the results.

Chapter 6

Summary and Conclusions

A numerical method for the static analysis of elastic membranes is presented in this thesis. The method is applicable to the study of tension fields associated with wrinkling in isotropic elastic membranes undergoing finite deformations.

The tension field generated by wrinkling has long been a problem of concern in the design of membrane structures, the analysis of wrinkling being important for the prediction of structural response. Wrinkling is initiated by the loss of prestress and appearance of compressive stresses, under the action of a specific loading and/or certain boundary conditions. It represents a localized buckling phenomenon. The configuration of the wrinkled region depends on the small bending stiffness of the material. Membrane theory in its usual form neglects this bending stiffness, delivering compressive stresses in the wrinkled regions. Such deformations are unstable and therefore not observable as equilibrium states. Stable solutions may be obtained by employing shell theory. Another alternative is tension field theory, which is much simpler from the point of view of the analysis. However, by employing a *relaxed strain energy density*, tension field theory is automatically incorporated into ordinary membrane theory, leading to stresses that are never compressive and therefore to deformations that satisfy this necessary condition for stability.

A *relaxed strain energy density* is constructed and employed in the method developed in this thesis, in order to accommodate the wrinkling effect while retaining the analytical simplicity of membrane theory.

The numerical procedure is based on the *Dynamic Relaxation Method*. This is an explicit, iterative technique in which the static solution is obtained as the steady state part of the damped dynamic response of the structure. Dynamic Relaxation does not require the construction or inversion of the stiffness matrix and is therefore particularly well suited for the present class of problems, which are characterized by ill-conditioned stiffness matrices, due to the presence of wrinkling. Dynamic Relaxation has also the advantage of delivering asymptotically dynamically stable solutions.

The numerical scheme is obtained from the spatial and temporal discretizations of the PDEs describing the damped motion of the membrane. The internal forces are obtained from the Euler-Lagrange equations. A finite difference technique derived from Green's theorem is used for the spatial discretization. The resulting system of ODEs is further integrated in time by a central difference time integrator. Fictitious mass and damping characteristics are chosen at each time step such that the static solution is achieved with the smallest number of steps.

Besides its simplicity, Green's theorem differencing method avoids the inconvenience of mapping techniques, being applicable to uniform as well as irregular types of meshes, which can be fitted to any shape of the boundary.

Also, this method allows for the solution of problems involving concentrated loads. The analytical formulations of such problems contain singularities. However, the present model can be used to obtain the associated deformation, since the concentrated loads are applied at nodal points of the mesh, whereas the stretches are evaluated at zone-centered points, where they remain finite.

Arbitrary, conservative loading and arbitrary, planar geometries of the stress-free reference configuration are considered. Solutions of a number of boundary value problems are obtained and analyzed. The effects of various boundary and loading

conditions on the response of the membrane are examined. A good agreement with existing exact solutions is observed. As well, the qualitative response obtained with experimental models confirms the predictions of the numerical method.

The method developed in this thesis can be further adapted in order to permit the analysis of problems involving initially curved surfaces, nonuniform pressure loading, the presence of gravity, the case of orthotropic materials (e.g. networks) as well as the case of anisotropic materials. Also, temperature effects may be included. The problem of self contact, a condition rarely encountered in elasticity, but which occurred in one of the boundary value problems considered in chapter 4, could as well be modeled in the present context. This are some possible directions to be pursued in the future.

Bibliography

Al-Shawi, F. A. N., Mardirosian, A. H., 1987, Improved Dynamic Relaxation Method for the Analysis of Plate Bending Problems, *Computers and Structures*, **27**, 237-240.

Alwar, R. S., Ramachandra Rao, N., 1973, Nonlinear Analysis of Orthotropic Skew Plates, *AIAA Jour.*, **11**, 495-498.

Alwar, R. S., Ramachandra Rao, N., 1974, Large Elastic Deformations of Clamped Skewed Plates by Dynamic Relaxation, *Computers and Structures*, **4**, 381-398.

Argyris, J. H., Angelopoulos, T., Bichat, B., 1974, A General Method for Shape Finding of Lightweight Structures, *Proc. of Int. Conf. on Tension Structures*, London, 35-47.

Ball, J.M., 1984, Material Instabilities and the Calculus of Variation, in: *Transformations and Material Instabilities in solids*, Gurtin, M.E., editor, MRC No. 52, Academic Press, Orlando, Fl., 1-19.

Barnes, M. R., 1974, Dynamic Relaxation Analysis of Tension Networks, *Proc. of Int. Conf. on Tension Structures*, London, 1-11.

Barnes, M. R., 1975, Applications of Dynamic Relaxation to the Topological Design and Analysis of Cable, Membrane and Pneumatic Structures, *Proc. of 2nd Int. Conf. on Space Structures*, Guildford, 211-219.

Barnes, M. R., 1976, Form-Finding of Minimum Surface Membranes, *Proc. of IASS World Congress on Space Enclosures*, Montreal, 115-124.

Barnes, M. R., 1980, Non-Linear Numerical Solution Methods for Static and Dynamic Analysis of Tension Structures, *Proc. of Symp. on Air-Supported Structures: The State of the Art*, London, 38-56.

Barnes, M. R., 1984, Form-Finding Analysis and Patterning of Tension Structures, *Proc. of Third Int. Conf. on Space Structures*, Guildford,730-736.

Barnes, M. R., 1986, Computer Aided Design of Cable and Membrane Structures with Applications to EXPO 88 and DQDC, Riyadh, *Proc. of Int. Conf. on Lightweight Structures in Architecture*, Sydney, 254-270.

Barnes, M. R., Wakefield, D. S., 1988, Form-Finding, Analysis and Patterning of Surface-Stressed Structures, *Proc. of 1st Oleg Kerensky Memorial Conf.*, London, 8-15.

Belytschko, T., 1983, An Overview of Semidiscretization and Time Integration Procedures, in *Computational Methods for Transient Analysis*, Belitschko, T., Hughes, T. J. R., editors, Elsvier, Amsterdam, 1-65.

Bergan, P. G., Soreide, T., 1973, A Comparative Study of Different Numerical Solution Techniques as Applied to a Nonlinear Structural Problem, *Computer Methods in Applied Mechanics and Engineering*, **2**, 69-81.

Brew, J. S., Brotton, D. M., 1971, Non-Linear Structural Analysis by Dynamic Relaxation, *Int. J. for Numerical Methods in Engineering*, **3**, 463-483.

Bunce, J. W., 1972, A Note on the Estimation of the Critical Damping in Dynamic Relaxation, *Int. J. for Numerical Methods in Engineering*, **4**, 301-304.

Caridis, P. A., Frieze, P. A., 1988, Flexural-Torsional Elasto-Plastic Buckling in Flat Stiffened Plating Using Dynamic Relaxation, Part 1: Theory, *Thin-Walled Structures*, **6**, 453-481.

Caridis, P. A., Frieze, P. A., 1989, Flexural-Torsional Elasto-Plastic Buckling Analysis of Stiffened Plates using Dynamic Relaxation, Part 2: Comparison with Test Results and other Formulations, *Thin-Walled Structures*, **7**, 37-72.

Cassel, A. C., Kinsey, P. J., Sefton, D. J., 1968, Cylindrical Shell Analysis by Dynamic Relaxation, *Proc. of Inst. of Civil Engineers*, London, **39**, 76-84.

Cassel, A. C., 1970, Shells of Revolution under Arbitrary Loading and the Use of Fictitious Densities in Dynamic Relaxation, *Proc. of Inst. of Civil Engineers*, London, **45**, 65-78.

Cassel, A. C., Hobbs, R. E., 1976, Numerical Stability of Dynamic Relaxation Analysis of Non-Linear Structures, *Int. J. for Numer. Methods in Engineering*, **10**, 1407-1410.

Cherepanov, G.P., 1963, On the Buckling under Tension of a Membrane Containing Holes, *Appl. Math. Mech. (PMM)*, **27**, 405-420.

Cohen, H., Wang, C.C., 1984, On the Response and Symmetry of Elastic and Hyperelastic Membrane Points, *Arch. Rat. Mech. Anal.*, **85**, 343-79.

Courant, R., Friedrichs, K., Lewy, H., 1928, On the Partial Differential Equations of Mathematical Physics, *Mathematische Anallen*, **100**, 32-74, English translation in: *IBM Journal*, 215-234, (1967).

Contri, P., Schrefler, B. A., 1988, A Geometrically Nonlinear Finite Element Analysis of Wrinkled Membrane Surfaces by a No-Compression Material Model, *Communications in Applied Numerical Methods*, **4**, 5-15.

Cundall, P. A., 1976, Explicit Finite Difference Methods in Geomechanics, *Proc. of E.F. Conf. on Numerical Methods in Geomechanics*, Blacksburg, VA.

Day, A. S., 1965, An Introduction to Dynamic Relaxation, *The Engineer*, London, **219**, 218-221.

Engeli, M., Ginsburg, T., Rutishauser, H., Stiefel, E., 1959, *Refined Iterative Methods for Computation of the Solution and Eigenvalues of Self-Adjoint Boundary Value Problems*, Birkhäuser Verlag, Basel.

Eriksson, A., 1987, Using Eigenvector Projections to Improve Convergence in Non-Linear Finite Element Equilibrium Iterations, *Int. J. for Numer. Methods in Engineering*, **24**, 297-512.

Estefen, S. F., Harding, J. E., 1986, Effect of Ring Stiffeners on Inter-Ring Cylindrical Panel Buckling, *Proc. of the 5th Int. Symp. on Offshore Engineering*, Rio de Janeiro, 460-476.

Felippa, C. A., 1974, Finite Element Analysis of Three-Dimensional Cable Structures, *Proc. of Int. Conf. on Computational Methods in Nonlinear Mechanics*, Austin, Texas, 231-256.

Forsythe, G. E., Wasow, W. R., 1981, Finite-Difference Methods for Partial Differential Equations, *Computer Methods in Applied Mechanics and Engineering*, **25**, 35-48.

Frankel, S. P., 1950, Convergence Rates of Iterative Treatments of Partial Differential Equations, *Mathematical Tables and other Aids to Computation*, National Research Council, Washington, **4**, 65-75.

French, D.A., Jensen, S., 1991, Behaviour in the Large of Numerical Solutions to One-Dimensional Nonlinear Viscoelasticity by Continuous Time Galerkin Methods, *Computer Methods in Applied Mechanics and Engineering*, **86**, 105-124.

Frieze, P. A., Hobbs, R. E., Dowling, P. J., 1978, Application of Dynamic Relaxation to the Large Deflection Elasto-Plastic Analysis of Plates, *Computers and Structures*, **8**, 301-310.

Graves, L.E., 1939, The Weierstrass Condition for Multiple Integral Variation Problems, *Duke Math. Journal*, **5**, 656-660.

Green, A.E., Adkins, J.E., 1970, *Large Elastic Deformations*, Calderon Press, Oxford.

Green, A.E., Naghdi, P.M., Wainwright, W.L., 1965, A General Theory of a Cosserat Surface, *Arch. Ration. Mech. Analysis*, **20**, 287.

Greenberg, D. P., 1970, Inelastic Analysis of Suspension Roof Structures, J. Struct. Div., ASCE, 96, ST5, 28-39.

Hancock, S.L., 1976, Finite Difference Equations for PISCES 2DELK, a Coupled Euler Lagrange Continuum Mechanics Computer Program, Physics Intl. Co., tech. Memo TCAM 76-2.

Hansen, W., 1956, *Theorie zur Errechnung des Wasserstandes und der Strömungen in Randmeeren nebst Anwendungen*, Tellus.

Haseganu, E.M., Steigmann, D. J., 1994a, Theoretical Flexural Response of a Pressurized Cylindrical Membrane, *Int. J. Solids Structures*, **31**, 27-50.

Haseganu, E.M., Steigmann, D. J., 1994b, Analysis of Partly Wrinkled Membranes by the Method of Dynamic Relaxation, *Computational Mechanics*, to appear.

Haug, E., Powell, G. H., 1971, Finite Element Analysis of Non-Linear Membrane Structures, *Proc. of IASS Pacific Symp.*, Part II, On Tension Structures and Space Frames, Tokyo, 165-175.

Haug, E., 1972, Finite Element Analysis of Pneumatic Structures, *Proc. of Int. Sym. on Pneumatic Structures*, Delft, 121-133.

Herrmann, W., Bertholf, L. D., 1983, Explicit Lagrangian Finite-Difference Methods, in: *Computational Methods for Transient Analysis*, Belytschko, T., Hughes, T. J. R., editors, Elsvier, Amsterdam, 361-416.

Hilgers, M. G., Pipkin, A. C., 1992, Elastic Sheets with Bending Stiffness, *Q. Jl. Mech. Appl. Math.*, **45**, 93-110.

Hoffman, R., 1975, Lagrange Explicit Finite-Difference Technology, Science Applications Inc., EPRI RP-307.

Jenkins, C. H., Leonard, J. W., 1991, Nonlinear Dynamic Response of Membranes: State of the Art, *ASME Applied Mechanics Rev.*, **44**, 319-328.

Jensen, J. J., 1971, An Investigation of the Static and Dynamic Behaviour of Suspension Structures, *Proc. of IASS Symposium on Tension Structures and Space Frames*, Tokyo, 27-34.

Jeong, D. G., Kwak, B. M., 1992, Complementary Problem Formulation for the Wrinkled Membrane and Numerical Implementation, *Finite Element Analysis and Design*, **12**, 91-104.

Jonatowski, J. J., 1974, Tensile Roof Structures: an Inelastic Analysis, *Proc. of Int. Conf. on Tension Structures*, London, 133-141.

Kant, T., Kommineri, J. R., 1993, Pseudo-Transient Large-Deflection Elastic Analysis of Fibre Reinforced Composite Plates, *Engineering Computations*, **10**, 159-173.

Key, S. W., Stone, C. M., Krieg, R. C., 1981, A Solution Strategy for the Quasi-Static, Large Deformation, Inelastic Response of Axisymmetric Solids, in: *Nonlinear Finite Element Analysis in Structural Mechanics*, Wunderlich, W., Stein, E., Bath, K. J., editors, Springer Verlag Berlin, 585-620.

Kondo, K., 1943, On the General Theory of the Curved Tension Field, *J. Soc. Aero. Sci.Nippon*, **10**, 98.

Kondo, K., Iai, T., Moriguti, S., Murasaki, T., 1955, Tension-Field Theory, in: *Memoirs of the Unifying Study of the Basic Problems in Engineering Science by Means of Geometry*, Vol. 1, C-V, 61-85, Gakujutsu, Bunken Fukyu-Kai, Tokyo.

Knops, R.J., Wilkes, E.W., 1973, Theory of Elastic Stability, in: *Handbuch der Physik*, Flügge, S., editor, Vol. VIa/3, Springer Verlag, Berlin.

Kulak, R. F., Fiala, C., 1988, NEPTUNE: A System of Finite Element Programs for Three-Dimensional Nonlinear Analysis, *Nuclear Engineering and Design*, **106**, 47-68.

Leech, J. W ., 1965, Stability of Finite-Difference Equations for the Transient Response of a Flat Plate, *AIAA Jour.*, **3**, 1772-1773.

Lewis, W. J., Jones, M. S., Lewis, G., Rushton, K. R., 1984, Cladding-Network Interaction in Pretensioned Cable Roofs Studied by Dynamic Relaxation, *Computers and Structures*, **19**, 885-897.

Lewis, W. J., 1989, The Efficiency of Numerical Methods for the Analysis of Prestressed Nets and Pin-jointed Frame Structures, *Computers and Structures*, **33**, 791-800.

Lewis, W. J., Shan, J., 1990, Numerical Modelling of the Non-Linear Static Response of Clad Cable Net Structures, *Computers and Structures*, **35**, 15-22.

Lewis, W. J., Goslilng, P. D., 1993, Stable Minimal Surfaces in Form-Finding of Lightweight Tension Structures, *Int. J. of Space Structures*, **8**, 149-166.

Li, X., Steigmann, D. J., 1993, Finite Plane Twist of an Annular Membrane, *Q.J. Mech. Appl. Math.*, **46**, 601-625.

Li, X., Steigmann, D. J., 1994, Point Loads on a Hemispherical Elastic Membrane, *Int. J. Non-linear Mech.*, to appear.

Lim, G. T., Turvey, G. J., 1985, Axisymmetrical Elasto-Plastic Large Deflection Behaviour of Circular Steel Plates with Initial Deflections - A Parametric Study, *Computers and Structures*, **21**, 1187-1196.

Lukasiewicz, S., Glockner, P. G., 1984-85, Stability of Lofty Air-Supported Cylindrical Membranes, *J. Struct. Mech.*, **12**, 543-555.

Lynch, R. D., Kelsey, S., Saxe, H. C., 1968, The Application of Dynamic Relaxation to the Finite Element Method of Structural Analysis, Technical Report No. Themis-Und-68-1, University of Notre Dame, Indiana.

Magara, H., Okamura, K., Kawaguchi, M., 1984, An Analysis of Membrane Structures, *Proc. of the Int. Symp. on Shell and Spatial Structures Engineering*, Rio de Janeiro, Pentech Press, London, 1-12.

Mansfield, E.H., 1970, Load Transfer Via a Wrinkled Membrane, *Proc. R. Soc. Lond.*, A, **316**, 269-289.

Marchestas, A. H., Kennedy, J. M., Pfeiffer, P. A., 1988, Reinforced Flexural Elements for TEMP-STRESS Program, *Nuclear Engineering and Design*, **106**, 87-102.

Meirovitch, L., 1986, *Elements of Vibration Analysis*, McGraw-Hill, New York.

Mikulas, M.M., 1964, Behaviour of Flat Membrane Wrinkled by the Rotation of an Attached Hub, NASA TND-2456.

Miller, R. K., Hedgepeth, J. M., 1982, An Algorithm for Finite Element Analysis of Partly Wrinkled Membranes, *AIAA Jour.*, **20**, 1761-1763.

Miller, R. K., Hedgepeth, J. M., Weingarten, V. I., Das, P., Kahyai, S., 1985, Finite Element Analysis of Partly Wrinkled Membranes, *Computers and Structures*, **20**, 631-639.

Mollman, H., Mortensen, P. L., 1966, The Analysis of Prestressed Suspended Cable Nets, *Proc. of Int. Conf. on Space Structures*, Guildford, 51-63.

Morrey, C.B., 1966, *Multiple Integrals in the Calculus of Variation*, Springer Verlag, Berlin.

Moncrieff, E., Topping, B. H. V., 1990, Computer Methods for Generating of Membrane Cutting Patterns, *Computers and Structures*, **37**, 441-450.

Motro, R., 1984, Forms and Forces in Tensegrity Systems, *Proc. of Third Int. Conf. on Space Structures*, Guilford, 283-288.

Motro, R., Najari, S., Jonanna, P., 1986, Tensegrity Systems, from Design to Realization, *Proc. of First Int. Conf. on Lightweight Structures in Architecture*, Sydney, 690-697.

Naghdi, P.M., 1972, Theory of Shells and Plates, in: *Handbuch der Physik*, Flügge, S., editor, Vol. VIa/2, pp. 425-640, Springer Verlag, Berlin.

Naghdi, P.M., Tang, P.Y., 1977, Large Deformation Possible in every Isotropic Elastic Membrane, *Phil. Trans. R. Soc. London*, A, **287**, 145-187 .

Nishimura, T., Tosaka, N., Honma, T., 1986, Membrane Structure Analysis Using the Finite Element Technique, in: *Shells, Membranes and Space Frames*, Heki, K., editor, Elsvier, Amsterdam, V. 2, 9-16.

O'Brien, G. G., Hyman, M. A., Kaplan, S., 1951, A Study of the Numerical Solution of Partial Differential Equations, *Jour. of Math. and Phys.*, **29**, 223-251.

Oden, J. T., 1972, *Finite Elements of Nonlinear Continua*, McGraw-Hill, New York.

Ogden, R.W., 1984, *Nonlinear Elastic Deformations*, Ellis-Horwood, Chichester, U.K.

Otter, J. R. H., Day, A. S., 1960, Tidal Flow Computations, *The Engineer*, London, **209**, 177-182.

Otter, J. R. H., 1965, Computations for Prestressed Concrete Reactor Pressure Vessels using Dynamic Relaxation, *Nuclear Structural Engineering*, Amsterdam, **1**, 61-75.

Otter, J. R. H., Cassell, A. C., Hobbs, R. E., 1966, Dynamic Relaxation, *Proc. of the Inst. of Civil Engineers*, London, **35**, 633-656.

Papadrakakis, M., 1981, A Method for the Automatic Evaluation of the Dynamic Relaxation Parameters, *Computer Methods in Applied Mechanics and Engineering*, **25**, 35-48.

Papadrakakis, M., 1986, Accelerating Vector Iteration Methods, *Jour. of Applied Mechanics*, **53**, 291-197.

Park, K. C., 1977, Practical Aspects of Numerical Time Integration, *Computers and Structures*, **7**, 343-353.

Park, K. C., Underwood, P. G., 1980, A Variable-Step central Difference Method for Structural Dynamics Analysis - Part 1: Theoretical Aspects, *Computer Methods in Applied Mechanics and Engineering*, **22**, 241-258.

Pica, A., Hinton, E. , 1980, Transient and Pseudo-Transient Analysis of Mindlin Plates, *Int. J. for Num. Methods in Engineering*, **15**, 189-208.

Pipkin, A.C., 1986a, The Relaxed Energy Density for Isotropic Elastic Membranes, *IMA J. Appl. Math.*, **36**, 85-99.

Pipkin, A.C., 1986b, Continuously Distributed Wrinkles in Fabrics, *Arch. Rat. Mech. Analysis*, **95**, 93-115.

Poskitt, T. J., 1967, Numerical Solutions of Non-Linear Structures, J. Struct., Div., ASCE, ST4, 36-48.

Ramesh, G., Krishnamoorthy, C. S., 1993, Post-Buckling Analysis of Structures by Dynamic Relaxation, *Int. J. for Numer. Methods in Engineering*, **36**, 1339-1364.

Rao, A. R. H., Shantaram, D., 1990, Nonlinear Finite Element Analysis by Dynamic Relaxation, *Int. J. of Structures*, **10**, 37-53.

Reissner, E., 1938, On Tension-Field Theory, *Proc. 5th International Congress on Applied Mechanics*, 88-92.

Rericha, P., 1986, Optimum Load Time History for Non-Linear Analysis using Dynamic Relaxation, *Int. J. for Numerical Methods in Engineering*, **23**, 2313-2324.

Richardson, L. F., 1911, The Approximate Arithmetical Solution by Finite Differences of Physical Problems Involving Differential Equations, with an Application to the Stresses in a Masonry Dam, *Philosophical Trans. of the Roy. Soc. of London*, A, **210**, 307-357.

Richardson, L. F., 1925, How to solve Differential Equations Approximately by Arithmetic, *Mathematical Gazette*, London, **12**, 415-421.

Roddeman, D. G., 1991, Finite Element Analysis of Wrinkling Membranes, *Communications in Applied Numerical Methods*, **7**, 299-307.

Roddeman, D. G., Drukker, J., Oomeens, C. W. J., Janssen, J. D., 1987, The Wrinkling of Thin Membranes: Part 1 - Theory, Part II - Numerical Analysis, *ASME J. of Applied Mechanics*, **54**, 884-887, 888-892.

Roxburgh, D.G., Steigmann, D.J., Tait, R.J., 1993, Azimuthal Shearing and Transverse Deflection of a Prestretched Annular Elastic Membrane, *Int. J. Engng. Sci.*, to appear.

Rushton, K. R., 1968a, Large Deflection of Variable-Thickness Plates, *Int. J. Mech. Sci.*, **10**, 723-735.

Rushton, K. R., 1968b, Dynamic Relaxation Solutions of Elastic-Plate Problems, *Jour. of Strain Analysis*, **3**, 23-32.

Rushton, K. R., 1969a, Dynamic Relaxation Solution for the Large Deflection of Plates with Specified Boundary Stress, *J. of Strain Analysis*, **4**, 75-80.

Rushton, K.R., 1969b, Simply Supported Plates with Corners Free to Lift, *Jour. of Strain Analysis*, **4**, 306-311.

Rushton, K. R., 1969c, Postbuckling of Tapered Plates, *Int. J. Mech. Sci.*, **11**, 461-480.

Rushton, K. R., 1972, Buckling of Laterally Loaded Plates Having Initial Curvature, *Int. J. Mech. Sci.*, **14**, 667-680.

Salehi, M., Turvey, G. J., 1991, Elastic large Deflection Response of Annular Sector Plates -a Comparison of DR Finite-Difference, Finite Element and Other Numerical Solutions, *Computers and Structures*, **40**, 1267-1278.

Sauve, R. G., Metzger, 1992, Advances in Dynamic Relaxation Techniques for Non-Linear Finite Element Analysis, *Proc. of 1992 Pressure Vessels and Piping Conference*, New Orleans, LA, 59-64.

Sauve, R. G., Badie, N., 1993, Non-Linear Shell Formulation for Time-Dependent Deformation, *Proc. of 1993 Pressure Vessels and Piping Conference*, Denver, CO, 269-275.

Shortley, G., Weller, R., Fried, B., 1942, Numerical Solution of Laplace's and Poisson's Equation with Application to Photoelasticity and Torsion, Studies, Engineering Series, Ohio State University, 107, 57-81.

Silling, S. A., 1985, CHIMP - A computer program for finite elastostatics, Report 54 California Institute of Technology, Division of Engineering and Applied Science.

Silling, S.A., 1987, Incompressibility in Dynamic Relaxation, *J. of Applied Mechanics*, **54**, 539-544.

Silling, S. A., 1988a, Finite Difference Modeling of Phase Changes and Localization in Elasticity, *Computer Methods in Applied Mechanics and Engineering*, **70**, 251-273.

Silling, S.A., 1988b, Numerical Studies of Loss of Elipticity near Singularities in an Elastic Material, *J. of Elasticity*, **19**, 213-239.

Silling, S. A., 1989, Phase Changes induced by Deformation in Isothermal Elastic Crystals, *J. of the Mechanics and Physics of Solids*, **3**, 293-316.

Steigmann, D. J., 1986, Proof of a Conjecture in Elastic Membrane Theory, *ASME J. Appl. Mech.*, **53**, 955-956.

Steigmann, D. J., 1990, Tension-Field Theory, *Proc. of Roy. Soc. of London*, A, **429**, 141-173.

Steigmann, D.J., 1991, A Note on Pressure Potentials, J. *Elast.*, **26**, 87-93.

Steigmann, D.J., 1992, Equilibrium of Prestressed Networks, *IMAJ. Appl. Math.*, **48**, 195-215.

Stein, M., Hedgepeth, J.M., 1961, Analysis of Partly Wrinkled Membranes, NASA TND-813.

Strang, G., 1980, *Linear Algebra and its Applications*, Academic Press, New York.

Stricklin, J. A., Haisler, W. E., 1977, Formulation and Solution Procedures for Nonlinear Structural Analysis, *Computers and Structures*, **7**, 125-136.

Swart, P.J., Holmes, P.J., 1992, Energy Minimization and the Formulation of Microstructure in Dynamic Anti-Plane Shear, *Arch. Rat. Mech. Anal.*, **121**, 37-85.

Swegle, J. W., 1978, Toody IV - A Computer Program for Two-Dimensional Wave Propagation, Sandia Labs, SAND-78-0552.

Szyszkowski, W., Glockner, P. G., 1984, Finite Deformation and Stability Behaviour of Spherical Inflatebles under Axisymmetric Concentrated Loads, *Int. J. Non-Linear Mech.*, **19**, 489-496.

Szyszkowski, W., Glockner, P. G., 1987a, On the Statics of Supports and the Geometry of Wrinkling of Large Spherical Pressure Vessels, *Proc. of 1987 Pressure Vessels and Piping Conference*, San Diego, CA, 81-86.

Szyszkowski, W., Glockner, P. G., 1987b, Spherical Membranes Subjected to Vertical Concentrated Loads: an Experimental Study, *Eng. Struct.*, **9**, 183-191.

Tarakanow, S. I., 1984, Convergence of the Dynamic Relaxation Method in Problems of Loading of Elastic Shells of Revolution, *Moskow University Mechanics Bulletin*, **39**, 53-56.

Thompson, W. T., 1988, *Theory of Vibration with Applications*, 3rd edition, Prentice-Hall, Englewood Cliffs, NJ.

Turvey, G. J., Lim, G. T., 1986, Parametric Study of the Axisymmetric Full-Range Response of Thickness-Tapered Circular Steel Plates, *Computers and Structures*, **22**, 459-468.

Turvey, G. J., Der Avanessian, N. G. V., 1986, Elastic Large Deflection of Circular Plates Using Graded Finite Differences, *Computers and Structures*, **23**, 763-774.

Turvey, G. J., Der Avanessian, N. G. V., 1989, Axisymmetric Elasto-Plastic Large Deflection Response of Ring Stiffened Circular Plates, *Int. J. Mech. Sciences*, **31**, 905-924.

Turvey, G. J., Der Avanessian, N. G. V., 1990, Full-Range Response of Clamped Ring-Stiffened Circular Steel Plates, *Computers and Structures*, **37**, 55-70.

Turvey, G. J., Salehi, M., 1990, DR Large Deflection Analysis of Sector Plates, *Computers and Structures*, **34**, 101-112.

Turvey, G. J., Osman, M. Y., 1993, Large Deflection Initial Failure Analysis of Angle-Ply Laminated Plates, *Composite Structures*, **25**, 529-539.

Underwood, P., 1979, Dynamic Relaxation, in: *Computational Methods for Transient Analysis*, Belytschko, T., Hughes, T. J. R. editors, Elsvier, Amsterdam, 245-265.

Underwood, P., 1983, Dynamic Relaxation, in: *Computational Methods for Transient Analysis*, Belytschko, T., Hughes, T. J. R. editors, Elsvier, Amsterdam, 245-265.

Underwood, P. G., Park, K. C., 1980, A Variable-Step Central Difference Method for Structural Dynamic Analysis - Part 2: Implementation and Performance Evaluation, *Computer Methods in Applied Mechanics and Engineering*, **23**, 259-279.

Underwood, P. G., Park, K. C., 1982, STINT/CD: A Stand-Alone Explicit Time Integration Package for Structural Dynamics Analysis, *Int. J. for Numer. Methods in Engineering*, **18**, 609-622.

Varga, O.H., 1966, *Stress-Strain Behaviour of Elastic Materials*, Wiley, New York.

Wagner, H., 1929, Ebene Blechwandträger mit sehr dünnen Stegblech, *Z. Flugtechnik u. Motorluftschiffahrt*, **20**, Nos 8-12.

Wakefield, D. D., 1986, TENSYL: The Development of an Integrated CAD System for Stressed Membrane Structures, *Proc. of the First Int. Conf. on Lightweight Structures in Architecture*, Sydney, 271-178.

Welsh, A. K., 1967, in Discussion on Paper "Dynamic Relaxation" by Otter, J.H.R. et al., *Proc. of Inst. of Civil Engineers*, London, **37**, 723-750.

Wilkins, M. L., 1964, Calculation of Elastic-Plastic Flow, in: *Methods in Computational Physics*, V.3, Alder, B., Fernbach, S., Rotenberg, M., editors, Academic Press, New-York, 211-163.

Wilkins, M. L., 1969, Calculation of Elastic-Plastic Flow, Lawrence Radiation Laboratory, Rept. UCRL-7322, Revised, Univ. of California, Livermore.

Wood, W., 1967, Comparison of Dynamic Relaxation with Three other Iterative Methods, *The Engineer*, London, **224**, 683-687.

Wood, W. L., 1971, Note on Dynamic Relaxation, *Int. J. for Numer. Methods in Engineering*, **3**, 145-147.

Wu, C.H., 1978, Nonlinear Wrinkling of Nonlinear Membranes of Revolution, *ASME J. Appl. Mech.*, **45**, 533-538.

Wu, C.H., Canfield, T. R., 1981, Wrinkling in Finite Plane-Stress Theory, *Q. Appl. Math.*, **39**, 179-199.

Zak, M., 1982, Statics of Wrinkling Films, *J. Elast.*, **12**, 51-63.

Zhang, L. G., Yu, T. X., 1989, Modified Adoptive Dynamic Relaxation Method and its Application to Elastic-Plastic Bending and Wrinkling of Circular Plates, *Computers and Structures*, **33**, 609-614.

Zhang, L. G., Yu, T. X., Wang, R., 1989, New Approach of Predicting Points of Elastic-Plastic Buckling of Plates and Shells, *Acta Mechanica Sinica*, **5**, 145-151.

Zienkiewicz, O. C., 1977, *The Finite Element Method*, 3rd ed., McGraw-Hill, London.

Zienkiewicz, O. C., Löhner, R., 1985, Accelerated "Relaxation" or Direct Solution? Future Prospects for FEM, *Int. J. for Num. Methods in Engineering*, **21**, 2-11.